

Elemental Abundance Survey of The Galactic Thick Disk

Bacham E. Reddy¹, David L. Lambert², Carlos Allende Prieto²

¹ *Indian Institute of Astrophysics, Bangalore 560034, India*

² *The W.J. McDonald Observatory, University of Texas, Austin, Texas 78712, USA*

17 November 2021

ABSTRACT

We have performed an abundance analysis for F- and G- dwarfs of the Galactic thick disk component. A sample of 176 nearby ($d \leq 150$ pc) thick disk candidate stars was chosen from the *Hipparcos* catalogue and subjected to a high-resolution spectroscopic analysis. Using accurate radial velocities combined with *Hipparcos* astrometry, kinematics (U , V , and W) and Galactic orbital parameters were computed. We estimate the probability for a star to belong to the thin disk, the thick disk or the halo. With a probability $P \geq 70\%$ taken as certain membership, we assigned 95 stars to the thick disk, 13 to the thin disk, and 20 to the halo. The remaining 48 stars in the sample cannot be assigned with reasonable certainty to one of the three components.

Abundances of C, O, Na, Mg, Al, Si, Ca, Sc, Ti, V, Cr, Mn, Fe, Co, Ni, Cu, Zn, Y, Ba, Ce, Nd, and Eu have been obtained. The abundances for thick disk stars are compared with those for thin disk members from Reddy et al. (2003). The ratios of α -elements (O, Mg, Si, Ca and Ti) to iron for thick disk stars show a clear enhancement compared to thin disk members in the range $-0.3 < [\text{Fe}/\text{H}] < -1.2$. There are also other elements – Al, Sc, V, Co, and possibly Zn – which show enhanced ratios to iron in the thick disk relative to the thin disk. The abundances of Na, Cr, Mn, Ni, and Cu (relative to Fe) are very similar for thin and thick disk stars. The dispersion in abundance ratios $[\text{X}/\text{Fe}]$ at given $[\text{Fe}/\text{H}]$ for thick disk stars is consistent with the expected scatter due to measurement errors, suggesting a lack of ‘cosmic’ scatter.

A few stars classified as members of the thick disk by our kinematic criteria show thin disk abundances. These stars, which appear older than most thin disk stars, are also, on average, younger than the thick disk population. They may have originated early in the thin disk history, and been subsequently scattered to hotter orbits by collisions. The thick disk may not include stars with $[\text{Fe}/\text{H}] > -0.3$. The observed compositions of the thin and thick disks seem to be consistent with models of galaxy formation by hierarchical clustering in a Λ CDM universe. In particular, the distinct abundance patterns observed in the thin and thick disks, and the chemical homogeneity of the thick disk at different galactocentric distances favor a scenario in which the majority of thick-disk stars were formed *in situ*, from gas rich merging blocks.

Key words: stars: atmospheric parameters – stars: abundances – stars: thick and thin disc – stars: kinematics – Galaxy: evolution – Galaxy: abundances

1 INTRODUCTION

Stars of the solar neighbourhood are overwhelmingly members of the Galactic disk, with a small admixture of halo stars. The assignment of a star to the disk or the halo is based on differences in chemical composition and kinematics. The local disk population is subdivided into stars of the thin disk and others belonging to the thick disk, with chemical composition and kinematics again playing a role in effecting this subdivision.

The modern division of the disk into the thin and thick

disk was proposed by Gilmore & Reid (1983). Star counts led them to divide the disk population in the solar neighbourhood into a thin disk with a scale height of 300 pc and a thick disk with the much greater scale height of 1450 pc. Thin disk stars outnumber thick disk stars by about twenty to one in the Galactic plane. Many other estimates of scale heights and relative densities of thin and thick disk populations now exist (e.g., Buser et al. 1999; Ojha 2001; Cabrera-Lavers, Garzón & Hammersley 2005; Juric et al. 2005). The thick disk stars are generally older than most thin disk stars.

The metallicity distribution of the thick disk population is shifted to lower values relative to the distribution for the thin disk by about 0.5 dex. Although both distributions can be reasonably approximated by Gaussians with a FWHM of roughly 0.5 dex, the thick disk includes a tail at lower metallicities. In contrast to the thin disk stars, which orbit the Galactic centre on nearly circular orbits, the thick disk stars are on moderately elliptical orbits that typically reach higher distances from the plane. Thick disk stars also revolve around the Galactic center slower than those in the thin disk.

The origin of the thick disk has occasioned much debate. Keys to the origin lie within the kinematics and the composition of the thick disk stars. A number of recent spectroscopic studies have set out to compare the chemical compositions of thick and thin disk stars. This avenue was explored by Gratton et al. (1996) and Fuhrmann (1998). Gratton et al. showed that O/Fe ratios for thick disk stars are distinctly different from thin disk stars but similar to halo stars. Fuhrmann confirmed this based on Mg abundances and showed a clear cut difference in the Mg/Fe ratio for thick and thin F-G dwarf stars of the same $[\text{Fe}/\text{H}]^1$. These studies stimulated several investigations of elemental abundances in samples of thick and thin disk stars – see, for example, Prochaska et al. (2000), Feltzing, Bensby, & Lundström (2003), Reddy et al. (2003, hereafter Paper I), Bensby, Feltzing, & Lundström (2003, 2004), Bensby et al. (2005), and Mishenina et al. (2004). Although the pattern of abundance differences between thick and thin disk is emerging, many details remain obscure, largely, one suspects, because these investigations cover small numbers of thick disk stars: Prochaska et al. considered ten, Bensby and colleagues analyzed 36, and Mishenina et al. less than 30 stars. Considering that the thick disk may span a range of 1 dex in $[\text{Fe}/\text{H}]$, these samples, even when combined, are probably too small to define in detail the differences between compositions of thick and thin disk stars over their full range in $[\text{Fe}/\text{H}]$, even if the two disk components were themselves chemically homogeneous as a function of metallicity. Additionally, different definitions of what constitutes a thick disk star have been adopted by different authors.

Tens of thousands of thick-disk stars at a few kpc from the plane have been spectroscopically observed as part of the Sloan Digital Sky Survey (York et al. 2000; Adelman-McCarthy et al. 2005). These spectra, however, have a much lower resolving power than the surveys mentioned above, and although they may yield abundance ratios for a number of metals that produce strong spectral lines, they have, to this date, been used to derive iron abundances only (Allende Prieto et al. 2005).

Exploration of the chemical compositions of local thin disk stars is now well advanced. In particular, several surveys have investigated many elements in F-G dwarfs whose spectra are amenable to quantitative analysis. Our recent study of 26 elements in 181 F-G dwarfs (Paper I) was the precursor for the work presented in this paper. The vast majority of the 181 stars belong to the thin disk, as judged

(see below) by their kinematics. Our Paper I sample may be combined with other large samples to which thin disk stars are the major contributor: e.g., Edvardsson et al. (1993) for 189 stars, and Chen et al. (2000) for 90 stars. A key result of our 2003 survey was the finding that ‘cosmic’ scatter in an abundance ratio X/Fe at a given Fe/H for thin disk stars was less than the small measurement errors. Here, we apply the same analytical techniques to a large sample of thick stars for which the cosmic scatter and, indeed, the form of the run of $[X/\text{Fe}]$ with $[\text{Fe}/\text{H}]$ was not known at the outset of this project. There were clear indications of the sign and magnitude of some abundance differences between thick and thin disk, as recognized by Fuhrmann (1998), and Prochaska et al. (2000) and further examined by Bensby and colleagues, and by Mishenina et al. (2004).

The present survey provides abundances for 23 elements from C to Eu for 176 stars in the solar neighbourhood, of which 95 are attributed to the thick disk. The full sample is introduced in the next section. The observations and abundance analysis are based closely on Paper I’s approach is described in Section 3 and 4. Full results, and comparisons with other studies are given in Section 5. Chemical evolution of the thick disk and evolution of the Galactic disk are discussed in Section 6. This section includes discussion on stars which have thick disk kinematics and thin disk abundances (TKTA), disk heating, and merger scenarios. Concluding remarks are given in Section 7.

2 THE THICK DISK SAMPLE

2.1 Preliminary selection

Stars were first selected from the *Hipparcos* catalogue according to the following criteria: a declination north of -30° so that they were observable from the W. J. McDonald Observatory; a B–V colour corresponding to an effective temperature of 5000 – 6500 K which eliminates the cool dwarfs with rich line spectra and the hotter dwarfs where rapid rotation may broaden lines; and an absolute visual magnitude in the range $2.5 \leq M_V \leq 6.0$ indicating evolution off the zero-age main sequence so that an age determination is possible; a distance of less than 150 pc to avoid significant uncertainties in the observed trigonometric parallaxes, and the introduction of a reddening correction. Application of these criteria provided about 9,300 stars from the catalogue’s total of 118,218.

The *Hipparcos* catalogue was the sole source of parallaxes and proper motions. Our initial selection of thick disk candidates was based on space motions computed using radial velocities collected from several catalogues: the *Hipparcos* Input Catalogue, Carney et al. (1994), Barbier-Brossat & Figon (2000), and Malaroda, Levato, & Galliani (2001). These sources provided radial velocity data for 1,970 of the 9,300 stars. The space velocities U, V, W were computed, where U is directed towards the Galactic centre, V is directed in the sense of Galactic rotation (clockwise as seen from the North Galactic Pole), and W is directed towards the North Galactic Pole. Then, the velocities $U_{LSR}, V_{LSR}, W_{LSR}$ relative to the local standard of rest were calculated assuming the solar motion of $(U, V, W) = (10.0, 5.3, 7.2)$ km s $^{-1}$, as derived by Dehnen & Binney (1998) from *Hipparcos* data. After calculation of their

¹ Here and throughout the paper we use the so-called *bracket* notation to indicate chemical abundance ratios of two elements X and Y: $[X/Y] \equiv \log N(X)/N(Y) - \log (N(X)/N(Y))_\odot$

Table 1. Given are the velocity dispersions, the asymmetric drift velocities relative to local standard of rest (V_{ad}), and the fractional population of three stellar components: thin, thick and the halo.

Component	σ_U	σ_V	σ_W	V_{ad}	Fraction
Thin disk	43	28	17	-9	0.93
Thick disk	67	51	42	-48	0.07
Halo	131	106	85	-220	0.006

U_{LSR} , V_{LSR} , and W_{LSR} , a selection by V_{LSR} and W_{LSR} was made to increase the yield of thick disk (and halo) stars: $V_{LSR} \leq -40 \text{ km s}^{-1}$ and $|W_{LSR}| \geq 30 \text{ km s}^{-1}$. These criteria led to a sample of 213 stars which was reduced to 176 when inspection of spectra revealed stars with broad lines and the double-lined spectroscopic binaries.

In the final computation of the U , V , W for the 176 stars, we made extensive use of three new sources of radial velocities: Latham et al. (2002), Nidever et al. (2002), and Nordström et al. (2004). The agreement between these sources for stars in common corresponds to about $\sigma = 0.2 \text{ km s}^{-1}$. For 146 of the 176 stars, the radial velocity is given in one or more of these sources. For the remaining 30 stars, we derived the radial velocity from our spectra with an accuracy of about 0.5 km s^{-1} .

Space velocities were recomputed using the new radial velocities. We examined the effects of errors in the input parameters (parallax, proper motion, and radial velocity), assuming these errors are uncorrelated. The uncertainties in U_{LSR} , V_{LSR} , and W_{LSR} are calculated as the quadratic sum of the individual uncertainties in the input parameters. In a typical case, the Galactic velocity components are accurate to about 5 km s^{-1} . An uncertain parallax (say, 30% accuracy) can lead to a much larger uncertainty; there are 12 stars for which the uncertainty in one of the component velocities is as large as $30\text{-}50 \text{ km s}^{-1}$.

2.2 Membership probabilities

In developing an understanding of the differences between the thin and thick disks, an obvious prerequisite is a reliable method, even if statistical, of assigning a star to the thin or thick disk, and of recognizing stars for which an assignment cannot be made with fair certainty. Since our goal is to quantify the differences in chemical composition between the thin and thick disk, composition cannot be a consideration in determining membership. Kinematic criteria are invoked for this purpose. We follow recent studies in developing and applying the criteria. The criteria are blunt instruments; the kinematics of especially thin disk stars but one suspects also of thick disk stars are complicated.

The thin disk, as represented by the F-G dwarfs in the solar vicinity, is neither a monolithic structure nor cleanly separated from the thick disk in U_{LSR} , V_{LSR} , W_{LSR} space. Structures include moving groups or stellar streams which are seen as regions of enhanced stellar density in phase space (see Nordström et al. 2004; Famaey et al. 2005). In addition, the mean location of stars and the dispersion about their mean velocity is dependent on the age of the stars.

Characteristics of thick disk stars are the generally neg-

ative V_{LSR} and the larger W_{LSR} (relative to the thin disk). At present, thick disk stars with accurate U_{LSR} , V_{LSR} , and W_{LSR} velocities are too few in number to identify moving groups should they exist. It is commonly agreed that the dispersions in the U_{LSR} , V_{LSR} and W_{LSR} velocities of the thick disk stars exceed those of the thin disk stars.

There are regions in U_{LSR} , V_{LSR} , W_{LSR} space where both thin and thick disk stars may occur. In such boundary layers shared by thin and thick stars, one must resort to a probability argument. Boundary layers also exist mixing thick disk with halo stars and again a probability argument must be used.

In this paper, the method of assigning the probability for each star to either the thin disk, the thick disk, or the halo is basically that adopted in the earlier studies by Bensby et al. (2003, 2004) and Mishenina et al. (2004). We assume the sample is a mixture of the three populations. These populations are each assumed to be represented by Gaussian distribution functions for the velocity components U_{LSR} , V_{LSR} , and W_{LSR} , with given mean values and dispersions. (The well-known age dependence of the quantities for the thin disk is ignored.) The remaining required ingredients are the relative numbers of thin disk, thick disk, and halo stars.

Given these assumptions, the equations establishing the probability that a star belongs to the thin disk (P_{thin}), the thick disk (P_{thick}), or the halo (P_{halo}) are

$$P_{thin} = f_1 \frac{P_1}{P}, \quad P_{thick} = f_2 \frac{P_2}{P}, \quad P_{halo} = f_3 \frac{P_3}{P} \quad (1)$$

where,

$$P = \sum f_i P_i,$$

$$P_i = K_i \times \exp \left[-\frac{U_{LSR}^2}{2\sigma_{U_i}^2} - \frac{(V_{LSR} - V_{ad})^2}{2\sigma_{V_i}^2} - \frac{W_{LSR}^2}{2\sigma_{W_i}^2} \right]$$

and

$$K_i = \frac{1}{(2\pi)^{\frac{3}{2}} \sigma_{U_i} \sigma_{V_i} \sigma_{W_i}} \quad (i = 1, 2, 3) \quad (2)$$

and V_{ad} is the asymmetric drift, the mean galactic rotation velocity for each stellar population relative to the LSR.

The parameters (σ 's and the mean velocities) defining the Gaussian distribution functions and the population fractions f_i given in Table 1 are taken from Robin et al. (2003; but see also Ojha et al. 1996, 1999 and Soubiran et al. 2003). The asymmetric drifts V_{ad} given by Robin et al. are referred to the Sun, and therefore we have corrected it for the solar motion relative to the LSR $V_{\odot} = +5.3 \text{ km s}^{-1}$. The mean values of U_{LSR} and W_{LSR} for any of the three populations are taken to be zero. For the thin disk, the estimates refer to stars of 5-7 Gyr in age, which is an average value for our sample (see §4.5), but this result is also in excellent agreement with the value inferred by Allende Prieto et al. (2004) from FGK stars in the solar neighborhood.

The relative numbers of thin disk, thick disk, and halo stars in the solar vicinity are taken to be $f_1 = 0.93$, $f_2 = 0.07$, and $f_3 = 0.006$, respectively. As a check, we have used Nordström et al.'s (2004) survey of Galactic F-G dwarfs in the solar neighborhood to estimate the fractions of the three

components. If we assume that all the stars having V_{LSR} between -150 and -40 km s^{-1} belong to the thick disk, stars with $V_{LSR} > -40$ km s^{-1} are part of the thin disk, and the rest are halo stars, we find fractions of 94%, 5%, and 1%. The differences between Robin et al.’s (2003) and these fractions are small and have no impact on the resolution of the sample into three components based on probabilities.² Our adopted fractions also compare well with the ratios ρ_{thick}/ρ_{thin} of 4% and 9% derived at the solar radius from star counts by Juric et al. (2005) using SDSS and by Cabrera-Lavers et al. (2005) based on 2MASS, respectively.

The probabilities – P_{thin} , P_{thick} , and P_{halo} – and the associated errors due to errors in the velocities U_{LSR} , V_{LSR} and W_{LSR} were computed. (Our program reproduces the probabilities given by Bensby et al. (2003, 2005) and Mishenina et al. (2004) when their input data are adopted.) We consider that a probability (P_{thick} – error) in excess 70% suffices to assign a star to either the thin disk, the thick disk, or the halo. Table 2 lists 95 thick stars with P_{thick} given in column 12, 13 thin disk stars with P_{thin} in column 12, and 20 halo stars with P_{halo} in column 12. Of the sample of 176 stars, there remain 48 stars with 34 belonging to either the thick or the thin disk with about equal probability, and 14 belong to the thick disk or the halo with approximately equal probability. In Table 2, P_{thick} is given for these 48 stars. (The same procedure applied to the 181 ‘thin’ disk stars of Paper I yielded 175 thin disk, just two thick stars with the other four assignable with roughly equal probability to either the thin or the thick disk.)

The present sample and that from Paper I are shown in Figure 1 with the velocities U_{LSR} , V_{LSR} , and W_{LSR} plotted against $[\text{Fe}/\text{H}] - [\text{Fe}/\text{H}]$ for the present sample is given below. Also, shown is the Toomre diagram with $(U_{LSR}^2 + W_{LSR}^2)^{1/2}$ against V_{LSR} . The biases from the selection criteria for the present sample – $V_{LSR} \leq -40$ km s^{-1} and $|W_{LSR}| \geq 30$ km s^{-1} – are quite evident in the three panels involving $[\text{Fe}/\text{H}]$. In addition, the sample from Paper I was biased towards less than solar metallicities, and, therefore, the thin disk is underrepresented at $[\text{Fe}/\text{H}] \sim 0$. The stars with approximately equal probability of membership of the thin or thick disks fall, as expected, at the thin-thick disk boundaries in the four panels.

Classification by probability with the parameters in Table 1 applied to our sample selected by our V_{LSR} and W_{LSR} criteria results in a collection of thin disk stars that may be deemed unusual by purists. The computed orbits of the thin disk stars are quite eccentric; compare the thin disk entries in Table 1 with those in Table 1 from Paper I – also see Figure 1 or the different locations of these thin disk stars and those from Paper I. The probability $P_{thin} > 70\%$ is largely set by the low $|W_{LSR}|$ which in turn implies the star remains close to the Galactic plane. In several of the panels of Figures 1 and 3, these thin disk stars fall at a boundary between the thin disk stars of Paper I and the present thick disk stars. Thus, one might regard them on kinematic grounds as either extreme representatives of the thin disk or

the thick disk. Their compositions may resolve this ambiguity (see below).

An informative illustration of the dependence of P_{thick} on the velocity components U_{LSR} , V_{LSR} , and W_{LSR} is provided in Figure 2. This gives equal probability contours for P_{thick} equal to 50, 70, 80, and ≥ 90 per cent for the range of $|U_{LSR}| = 0$ to 200 km s^{-1} , $V_{LSR} = +100$ to -200 km s^{-1} , and $|W_{LSR}| = 0$ to 150 km s^{-1} . In the figure, probabilities increase from outside ($P_{thick}=0.50$) to inside ($P_{thick}=0.97$ for panels (a) to (c) and to $P_{thick} = 0.90$ for the panel (d)). In these panels, if a star’s V_{LSR} and W_{LSR} is such that it falls outside of the thick disk $P_{thick}=0.50$ contour, the star most likely belongs to the halo and it is most likely a thin disk star if it falls in empty bottom right corners of the plots.

2.3 Orbital Parameters

Orbital parameters such as the eccentricity, maximum distance above the Galactic plane, the apogalactic and the perigalactic distance for the sample were computed using the same Galactic potential model adopted for Paper I. The distance of 8.5 kpc for the Sun from the Galactic center is adopted. The mean Galactocentric distance (R_m) for each star is taken as the mean of the apogalactic and perigalactic distances. Key Galactic orbital parameters for the thick disk sample are shown in Figure 3 against $[\text{Fe}/\text{H}]$ for both the current sample and that from Paper I. Again, it must be recognized that our selection criteria affect the distribution of points in the panels of Figure 3.

3 OBSERVATIONS

High-resolution spectra of the programme stars were obtained during the period, December 2002 - June 2004 at the Harlan J. Smith 2.7-m telescope of the W. J. McDonald Observatory, using the 2dcoudé echelle spectrometer (Tull et al. 1995) with a 2048×2048 Tektronix CCD as detector.

Spectral coverage at a resolving power of about 60,000 was complete from 3500 Å to 5600 Å and substantial but incomplete from 5600 Å to about 9000 Å. The Echelle spectroscopic data were reduced to one dimensional spectra with Y-axis as normalized flux and X-axis as wavelength using spectral reduction programme *IRAF*³ as outlined in Paper I. The final reduced spectra have S/N $\approx 100 - 200$. Selection and measurement of suitable absorption lines followed the procedures described in Paper I.

4 ANALYSIS

The LTE abundance analysis was modelled as closely as possible on that described in Paper I. The model atmosphere grid and the methods of determining the fundamental atmospheric parameters were retained. A minor alteration in the determination of the effective temperature for about 40 stars is noted below. The line list and basic atomic data was

² Venn et al. (2004) seem to have computed membership probabilities on the assumption that the fractional populations are the same for the three components. This assumption can give very different and misleading results.

³ IRAF is distributed by the National Optical Astronomical Observatories, which is operated by the Association for Universities for Research in Astronomy, Inc., under contract to the National Science Foundation.

taken over from Paper I. The abundance analysis was again performed with the 2002 version of the code MOOG (Snedden 1973). The reader interested in the details is referred to Paper I.

The distribution of stars in our sample with T_{eff} , $\log g$, and $[\text{Fe}/\text{H}]$ is shown in Figure 4 where is also given the distribution of $\log g$ with $[\text{Fe}/\text{H}]$. This figure may be compared with its counterpart in Paper I. The comparison shows the anticipated difference in the $[\text{Fe}/\text{H}]$ range of the two samples. A point of note is that the samples differ in the spans of T_{eff} ; the thin disk stars are in the mean systematically warmer than the present sample with the peak in the thick disk distribution being about 300 K cooler than that in Paper I.

4.1 The Effective Temperature

In Paper I, effective temperatures (T_{eff}) were estimated from a star's Strömgren ($b - y$) colour using the calibration provided by Alonso et al. (1996) who obtained T_{eff} from the infra-red flux method (IRFM). The $wby\beta$ data was adopted from Hauck & Mermilliod's (1997) catalogue. This approach was used for the 135 of the 176 stars in the present sample for which Strömgren photometry has been reported.

An alternative approach was developed for the other 41 stars. We chose to use the ($V - K$) colour and the corresponding calibration, again from Alonso et al. The V magnitude was taken from the *Hipparcos* catalogue. The K magnitude is not available for all of these stars, but the 2MASS Catalogue⁴ (Cutri et al. 2003) provides the magnitudes K_s for all 41 stars. To estimate a possible systematic offset between the (K_s) magnitudes of 2MASS and the Alonso et al. scale (K), we took a sample of 100 stars from the 2MASS catalogue with observations from Alonso et al (1996). The mean difference is very small: ($K_s - K$) = -0.004 with a σ of 0.09 and no trend (Figure 5). Therefore, we adopted the 2MASS K_s and equated it with K .

The ($b - y$) and ($V - K$) \equiv ($V - K_s$) colours give very similar T_{eff} values – see Figure 6. The mean difference $T_{\text{eff}}(b-y) - T_{\text{eff}}(V-K) = -15$ K with a $\sigma = 69$ K with a few outliers. For the outliers, we obtained T_{eff} spectroscopically by demanding excitation equilibrium for a set of Fe I lines.

Observed colours were not corrected for interstellar extinction for stars closer than 100 pc. For the 37 stars with distances greater than 100 pc (but less than 150 pc), a correction was estimated from Neckel, Klare & Sarcander (1980) maps. The maximum extinction is about 0.1 magnitudes in V and thus 0.01 magnitudes in K . Correction for this level of extinction, a maximum for our sample, increases the T_{eff} by about 140 K.

⁴ This publication makes use of data products from the Two Micron All Sky Survey, which is a joint project of the University of Massachusetts and the Infrared Processing and Analysis Center/California Institute of Technology, funded by the National Aeronautics and Space Administration and the National Science Foundation

4.2 Metallicity, surface gravities, and microturbulence

Metallicity usually refers to the iron abundance (relative to the solar abundance) which here was obtained for each star from numerous well defined Fe I lines and a few Fe II lines. Since the stellar T_{eff} except for a few exceptional cases (see above) and the surface gravity in all cases were obtained without recourse to the Fe I and Fe II lines, it is of interest to see if the Fe I and Fe II lines return the same value for the iron abundance. Non-LTE effects may affect these iron abundance estimates; overionization of neutral iron (relative to LTE) is believed to be the principal non-LTE effect so that, in an LTE analysis, the abundance from Fe I lines is less than that from Fe II lines. Figure 7 (top panel) shows the abundance difference from Fe I and Fe II as a function of the abundance from the neutral lines. On average the Fe I lines give a lower abundance by 0.04 ± 0.08 dex with no significant trend with $[\text{Fe}/\text{H}]$. (The corresponding difference for the thin disk stars in Paper I was 0.02 ± 0.05 dex for stars with $[\text{Fe}/\text{H}]$ from about 0.0 to -0.6 .) Following Paper I, we adopt the iron abundance given by the Fe I lines because the neutral lines are many and the ionized lines few.

Photometric recipes exist for determining the metallicity, here identified with $[\text{M}/\text{H}]$. Here, we adopt the metallicity calibration of Strömgren photometry provided by Hauck & Mermilliod (1997). Figure 7 (lower panel) shows the difference between the photometric $[\text{M}/\text{H}]$ and the spectroscopic $[\text{Fe}/\text{H}]$ from the Fe I lines as a function of the spectroscopic $[\text{Fe}/\text{H}]$. The differences are generally small and the mean difference $[\text{M}/\text{H}] - [\text{Fe}/\text{H}] = -0.01 \pm 0.10$. (In Paper I, the mean difference was 0.05 ± 0.09 with no detectable trend over the interval $[\text{Fe}/\text{H}]$ from -0.2 to -0.8 .) We note that discrepant iron abundances are inferred from Fe I and Fe I lines for slightly lower values of T_{eff} and especially more metal rich stars than in our sample (Feltzing & Gustafsson 1998; Schuster et al. 2003; Yong et al. 2004; Allende Prieto et al. 2004).

Surface gravities were obtained, as in Paper I, by a combination of stellar isochrones (Bertelli et al. 1994), T_{eff} , $[\text{Fe}/\text{H}]$, and the *Hipparcos* astrometry. The resulting $\log g$ values are compared for the common stars between this study and few others (see Table 3). For the microturbulent velocities (ξ_t) we used the relation between ξ_t , T_{eff} , and $\log g$ derived in Paper I. The relation used from Paper I is derived using mainly thin disk stars which cover slightly different ranges in the parameters than the thick disk sample stars. To check the validity of the relation we derived ξ_t values for 15 thick disk stars using Fe I lines. The adopted values from the relation are larger by only 0.14 ± 0.17 km s⁻¹ than the spectroscopically derived values. The effect of such difference on the abundances is negligible.

4.3 Model Atmospheres

Stellar abundances are obtained assuming LTE line formation. Abundances are given with respect to the Sun which was analyzed as described in Paper I. We used Kurucz's (1998) LTE, plane parallel, line-blanketed models with convective overshoot and the revised (2002) stellar abundance code MOOG (Snedden 1973). The oscillator strengths for the basic set of about 160 lines are a mixture of laboratory mea-

sured values and the astrophysically derived by inverting solar and the stellar spectra (see Paper I).

The rationale for adopting Kurucz models with convective overshoot is described in Paper I; the thin disk sample in Paper I are similar to the Sun for which the convective overshoot model gives a good representation. However, the current thick disk stars are cooler, metal-poor and higher gravity stars than the thin disk sample; they are not close analogs of the Sun. The models with convective overshoot are not widely used in abundance analysis. For this reason, we computed the $[X/Fe]$ of 12 representative elements using both models with and without convective overshoot. Twelve stars are chosen so that they cover T_{eff} (5000 K to 6100 K) and $[Fe/H]$ (0.2 to -1.6) range of the thick disk sample. Differences ($\delta[X/Fe]$) in $[X/Fe]$ from the two kinds of models were $\delta[X/Fe] \leq 0.01$ for all the elements except carbon for which 0.04 was representative.

4.4 Abundance errors

The principal goal of this study is to define the differences in composition between thin and thick disk stars. It is known that the differences, even in the most striking cases, are small (≤ 0.2 dex) and, therefore, attention must be paid to the errors thought to affect the abundance determinations. In addition, our sample of thick disk stars is of a sufficient size that we may attempt to estimate the dispersion in the abundances at a given metallicity and wonder if the dispersion is due to measurement errors or may contain cosmic scatter.

The recipe used to assess the errors follows that used in Paper I. Two qualitative differences may be noted. First, the spectra for the thick disk sample are of lower quality than those used for Paper I: $S/N \simeq 100 - 200$ versus $S/N \simeq 200 - 400$. Also, two spectra were generally obtained for each thin disk star but a single one for a thick disk star; the thick disk stars are relatively fainter than the selected thin disk stars. Second, the thick disk stars are systematically cooler (and more metal poor) than the thin disk stars; these differences lead to different sensitivities of the abundances on the atmospheric parameters.

For these reasons, we estimated uncertainties in $[X/Fe]$ due to uncertainties in model parameters and measurement errors afresh for the present sample. We assumed that the errors are uncorrelated. The predicted uncertainty, σ_{mod} for a whole sample, in each abundance ratio due to measurement errors can be written as a simple mean of the σ s estimated for n representative stars

$$\sigma_{\text{mod}} = \frac{1}{n} \sum_i \sigma_i = \frac{1}{n} \sum_i \sqrt{\sum_j \left(\frac{\partial}{\partial p_j} [X/Fe] \right)^2 (\delta p_j)^2} \quad (3)$$

and the parameters p_j considered here are the effective temperature, surface gravity, metallicity, microturbulence, and the equivalent width measurements. We examined five representative thick disk stars spanning the sample's range in T_{eff} , $[Fe/H]$, and $\log g$. Assuming that $\delta T_{\text{eff}} = 100$ K, $\delta \log g = 0.2$, $\delta [M/H] = 0.2$, $\delta \xi_t = 0.25$ km s $^{-1}$, and $\delta W_\lambda = 2$ mÅ. The error in W_λ is estimated in the same way as in Paper I, and the resulting error in the abundance is divided by \sqrt{N} where N is the number of lines used in deriving the abundance $[X/H]$. In Table 4, σ s for each abundance ratio for

five stars and the final mean value σ_{mod} and the standard deviation are given.

4.5 Ages

Stellar ages for the present sample have been computed by the method used in Paper I. Briefly, we used the stellar isochrones of Bertelli et al. (1994) and the method described in Paper I and Allende Prieto et al. (2004). The adopted isochrones do not consider compositions in which the α -elements have enhanced abundances (relative to iron). For thin disk stars, this is a fair approximation. However, in the present sample there are stars belonging to the thick disk and in halo which show α/Fe ratios significantly different from zero. Neglecting the α -enhancements in the isochrones would overestimate the ages for the most metal-poor thick disk and halo stars by up to 2 Gyr. We thus adopted the relationship between metallicity (Z), iron abundance ($[Fe/H]$), and the α -enhancement proposed by Degl'Innocenti, Prada Moroni & Ricci (2005), in selecting the appropriate isochrones from the Padova grid. Reliable ages are determinable only for those stars which have evolved away from the zero age main sequence. Ages were estimated for 65 stars (see Table 2, column 11).

In Figure 8, we compare our age determinations with those published in the recent survey by Nordström et al. (2004). Nordström et al. used the Padova isochrones (no α -enhancement) of Girardi et al. (2000). The 45 stars which are in common between the two surveys are overwhelmingly thin disk stars, and therefore, in spite of the difference in the selection of the isochrones' metallicity, the two determinations agree fairly well with an average difference of 0.1 Gyrs with $\sigma \approx 2$ Gyrs.

5 THIN AND THICK DISK COMPOSITIONS

5.1 Some Comparisons

Clear evidence that thick and thin disk stars of the same $[Fe/H]$ showed different abundances (relative to Fe) of other elements was provided by Fuhmann's (1998) demonstration that $[Mg/Fe]$ was systematically greater in the thick disk stars. Extension of this result to other elements was made by Prochaska et al. (2000), who determined the abundances of up to 20 elements in a sample of 10 stars with V_{LSR} from -20 to -100 km s $^{-1}$ and a W_{LSR} that takes a star to at least 600 pc above the Galactic plane, which virtually guarantees that the stars belong to the thick disk.

Prochaska et al.'s survey augmented by the occasional inclusion of thick disk stars in quite extensive studies of local stars (Edvardsson et al. 1993; Chen et al. 2000; Fulbright 2000; Reddy et al. 2003) led to the finding that abundance differences between thick and thin disk stars appear to define two broad categories. In the first category (here, Mg-like elements) are elements like Mg in which $[X/Fe]$ for a thick disk star exceeds that in a thin disk star of the same $[Fe/H]$. The thick-thin difference is not the same for all elements in this category and may also be a function of $[Fe/H]$. The second category (here, Ni-like elements) are those elements for which $[X/Fe]$ appears unchanged between the thin and

Table 4. Abundance uncertainties due to estimated uncertainties in atmospheric parameters for five representative stars. The σ 's are quadratic sum of variations in abundance ratios, $[X/Fe]$, due to uncertainties in model parameters. The column σ_{mod} , is the mean of the σ 's and the quoted error std is the standard deviation per measurement.

	HIP 17666	HIP 15405	HIP 5122	HIP 3086	HIP 16738	
T_{eff}	5000 K	5107 K	5204 K	5697 K	6000 K	
$[Fe/H]$	-1.03	-0.73	-0.55	-0.23	+0.36	
	σ_1	σ_2	σ_3	σ_4	σ_5	$\sigma_{mod} \pm std$
$[Fe/H]$	0.07	0.09	0.09	0.08	0.09	0.08±0.01
$[C/Fe]$	0.07	0.21	0.10	0.16	0.16	0.14±0.06
$[O/Fe]$	0.21	0.21	0.20	...	0.15	0.19±0.03
$[Na/Fe]$	0.06	0.05	0.04	0.03	0.04	0.05±0.02
$[Mg/Fe]$	0.05	0.05	0.04	0.04	0.06	0.05±0.01
$[Al/Fe]$	0.04	0.05	0.05	0.05	0.05	0.05±0.01
$[Si/Fe]$	0.09	0.10	0.08	0.03	0.06	0.07±0.03
$[S/Fe]$	0.07	0.18	0.17	0.12	0.13	0.13±0.04
$[Ca/Fe]$	0.07	0.04	0.03	0.02	0.01	0.03±0.03
$[Sc/Fe]$	0.10	0.13	0.11	0.09	0.13	0.11±0.02
$[Ti/Fe]$	0.09	0.07	0.06	0.04	0.04	0.06±0.02
$[V/Fe]$	0.10	0.07	0.05	0.03	0.02	0.06±0.03
$[Cr/Fe]$	0.05	0.03	0.03	0.02	0.02	0.03±0.01
$[Mn/Fe]$	0.05	0.08	0.07	0.05	0.04	0.06±0.02
$[Co/Fe]$	0.02	0.03	0.03	0.03	0.02	0.03±0.01
$[Ni/Fe]$	0.05	0.04	0.03	0.03	0.04	0.04±0.01
$[Cu/Fe]$	0.05	0.03	0.04	0.05	0.03	0.04±0.01
$[Zn/Fe]$	0.09	0.11	0.11	0.07	0.10	0.10±0.02
$[Y/Fe]$	0.09	0.12	0.13	0.12	0.07	0.11±0.03
$[Ba/Fe]$	0.11	0.11	0.13	0.13	0.13	0.12±0.01
$[Ce/Fe]$	0.10	0.11	0.12	0.11	...	0.11±0.01
$[Nd/Fe]$	0.08	0.11	0.13	0.12	...	0.11±0.02
$[Eu/Fe]$	0.12	...	0.14	0.13	...	0.13±0.01

thick disk. In reality, the thick-thin disk abundance differences may span a continuous range.

Before presenting and discussing our results in detail, we offer a few comparisons with several recent abundance analyses of thick disk stars to highlight differences in the sizes of the samples and to examine the consistency between the different investigations with respect to the abundance ratios. The chosen analyses are those by Bensby and colleagues, Mishenina et al. (2004), and Fuhrmann (2004). For each case, we reassessed the assignments to the thick and thin disks using our recipe for the membership probabilities.

Bensby and colleagues determined abundances for many elements in a sample of 102 F-G dwarfs of which 35 were attributed by them to the thick disk. According to our recipe, 18 of the 102 are thick disk stars. Though the recipes for choosing thick disk stars are basically the same, they differ in the normalization. Bensby et al. chose a relative probability ratio of thick disk and thin disk > 1.0 , and halo and thick disk ratio < 1.0 for a star to belong thick disk. Their criteria approximately translate into our criteria if $P_{thick} > 50\%$ for a star to belong thick disk.

Mishenina et al. analysed 174 F-G-K dwarfs for their Mg, Si, Fe, and Ni abundances. (Non-LTE effects were considered in the Mg analysis.) Thirty stars were assigned to the thick disk. Adoption of our method of calculating the membership probability reduces the number of thick disk stars to 13. The main difference between us and Mishenina et al. is in the adopted fraction for thin and thick disk stars. Mishenina et al. assumed 25% thick disk and 75% thin disk

Table 3. Mean differences and standard deviations of the abundance ratios $[X/Fe]$ for stars that are common among Bensby et al. (2003,2004), and Mishenina et al. (2004).

Quantity	Bensby - Ours		Mishenina- Ours	
	diff.	σ	diff.	σ
T_{eff}	88	80	102	116
$\log g$	-0.05	0.08	-0.18	0.18
$[Fe/H]$	0.03	0.05	-0.03	0.09
$[Na/Fe]$	-0.02	0.05	0.03	0.08
$[Mg/Fe]$	0.00	0.06	0.05	0.05
$[Al/Fe]$	0.04	0.08	0.12	0.10
$[Si/Fe]$	0.00	0.06	0.16	0.09
$[Ca/Fe]$	0.04	0.06	0.07	0.04
$[Ti/Fe]$	0.08	0.04	0.10	0.08
$[V/Fe]$	0.05	0.09
$[Cr/Fe]$	0.04	0.05	0.08	0.03
$[Ni/Fe]$	0.01	0.04	0.05	0.02
$[Zn/Fe]$	0.02	0.05
$[Y/Fe]$	-0.08	0.04	0.01	0.05
$[Ba/Fe]$	0.12	0.08	0.12	0.10

stars. This led to larger number of thick disk stars in their study.

Fuhrmann (2004) following his earlier work (Fuhrmann 1998) obtained Mg and Fe abundances for a sample of 71 nearby stars. Out of which 25 or more are deemed thick disk stars.

In Figure 9, we show $[Mg/Fe]$ against $[Fe/H]$ as provided by our sample and the three published analyses. The

larger filled black symbols in the plot represent thick disk stars based on our criteria. Stars for which the probability of thin or thick disk membership is below 70% but greater than 50% are included in the panels but with a smaller symbol. Figures 10 and 11 show the corresponding results for [Si/Fe], and [Ti/Fe], respectively. These figures show clearly the increase in the number of thick disk stars provided by our sample. They also show broad agreement between the different studies over the behaviour of Mg-like elements with [Fe/H] in thin and thick disks: [X/Fe] of the thick disk exceeds that of the thin disk at a common [Fe/H] for [Fe/H] ≤ -0.3 with an apparent merger of thin and thick disk behaviour for greater [Fe/H]. Inspection of Figures 9, 10, and 11 shows that a majority of stars from Bensby et al.’s sample which we put in the thin-thick group with [Fe/H] ≤ -0.3 are thick disk stars as judged by Mg, Si, and Ti abundances. Mishenina et al.’s results give marginal support to the difference in [Mg/Fe] and [Si/Fe] between thin and thick disks.

A comparison of abundances for stars in common shows that the different studies are consistent. We have ten stars (no distinction is made according to thin or thick disk) in common with Bensby and colleagues’ total sample of 102 stars. We have five stars in common with Mishenina et al. (2004). Mean difference and standard deviations for the samples of common stars are summarised in Table 3 for the atmospheric parameters, the Fe abundance, and the [X/Fe] values. We have six stars in common with Fuhrmann (2004). The mean difference between him and us, for [Fe/H] is 0.0 ± 0.05 and [Mg/Fe] is 0.03 ± 0.12 . Fuhrmann’s T_{eff} and $\log g$ values are systematically hotter by 125 ± 23 K and lower by 0.19 ± 0.06 dex, respectively. Brewer & Carney (2005) analyzed 23 G dwarfs of which four were analyzed by us. Their and our adopted atmospheric parameters and derived abundances are in excellent agreement, e.g. differences in T_{eff} , $\log g$, and [Fe/H] run from -43 to $+14$ K, -0.2 to 0.0 cgs units, and -0.08 to $+0.06$ dex, respectively.

An analogous and equally satisfactory comparison was made in Paper I for thin disk stars and the large surveys by Edvardsson et al. (1993), Chen et al. (2000), and Fulbright (2000). These analyses of stars in common with our studies suggest that results from different studies could be combined to enlarge the sample size for thick and thin disk stars.

5.2 Thin and Thin-Thick Disk stars

Our discussion of the thick disk’s composition is based on the 95 thick stars chosen by the requirement that $P_{\text{thick}} > 70\%$. Here, we consider the 13 stars assigned to the thin disk and the 34 stars in the thin-thick disk category. Figure 12 shows in separate panels the run of $[\alpha/\text{Fe}]$ ratio versus [Fe/H] for thick, thin-thick, and thin disk stars from our present sample with the thin disk stars from Paper I shown in each panel. The ratio $[\alpha/\text{Fe}]$ is defined as simple mean of the four ratios [Mg/Fe], [Si/Fe], [Ca/Fe], and [Ti/Fe]. Clearly, the samples of thick/thin, and thin disk stars both contain thick stars, as judged by $[\alpha/\text{Fe}]$. This mixing and contamination must in part result from the fact that the assignment to the thin or the thick disk is based on a probability. Given that Figure 12 (and other figures) convey the impression that thin and thick disk abundance relations are distinct, the collection of thick disk stars might be augmented by stars from the thin-thick disk category, and even the thin

disk category. We do not act on the second suggestion, but reconsideration of the procedure for categorising disk stars would be a useful exercise.

5.3 Our halo stars

The probability criteria yielded 20 halo stars. Most of them, as expected, have very negative $V_{\text{LSR}} \leq -180$ km s $^{-1}$ and orbits of extreme eccentricity (0.7 to 1.0). A few stars are on retrograde orbits, i.e., $V_{\text{LSR}} < -220$ km s $^{-1}$. The halo stars in the sample span the [Fe/H] range -0.6 to -2.0 .

Mg-like elements show overabundances similar to thick disk stars and may show a mild trend of [X/Fe] with [Fe/H]. At overlapping metallicities, the $[\alpha/\text{Fe}]$ of the halo stars are in agreement with the thick disk ratios. Ni-like elements for the halo stars track the Fe similar to thin and thick disk stars. The scatter in [X/Fe] ratios for both the Mg-like and Ni-like elements for the halo stars appears similar to that for the thick disk stars.

The $[\alpha/\text{Fe}]$ ratio, for the halo stars in our sample is about 0.25 dex, in agreement with our thick disk stars. This value is in good agreement with the $[\alpha/\text{Fe}]$ results for halo stars from Gratton et al. (2003) in the same [Fe/H] range. Their results also do not show a trend of $[\alpha/\text{Fe}]$ with [Fe/H].

5.4 The Mg-like elements

One subset of the Mg-like elements are the so-called α -elements: C, O, Mg, Si, Ca, and Ti. Our results for these elements are shown in Figures 13 and 14. Other Mg-like elements are Al, Sc, V, Co, and possibly Zn (Figure 15).

The trend of [X/Fe] against [Fe/H] for Mg-like elements in the thick disk may be characterized by a shallow slope for [Fe/H] ≤ -0.3 and from the trend for thin disk stars. For each Mg-like element, we compute the slope (B_{thick}) from a linear regression fit to the [X/Fe] from [Fe/H] = -0.3 to -1.0 . The offset between the thick and thin trends is obtained by calculating the mean value (M_{thick} or M_{thin}) in the bin of [Fe/H] from -0.45 to -0.55 . Quantities B_{thin} , B_{thick} , M_{thin} and M_{thick} are given in Table 6 together with the thick-thin disk offset $\Delta[X/\text{Fe}] = M_{\text{thick}} - M_{\text{thin}}$. The behavior of the Mg-like elements for [Fe/H] > -0.3 is discussed below. Below we make few remarks on individual elements.

Carbon: We obtained abundances for stars with [Fe/H] ≥ -1.2 ; the chosen C I lines are too weak to measure in more metal-poor stars. Abundance ratios [C/Fe] for the thick disk sample stars below [Fe/H] < -0.4 as shown in Figure 13 are on average larger than the thin disk stars of the same [Fe/H]. Although the scatter is quite large, carbon is seen to behave like Mg and other α -elements. Similar behaviour of [C/Fe] with [Fe/H] is seen by Shi, Zhao & Chen (2002) and Takeda-Hidai et al. (2005) for nearby F, G, and K dwarfs. They also noted that the non-LTE corrections are negligibly small. Our thin disk [C/Fe] (Paper I), also from the C I lines, are in agreement with results obtained from [C I] line at 8727 Å by Gustafsson et al. (1999) and Allende Prieto et al. (2004) for samples dominated by thin disk stars. Contrary to the above studies, the recent study by Bensby et al. (2005) based on the [C I] line at 8727 Å for a small sample of both thick and thin disk stars shows almost a flat trend of [C/Fe] below [Fe/H] ≈ -0.2 .

Oxygen: The permitted O I lines at 7771 Å are used to get O abundances for all stars. These lines are known to be subject to non-LTE effects. We apply the empirical calibration to correct for these effects that was developed in Paper I using abundances from the [O I] and O I lines for the same stars. The resulting [O/Fe] ratios are shown against [Fe/H], which shows oxygen to behave as a Mg-like element (Figure 13). Full non-LTE corrected O abundances will be discussed in a separate publication (see Ramírez, Allende Prieto, & Lambert, 2005).

The α -elements: Mg, Si, Ca, and Ti: The runs of abundance ratios [X/Fe] against [Fe/H] are shown in Figure 14. For [Fe/H] < -0.3, [X/Fe] for thick disk stars are distinctly larger than for thin disk stars. In the [Fe/H] range -0.3 to -0.6 where thin and thick disk stars are well represented, there is a clear separation between [α /Fe] of Mg, Si, Ti, and probably also Ca for thin and thick disk stars. For metal-rich stars of [Fe/H] \geq -0.3, the thin and thick disk stars show similar abundances. We comment below (see Sec 6) on the possibility that there is a smooth transition for [X/Fe] from a positive displacement above its thin disk value for [Fe/H] < -0.3 to the thin disk value for [Fe/H] > 0.0. The thick disk [X/Fe] ratios smoothly merge with the halo ratios in the overlapping metallicity range.

Our results for the α -elements in the thick disk agree very well with Prochaska et al.'s (2000) results for their sample of ten stars with [Fe/H] between -0.5 and -1.2. Our results also agree with the results from Fuhrmann (1998, 2004) for Mg and Bensby et al. (2005) for Mg, Si, Ca, and Ti (see Figures 9, 10, and 11).

Aluminium: An odd-Z element Al might have been expected to behave like Na, another odd-Z light element. This expectation is not met (Figure 15); Al is Mg-like and Na is Ni-like. Our results below solar metallicity agree with those by Prochaska et al. (2000) and Bensby et al. (2005). Above [Fe/H] = 0.0, Bensby et al., also Chen et al. (2000), show [Al/Fe] increasing with increasing [Fe/H]. Our samples contain too few metal-rich stars to detect this interesting trend. Below the metal-poor end of our sample, [Al/Fe] ratios for halo stars are seen to be sharply decreasing with decreasing [Fe/H] (e.g; Spite & Spite 1980; Gehren et al. 2004).

Scandium: The ratio [Sc/Fe] with [Fe/H] shows an interesting trend. Above [Fe/H] = -0.3, [Sc/Fe] ratios are similar for thin and thick disk stars. Below [Fe/H] = -0.3, [Sc/Fe] appears constant with an excess - albeit slight - above thin disk values, a characteristic of a Mg-like element. A keen eye may suggest that [Sc/Fe] slowly increases and then decreases at around [Fe/H] \approx -0.5 and returns to the solar ratio.

A similar trend of increasing [Sc/Fe] with [Fe/H] and then decreasing was seen for disk F- and G- dwarfs (Nissen et al. 2000; Prochaska and McWilliam 2000). For their thick disk stars with [Fe/H] range of -0.4 to -1.2, Prochaska et al.'s results agree with our larger data set in magnitude and trend.

Vanadium: Below [Fe/H] = -0.3, [V/Fe] of thick disk stars is slightly larger than for thin disk stars. In the [Fe/H] range -0.3 to -1.6, [V/Fe] is almost flat with [Fe/H]. Our thick disk results are consistent with those from Prochaska et al. (2000).

Peterson (1981) derived [V/Fe] ratios for 22 moderately metal-poor ([Fe/H] = -0.5 to -1.5) F-G-K dwarfs. Her re-

sults show a clear and approximately uniform enhancement of [V/Fe] relative to solar except for two stars at the low [Fe/H] limit of the sample. A quick look at the kinematics of her sample showed many of them to have $V_{LSR} \leq -40$ km s⁻¹, indicating membership of the thick disk or the halo.

Cobalt: Figure 15 shows that cobalt is a Mg-like element. For thick disk stars, [Co/Fe] is almost flat with [Fe/H], in good agreement with the results obtained by Prochaska et al. (2000). For thin-disk stars, a weak trend of decreasing [Co/Fe] with increasing [Fe/H] is apparent in the range -0.5 < [Fe/H] < 0.0. This is consistent with the results of Allende Prieto et al. (2004) for that interval (with the exception of a small scale offset).

Zinc: Zinc appears to be indistinguishable between thin disk and thick disk stars in the common metallicity range. We note, however, that for thin disk stars there is evidence for a mild trend of increasing [Zn/Fe] with decreasing [Fe/H], as previously reported by Nissen et al. (2004), Allende Prieto et al. (2004), and Bensby et al. (2005). The latter two studies also reported an increase of the Zn/Fe ratios at [Fe/H] > 0.

5.5 The Ni-like elements

The Ni-like elements include Na, Mn, Cr, Ni and Cu. Prochaska et al. were the first to show that these elements (relative to Fe) behaved similarly in thick and thin disk stars. Bensby et al. (2005) confirmed the Ni-like behavior of Na, Cr and Ni but did not consider either Mn or Cu in their analyses. Our results for the quintet are shown in Figure 16. Of especial interest, perhaps, is the example of Mn where [Mn/Fe] is a quite steeply increasing function of Fe, yet thin and thick disk stars form a single relation. The contrast between the odd-even Na (Ni-like) and Al (Mg-like) is also interesting.

Sodium: This odd-Z and proton-capture element seems to be a difficult one for which to obtain consistent values. We suspect departures from LTE are behind these difficulties. There are several studies but no two are in very good agreement. For example, Chen et al.'s (2000) study of disk F- and G- dwarfs shows a flat trend of [Na/Fe] with [Fe/H] without Na enhancement. Edvardsson et al (1993) results suggest [Na/Fe] increases with [Fe/H] for stars of [Fe/H] > 0.0 and an apparent slow rise in [Na/Fe] with decreasing [Fe/H] for stars with [Fe/H] < 0.0. Prochaska et al. (2000) found an enhancement of Na for 10 thick disk stars without any trend with [Fe/H].

The results from our study are based on two Na I lines 6154 Å and 6160 Å. Results indicate no visible (Figure 16) demarcation between the thin and thick disk samples. Examination of the plot indicates a possible slow increase of [Na/Fe] with decreasing [Fe/H] reaching a maximum value of [Na/Fe] \approx 0.15 at [Fe/H] \approx -0.6. From the maximum, [Na/Fe] may fall with decreasing [Fe/H]. Recent analysis of disk dwarfs by Shi, Gehren, & Zhao (2004) using the same lines as we did but with NLTE treatment suggests a similar trend of [Na/Fe] in [Fe/H] range 0.0 to -1.0. For metal-rich stars, they confirm Edvardsson et al. (1993) results.

Chromium and Nickel: Chromium shows [X/Fe] \approx 0.02 \pm 0.04 between thick and thin disk stars. Chromium tracks Fe well up to around [Fe/H] \approx -0.6, but [Cr/Fe] is negative for lower [Fe/H]. Nickel tracks Fe throughout the [Fe/H] range. Possibly, [Ni/Fe] is larger for thick disk

stars compared to thin disk but the mean difference is just 0.04 ± 0.03 . A small overabundance of Ni for the thick disk stars is suggested by the equivalent figures given by Prochaska et al. (2000) and Bensby et al. (2005).

Manganese: As shown in Figure 16, $[\text{Mn}/\text{Fe}]$ is a function of $[\text{Fe}/\text{H}]$. $[\text{Mn}/\text{Fe}]$ ratios at a given $[\text{Fe}/\text{H}]$ for thin, thick, and halo stars are the same. Below $[\text{Fe}/\text{H}] = -1.0$, $[\text{Mn}/\text{Fe}]$ shows a flat trend with $[\text{Fe}/\text{H}]$. Above $[\text{Fe}/\text{H}] = -1.0$, Mn steadily increases with increasing $[\text{Fe}/\text{H}]$. Our results are in agreement with Mn results for disk and halo stars (Nissen et al. 2000) and the 10 thick disk stars analysed by Prochaska et al. (2000).

Copper: Copper is a Ni-like element in the $[\text{Fe}/\text{H}]$ interval populated by both thin and thick disk stars; there is a hint that $[\text{Cu}/\text{Fe}]$ is slightly greater for the thick disk stars: $\Delta[\text{Cu}/\text{Fe}] = +0.07$ (Table 6). This result was shown by Prochaska et al. (2000). At $[\text{Fe}/\text{H}] < -0.8$, $[\text{Cu}/\text{Fe}]$ falls below the solar value, possibly in a precipitous way. Our results generally confirm earlier results for disk and halo stars (Snedden et al. 1991; Mishenina et al. 2002; Bihain et al. 2004; Simmerer et al. 2004).

5.6 The *s*- and *r*-process elements

Synthesis of elements beyond the iron group occurs by two neutron-capture processes: the *s*-process occurring in AGB stars, and the *r*-process occurring (probably) in Type II supernovae. In the solar system mix of elements, barium is predominantly a *s*-process product and europium an *r*-process product. Our suite of elements includes not only Ba and Eu but also Y, Ce, and Nd. According to Burris et al.’s (2000) resolution of the solar elemental abundances the contributions from the *s*-process are 72% for Y, 85% for Ba, 81% for Ce, 47% for Nd, and merely 3% for Eu. Bensby et al. (2005) determined abundances for Y, Ba, and Eu showing differences in the behavior of the *s*- and *r*-process contributions between the thin and thick disks.

Our abundances for Y, Ba, Ce, Nd, and Eu are based with one exception on the lines used in Paper I. The exception concerns Eu for which we use the resonance line at 4129 Å but in Paper I we used the subordinate line at 6645 Å. The atomic data for the 4129 Å line are taken from Kurucz (1998) and the isotopic abundance ratio was set at the solar value: $^{151}\text{Eu}/^{153}\text{Eu} = 53/47$. The 4129 Å line was analyzed in all stars of the present sample and also those in Paper I. The Eu abundances from the 4129 Å and the 6645 Å lines are in good agreement for Paper I’s stars.

The trends of the abundances of Y, Ba, Ce, Nd, and Eu with $[\text{Fe}/\text{H}]$ (Figure 17) show a difference between the contributions of the *s*-process and the *r*-process to the thin and thick disks, as found by Bensby et al. The elements – Y, Ba, and Ce – expected to have a dominant *s*-process contribution are Ni-like elements. Our results for Y agree with thick disk results from Prochaska et al. (2000). However, Bensby et al. (2005) found $[\text{Y}/\text{Fe}]$ ratios showing a slow decreasing trend with decreasing $[\text{Fe}/\text{H}]$, but the $[\text{Y}/\text{Fe}]$ ratios at given $[\text{Fe}/\text{H}]$ are almost same for both thin and thick disk stars similar to our present results. In the case of Ba, our $[\text{Ba}/\text{Fe}]$ ratios for thick disk stars are on average smaller by 0.1 dex than for thin disk stars. There also may be small trend of decreasing $[\text{Ba}/\text{Fe}]$ with decreasing $[\text{Fe}/\text{H}]$. Again our and Prochaska et al. results for Ba agree, both in trend

Table 6. The predicted uncertainty, σ_{mod} and the σ_{gau} resulting from a Gaussian fit to the residuals for thin and thick disk stars are given.

[X/Fe]	Thin Disk		Thick Disk	
	σ_{mod}	σ_{gau}	σ_{mod}	σ_{gau}
[Fe/H]	0.07	...	0.08	...
[C/Fe]	0.14	0.07	0.14	0.09
[O/Fe]	0.16	0.07	0.19	0.07
[Na/Fe]	0.03	0.04	0.05	0.07
[Mg/Fe]	0.04	0.04	0.05	0.07
[Al/Fe]	0.04	0.05	0.05	0.08
[Si/Fe]	0.05	0.04	0.07	0.06
[Ca/Fe]	0.03	0.04	0.03	0.06
[Sc/Fe]	0.11	0.05	0.11	0.09
[Ti/Fe]	0.03	0.04	0.06	0.06
[V/Fe]	0.04	0.04	0.06	0.10
[Cr/Fe]	0.02	0.03	0.03	0.04
[Mn/Fe]	0.04	0.04	0.03	0.04
[Co/Fe]	0.02	0.04	0.03	0.06
[Ni/Fe]	0.02	0.03	0.04	0.04
[Cu/Fe]	0.02	0.06	0.04	0.08
[Zn/Fe]	0.05	0.06	0.10	0.06
[Y/Fe]	0.09	0.07	0.11	0.12
[Zr/Fe]	0.10	0.07	0.11	0.12
[Ba/Fe]	0.12	0.08	0.12	0.11
[Ce/Fe]	0.11	0.08	0.11	0.10
[Nd/Fe]	0.10	0.07	0.11	0.09
[Eu/Fe]	0.11	0.08	0.13	0.08

and magnitude. Both Bensby et al. (2005) and Allende Prieto et al. (2004) found thin disk stars to show a possible maximum of $[\text{Ba}/\text{Fe}]$ at $[\text{Fe}/\text{H}] \sim -0.2$, but such feature is not present in our data.

Europium is a Mg-like element. The scatter in $[\text{Eu}/\text{Fe}]$ at a given $[\text{Fe}/\text{H}]$ is attributable to the measurement errors. The large scatter in Eu results for the thick compared to the thin disk may be attributed to large number of cooler stars in thick disk sample. Continuum placement at 4129 Å is more difficult for the cooler stars, and also sensitivity to the model parameters is different. Eu results agree quite well with the Eu results from Prochaska et al. (2000) and Bensby et al. (2005).

Neodymium which is provided about equally by the *s*- and *r*-process in the solar mix of abundances can be imagined from Figure 17 to be a mix of a Mg-like and a Ni-like element. We do not confirm the trend of increasing $[\text{Nd}/\text{Fe}]$ with decreasing $[\text{Fe}/\text{H}]$ reported by Allende Prieto et al. (2004) for thin disk stars.

5.7 Cosmic scatter

In Paper I, we showed that the scatter of the $[\text{X}/\text{Fe}]$ values about the mean trend was entirely dominated by the measurement errors, i.e., there was no hint of a cosmic scatter in the values found for the thin disk stars. It is of value to determine if the thick disk stars betray cosmic scatter in their $[\text{X}/\text{Fe}]$ values.

We estimate the scatter in $[\text{X}/\text{Fe}]$ for the thick disk by removing the linear fit made to the data points for $[\text{Fe}/\text{H}] < -0.3$ and fitting a Gaussian to the residuals – see Figure 18 for $[\text{Si}/\text{Fe}]$. In Table 5, we list the Gaussian σ_{gau} and

the expected σ_{mod} from the congerie of measurement errors. The same quantities from Paper I are also tabulated. The comparison of σ_{gau} with σ_{mod} (Figure 19) shows that they are very similar, i.e., there is no detectable cosmic scatter for the sampled elements for thick disk stars with $[\text{Fe}/\text{H}] < -0.3$. Oxygen's σ_{mod} determined from the $[\text{O}/\text{Fe}]$ obtained from the O abundances based on the O I 7772 Å line, after introducing an empirical correction for departures from LTE, greatly exceeds the measured scatter (σ_{gau}) which is apparently overestimated for these high-excitation lines.

6 CHEMICAL EVOLUTION OF THE THICK DISK

By chemical evolution is meant the run of $[\text{X}/\text{Fe}]$ versus $[\text{Fe}/\text{H}]$ for a suite of elements X sampling the major sites and processes of stellar nucleosynthesis. Here, the Mg-like elements separate thick from thin disk stars, and it is their evolution that we address first. To reduce the observational uncertainties as much as possible, we use the composite index $[\alpha/\text{Fe}]$ from the average of the four indices $[\text{X}/\text{Fe}]$ for $\text{X} = \text{Mg}, \text{Si}, \text{Ca},$ and Ti . The individual indices are given equal weight. The index $[\alpha/\text{Fe}]$ versus $[\text{Fe}/\text{H}]$ is shown in Figure 20. Two representations of the thick disk's chemical evolution are suggested by inspection of Figure 20.

First, as proposed by Bensby et al. (2003), $[\alpha/\text{Fe}]$ of the thick disk is greater than for the thin disk for $[\text{Fe}/\text{H}] < -0.3$ but at about a $[\text{Fe}/\text{H}]$ of -0.3 , the $[\alpha/\text{Fe}]$ appears to tend towards thin disk values and for $[\text{Fe}/\text{H}] > -0.2$, thick and thin disk stars are chemically identical to within the measurement errors. Bensby et al. speak of a 'knee' linking the thick disk stars of $[\text{Fe}/\text{H}] < -0.3$ with those of $[\text{Fe}/\text{H}] > -0.2$. This puts all but a few of our thick disk stars into a single relation. The exceptions are five stars in Figure 20 with $[\text{Fe}/\text{H}] < -0.3$ with thick disk kinematics but a thin disk $[\alpha/\text{Fe}]$.

In an alternative representation proposed here, the thick disk is restricted to $[\text{Fe}/\text{H}]$ less than about -0.3 , and the above five exceptions with thin disk compositions but thick disk kinematics are considered to form a single relation with the thick disk stars of $[\text{Fe}/\text{H}] > -0.3$. Thirteen of our thick disk stars from across the $[\text{Fe}/\text{H}]$ spanned by the thin disk form this latter relation which is considered distinct from the more populated thick disk relation between $[\alpha/\text{Fe}]$ and $[\text{Fe}/\text{H}] < -0.3$. In this representation, there is no knee connecting thick and thin disk stars.

Before commenting further on the two representations, we remark upon the stars – five in one and thirteen in the other representation – with the kinematics of the thick disk but abundances of the thin disk: here, we refer to these as the TKTA stars.

6.1 The TKTA stars

TKTA stars have *contaminated* some previous studies. For example, the eight thick disk stars in Mishenina et al. (2004) sample with $[\text{Fe}/\text{H}] > -0.3$ had the abundance pattern of the thin disk. Application of our membership criteria reduces the octet to a single thick disk star. Although all eight have a negative V_{LSR} (-40 to -100 km s^{-1}) outside the normal range for thin disk stars, they with a single exception

have a low W_{LSR} and so remain close to the Galactic plane, a fact noted by Mishenina et al. The exception at $[\text{Fe}/\text{H}]$ of $+0.12$ is a TKTA star by our definition.

Bensby et al. (2003, 2005) were the first to suggest that thin and thick disk abundance patterns converged for $[\text{Fe}/\text{H}] > -0.2$. According to our criteria, 17 of their stars belong to the thick disk. One of the 17 is a TKTA star with $[\text{Fe}/\text{H}] = -0.37$. Other potential TKTA stars are at metallicities for which thin and thick disk have the same abundance pattern.

In our larger sample, we have five TKTA stars at a low $[\text{Fe}/\text{H}]$ such that their abundances clearly separate them from the majority of the thick disk stars. It is unlikely that the five are mistakenly identified as TKTA stars through a conspiracy of errors. The individual $[\text{X}/\text{Fe}]$ contributing to the $[\alpha/\text{Fe}]$ each mark them out as having thin disk abundances. One of the five (HIP 50671) was earlier analysed by Edvardsson et al. (1993) who obtained a similar $[\text{Fe}/\text{H}]$ (-0.42 vs our -0.48) and $[\alpha/\text{Fe}]$ (0.05 vs our 0.06). Another (HIP 31188) was treated by Fuhrmann (1998) whose $[\text{Fe}/\text{H}]$ was -0.81 vs our -0.59 and $[\text{Mg}/\text{Fe}]$ was $+0.22$ vs our $+0.12$. If placed in Figure 9, the star would fall on an extension of Fuhrmann's thin disk abundances and below his thick disk abundance of $[\text{Mg}/\text{Fe}]$ of 0.4 for his $[\text{Fe}/\text{H}]$. It should be considered a possible TKTA star when judged solely by Fuhrmann et al.'s abundances. A fresh study of HIP 31188 may be desirable but we note that our Si, Ca, and Ti abundances support our low value of $[\text{Mg}/\text{Fe}]$.

The set of thirteen TKTA stars with the additional examples from Mishenina et al. and Bensby and colleagues run in $[\text{Fe}/\text{H}]$ over the entire metallicity spread of the thin disk. The close correspondence between the compositions of TKTA stars and the thin disk suggest that there is a close relation between the two groups. Heating of the thin disk is a well known phenomena: the dispersion of the components ($U_{LSR}, V_{LSR}, W_{LSR}$) increases with age. Nordsöm et al. (2004)- provide a recent determination of the dispersion – age relations. Perhaps, the TKTA stars are thin disk stars which have been heated to resemble the genuine thick disk stars. The old ages of the TKTA stars favour above average heating and, perhaps, owing to the stochastic nature of the heating processes, the TKTA stars were subjected to much greater than normal heating. Low mass analogues of the runaway B stars are a possibility. Against the association of the TKTA stars with the thin disk is the fact that on average the TKTA stars appear to be systematically a couple of Gyr older than the oldest thin disk stars (Figure 24 below).

The TKTA stars appear to be confined to certain parts of the ($U_{LSR}, V_{LSR}, W_{LSR}$) space. Figure 21 using $[\alpha/\text{Fe}]$ to distinguish thick from thin disk stars shows that the TKTA tag on to the low V_{LSR} tail of the thin disk stars. The TKTA stars favour positive U_{LSR} over negative values but are distributed in W_{LSR} in a similar way to thick disk stars. A wider exploration of ($U_{LSR}, V_{LSR}, W_{LSR}$) space may reveal some clumping of TKTA stars, an indication of a moving group.

6.2 The knee

In the representation in which TKTA stars are given an identity apart from the thick disk stars (i.e., thin-disk stars with special kinematics), thick disk stars are restricted to $[\text{Fe}/\text{H}]$ less than about < -0.3 or -0.2 . The alternative rep-

resentation proposed by Bensby et al. (2003) introduces a knee in the thick disk's $[X/Fe]$ vs $[Fe/H]$ for a Mg-like element such that the near-constant $[X/Fe]$ for $[Fe/H] < -0.3$ merges smoothly with the lower $[X/Fe]$ values of thin and thick disk results for $[Fe/H] > -0.1$ or so. (The TKTA stars with $[Fe/H] < -0.3$ still require a special interpretation in this scenario.) Interpretations of the chemical evolution of the thick disk differ for these different representations.

The leading suggestion of a 'knee' was made by Bensby and colleagues. Comparison with our results is made by combining the index $[\alpha/Fe]$ from the abundances obtained by Bensby and colleagues with our probability criteria for stellar populations. Figure 22 shows the result where thick disk stars by our criteria are shown by the larger filled triangles and thin disk stars by small open triangles. Small filled triangles represent stars with a probability of 50 to 70% of belonging to the thick disk (these were assigned to the thick disk by Bensby et al.). Compare this figure with Figure 20. Although a knee could be drawn in Figure 22, our representation of a thick disk terminating at about $[Fe/H]$ of -0.3 and a separate thin disk relation with superposed TKTA stars would appear to be as satisfactory a fit. Figure 22 shows one TKTA star (HIP 3704) with $[Fe/H] < -0.3$ but three with $[Fe/H] > -0.1$. The thick disk relation may show a slight drop in $[\alpha/Fe]$ near $[Fe/H] = -0.3$.

Bensby et al. would likely contend that the principal evidence for the knee lies in their results for oxygen (Bensby et al. 2004, 2005) which show a near-linear and continuous relation for $[O/Fe]$ vs $[Fe/H]$ in thick disk stars with no hint of a discontinuity at $[Fe/H] \sim -0.3$. Existence of the knee would appear to depend, however, on the $[O/Fe]$ values for just two to four stars in the interval $[Fe/H]$ of about -0.3 to 0.0 . The oxygen abundances derived from the $[O\text{I}]$ 6300 Å line (corrected for a blending Ni I line) provide the clearest evidence for the continuous relation. Abundances from the $O\text{I}$ 7772 Å triplet do not offer decisive evidence in favor of a continuous relation for the thick disk stars. Ramírez et al. (2005), who performed a non-LTE analysis of the $O\text{I}$ 7772 Å triplet for a large sample of thick disk stars (our present sample plus about an additional 20 stars) suggest that the thick disk $[O/Fe]$ versus $[Fe/H]$ relation show no clear signs of a knee.

Marsakov & Borkova (2005) attempt to separate chemical evolution for thick and thin disks by discussing $[Mg/Fe]$ indices compiled from published values collated by Borkova & Marsakov (2005) who attempt to place the collated results for $[Fe/H]$ and $[Mg/Fe]$ from about 80 publications on common scales. Velocity components (U, V, W) are also provided. Thick disk stars are separated from thin disk stars by criteria that give results similar to ours. Marsakov & Borkova conclude that $[Mg/Fe]$ for the thick disk starts to decline steeply from $[Mg/Fe] \simeq +0.4$ at $[Fe/H] \simeq -0.5$ to $[Mg/Fe] \simeq +0.1$ at $[Fe/H] = -0.3$ with a subsequent less steep decline. This interpretation is based on abundances for 133 thick disk stars.

The separation in $[Mg/Fe]$ at $[Fe/H] \simeq -0.3$ between thick and thin disk stars is not large (say, 0.2 dex) and, therefore, close attention must be paid in combining measurements from different authors to relative precision and to normalization to common abundance scales for Mg and Fe. If selection of thick disk stars is restricted to those stars with $[Mg/Fe]$ from two or more sources, the evidence for the knee

is greatly weakened (see Marsakov & Borkova's Fig. 2b) for lack of thick disk stars with $[Fe/H] > -0.3$ (three only). Only when stars with a single measurement of $[Mg/Fe]$ are included is the thick disk quite well represented across the full $[Fe/H]$ range (their Fig. 2c) but the clean separation between thin and thick disk stars clearly obtained by Bensby et al. and by us is not found. This lack of a separation must cast doubt on the conclusions drawn by Marsakov & Borkova.

On applying our criteria to the space velocities given in Borkova & Marsakov's (2005) catalogue and adopting their recommended $[Mg/Fe]$, we obtain the results shown in Figure 23 for stars with $[Fe/H] > -2.0$. The top panel shows results for thick disk stars alone; the majority of these 84 stars are drawn from the studies we have commented upon. This panel provides no support for a knee. The lower panel includes the thin and halo stars drawn again using our criteria from the catalogue. There is a large number of stars classified as belonging to the thin disk with a $[Mg/Fe]$ of the thick disk.

Very recently, Brewer & Carney (2005) offered evidence in favour of a knee. Their sample of 23 G dwarfs contained, by their method of assigning population membership (see Venn et al. 2004), nine thin disk and 14 thick disk stars. The method overlooks the fact the three categories of membership (halo, thin and thick disk) are not represented equally in the solar neighbourhood (thin disk stars dominate the stellar population). On applying the method in Section 3.2 in which the membership fractions are considered, we find that 18 of the 23 stars are thin disk stars, the other five fall in our thin/thick disk group with a maximum probability of belonging to the thick disk of under 50%, and not a single star would be assigned thick disk status by us. Nonetheless, consistent with our results in Figure 12, Brewer & Carney's precise abundances delineate the thin and thick disk trends of $[\alpha/Fe]$ with $[Fe/H]$. There may be evidence from stars with $[Fe/H] \sim -0.2$ and higher of a knee, but this comes from stars we would classify as belonging to the thin disk (see Figure 12 – bottom panel).

6.3 Stellar ages

Interpretations of the chemical evolution of the thick disk, as represented by a plot of $[X/Fe]$ vs $[Fe/H]$, should take account of the ages of thick and thin disk stars. There is a consensus that the mean age of the thick disk is about five Gyr greater than that of the thin disk when isochrone ages are estimated for stars in the solar neighbourhood. Evidence, described as tentative, also exists that thick disk stars describe an age-metallicity relation (Bensby et al. 2004, 2005). Here, the age-metallicity relation and some connections between the ages and other properties are presented for our sample of thick disk stars.

Determination of stellar ages was discussed in Sec. 4.5. Ages were obtained for 43 of the 95 thick disk stars. Figure 24 shows $[Fe/H]$ versus age for these stars together with ages for 150 thin disk stars from Paper I. This figure gives an impression of a continuous age-metallicity relation. For the thin disk stars this is a false impression because Paper I did not fairly represent stars with $[Fe/H] > -0.2$ for which the age spread is very similar to that of the thin disk stars with $[Fe/H] < -0.2$. The thick disk stars were not knowingly selected by $[Fe/H]$ but by kinematic criteria. There is an age-

metallicity relation for the thick disk: metallicity increases to about $[\text{Fe}/\text{H}] \sim -0.3$ in 5 Gyr from -1.5 . This result is consistent with previous studies. The maximum ages given the measurement errors are consistent with the *WMAP* age of just under 14 Gyr. As emphasized recently by Schuster et al. (2005) from ages of halo stars the mean stellar age, star formation began within 1 Gyr of the Big Bang. With two exceptions, thick disk stars appear older than 8 Gyr, in agreement with the results of Allende Prieto et al. (2005) for a sample from the SDSS.

Those stars with well-determined ages may be used to examine the velocity-age relations. Nordström et al. (2004, their Fig. 30) show the growth of U_{LSR} , V_{LSR} , and W_{LSR} with age for their sample, which is dominated by thin disk stars. This figure serves to indicate the outer boundaries for the growth in these velocity components arising from dynamical heating of thin disk stars. (We showed earlier that our ages were in fair agreement with Nordström et al.'s.) In Figure 25, we show these boundaries in the three panels showing velocity versus age. Stars of Paper I fall in the main between the broken lines. In Nordström et al.'s Figure 30, the area between the broken lines is filled with stars to about ages of 15 Gyr, but note that their ages systematically differ from ours for the most-metal poor stars (see §4.5).

Our thick disk stars are, as expected, displaced outside the area between the broken lines in the V_{LSR} versus age plot. In W_{LSR} versus age, the thick disk stars fall along the broken lines, and in U_{LSR} versus age the thick disk stars fall within and outside the area between the broken lines.

7 MERGERS AND ABUNDANCES

Today, the origin of the thick disk is believed to lie in the formation of the early Galaxy through mergers of smaller (proto-) galaxies in the context of a Λ CDM universe. Simulations of galaxy construction by mergers are regularly reported in the literature. Reviews are written to correlate observational and theoretical evidence on the thick disk not only of the Galaxy but of (edge-on) spiral galaxies. Here, we restrict remarks largely to interpretations of the abundance differences between thick and thin disk and the similarities between the thick disk and the halo. The reader is referred to comprehensive reviews for a more detailed discussion of observations and theory – see, for example, Majewski (1993) and Freeman & Bland-Hawthorn (2002). Our discussion is obviously influenced by recent commentaries by Dalcanton (2005) and Wyse & Gilmore (2005).

Recent detections of accretion of dwarf galaxies show that merger is a continuing way of life for the Galaxy (e.g., Ibata et al. 1997, Yanny et al. 2003). Theoretical ideas about mergers in the usual Λ CDM universe predict that the rate of mergers was much higher in the past with a marked decline in the rate at (say) a redshift $z \sim 1$ or about 8 Gyr ago. Coupling of the history of mergers with the formation of thick disk stars explains why the Galactic thick disk stars are old. One additional condition is required: the system of thick disk stars must be created free of gas in order that star formation is cut off and young thick disk stars are not formed. Thin disk stars form from gas – likely, a mixture of pre-merger gas of the Galaxy and infall of gas following the mergers.

A defining characteristic of the thick disk is the large vertical scale height, that is the high vertical velocity dispersion (σ_W). Dalcanton (2005) notes that there are three ways in which a high σ_W may be achieved through merging: (A) heating of a thin disk in a merger (which may or may not lead to the disruption of the thin disk); (B) direct accretion of stars from satellite galaxies; and (C) star formation in merging gas-rich systems. There is the real possibility that the three ways each contributed to formation of our thick (and thin) disk.

7.1 Scenario A

The Galaxy develops a thin disk with on-going star formation. Merger with one or more satellite galaxies occurs. Thin disk stars are heated in the merger to create a thick disk of stars but not gas. Thick disk stars are fossils from the early years of the thin disk. This thin disk of gas is largely destroyed but reforms following the mergers by accreting gas from the original thin disk, the satellites, and, perhaps, the proverbial infall of (primordial?) gas. After a hiatus, star formation resumes in the thin disk from gas having an initial abundance set by the compositions of the contributors of gas and may be also by the Type Ia supernovae from the generations of thick disk stars. Quinn, Hernquist & Fullagar (1993) is commonly cited as providing a description of thick disk formation through a merger.

As pointed out by Dalcanton (2005), vertical heating does not change angular momentum significantly. For example, Quinn et al. (1993) show only a mild reduction of about 10 km s^{-1} in the rotational velocities of the stars after disk heating by a satellite merger. Thus, in this scenario it may be difficult to explain the larger differences observed between the asymmetric drifts of the thin and thick disks.

7.2 Scenario B

An alternative consequence of galaxy growth through mergers is that the thick disk is composed of stars accreted from satellite galaxies. Abadi et al. (2003a, 2003b) describe results from a single simulation of galaxy formation in a Λ CDM universe. Many structural and dynamical properties of the Galaxy are satisfactorily reproduced including a disk with well-defined thin and thick disk components. The majority (about 60%) of the thick disk stars are stars captured from satellite galaxies. This percentage increases with age; ninety per cent of thick disk stars older than about 10 Gyr were provided by satellite galaxies. In addition, about 15% of the oldest thin disk stars are from the satellites.

One of the most interesting predictions of the Abadi et al. scenario is that thick disk stars acquired from any given satellite do not end up at all galactocentric distances, but they rather form a ring-like structure. Thus, different satellites may dominate the thick disk population at different radii. However, the peak of the metallicity distribution of thick disk stars appears to be fairly uniform between 4 and 14 kpc from the galactic center (Allende Prieto et al. 2005).

The demonstrated uniformity of composition among thick disk stars in the solar neighborhood (see Sec. 5.7), and the lack of cosmic scatter, would suggest that these stars may not have come from a variety of satellites, each with a

Table 7. Mean $[X/Fe]$ values (M) in the bin of $[Fe/H]$ -0.45 to -0.55 and the coefficients (B) of the slope of the linear regression fit to the runs of $[X/Fe]$ versus $[Fe/H]$ in the metallicity range -0.3 to -1.0 for thin and thick disk stars. The value $\Delta[X/Fe]$ in column 6 is the difference between M_{thick} and M_{thin} .

$[X/Fe]$	M_{thin}	B_{thin}	M_{thick}	B_{thick}	$\Delta[X/Fe]$
[C/Fe]	0.22±0.08	-0.23±0.04	0.35±0.08	-0.23±0.06	0.13
[O/Fe]	0.24±0.07	-0.19±0.03	0.36±0.19	-0.25±0.05	0.12
[Na/Fe]	0.09±0.04	-0.15±0.03	0.12±0.05	-0.06±0.04	0.03
[Mg/Fe]	0.11±0.06	-0.15±0.03	0.32±0.06	-0.10±0.03	0.21
[Al/Fe]	0.12±0.06	-0.11±0.03	0.30±0.09	-0.01±0.06	0.18
[Si/Fe]	0.08±0.05	-0.09±0.02	0.22±0.06	-0.11±0.03	0.14
[Ca/Fe]	0.06±0.04	-0.13±0.02	0.18±0.06	-0.12±0.02	0.12
[Sc/Fe]	0.05±0.05	-0.17±0.04	0.17±0.10	+0.14±0.05	0.12
[Ti/Fe]	0.06±0.05	-0.18±0.02	0.21±0.09	-0.03±0.03	0.15
[V/Fe]	-0.01±0.04	-0.10±0.03	0.10±0.08	+0.02±0.04	0.11
[Cr/Fe]	-0.02±0.02	+0.03±0.01	0.00±0.04	+0.04±0.03	0.02
[Mn/Fe]	-0.18±0.05	+0.16±0.02	-0.22±0.05	+0.38±0.04	-0.04
[Co/Fe]	0.00±0.05	-0.10±0.02	0.11±0.06	-0.03±0.03	0.11
[Ni/Fe]	0.00±0.02	-0.00±0.01	0.04±0.03	-0.03±0.04	0.04
[Cu/Fe]	-0.01±0.04	-0.05±0.04	0.06±0.09	+0.48±0.06	0.07
[Zn/Fe]	0.09±0.07	-0.14±0.07	0.12±0.07	-0.11±0.08	0.03
[Y/Fe]	-0.03±0.1	0.16±0.04	0.01±0.08	-0.10±0.06	-0.04
[Ba/Fe]	-0.04±0.11	+0.09±0.06	-0.19±0.08	-0.10±0.07	-0.10
[Ce/Fe]	-0.01±0.10	+0.00±0.05	0.03±0.09	+0.00±0.06	0.04
[Nd/Fe]	0.04±0.18	-0.03±0.06	0.15±0.10	-0.04±0.04	0.11
[Eu/Fe]	0.15±0.06	-0.26±0.03	0.38±0.11	-0.20±0.09	0.23

different, if similar, chemical history. It may be noted too that abundance analyses of stars in dwarf spheroidal galaxies and the Magellanic clouds (Hill 2004; Shetrone et al. 2003) show a variety of $[X/Fe]$ versus $[Fe/H]$ relations, each unlike those of the thick disk. However, the satellites that merged long ago may have had abundance patterns distinct from those of the surviving dwarf spheroidal and irregular galaxies. Abadi et al. stress that they have only a single simulation and, perhaps, other simulations will provide a Galaxy with a thick disk free of a significant population of accreted stars. (Abadi et al. predict that one in two stars in the halo are from satellite galaxies. Star-to-star scatter in $[X/Fe]$ including $[\alpha/Fe]$ may exist among halo stars.)

The mergers disrupt the gas of the early thin disk. Just prior to its disruption, a part of the thin disk had attained $[Fe/H] \simeq -0.3$, the maximum metallicity of the thick disk. After the merger, the thin disk is reconstituted from gas of the former thin disk and metal-poor (presumably) gas of the satellite galaxies. One supposes that the present thin disk began life with $[Fe/H] \sim -0.7$, the low metallicity bound to the present thin disk stars. In the hiatus before reconstitution of the thin disk, the gas is contaminated by ejecta from Type Ia supernovae, as in scenario (C) – see, our discussion of Figures 26 and 27 which is also pertinent to this scenario.

7.3 Scenario C

The thick disk is formed during an early period of multiple mergers involving gas-rich systems. A high star formation rate is associated with this period. Interactions between the merging systems and the nascent galaxy lead to a relatively hot system of stars supported by rotation – that is a thick disk. Subsequent to this early period, the thin disk is formed from infalling gas.

This scenario is developed by Brook et al. (2004, 2005a,

2005b). Their 2005 paper presents abundance predictions, specifically $[\alpha/Fe]$ versus $[Fe/H]$, for several simulated galaxies provided from an N-body SPH code. These predictions (Figures 12 to 15 from Brook et al. 2005a) bear a remarkable resemblance to the observed abundance patterns of the halo, thick and thin disks.

For example, the predicted metal content of thick disk stars at different galactocentric distances is approximately uniform, and so is also with distance from the Galactic plane, in agreement with recent SDSS observations (Allende Prieto et al. 2005). Of particular note is the clear separation in the $[\alpha/Fe]$ versus $[Fe/H]$ relations of the thick and thin disk with each trend showing a weak $[Fe/H]$ dependence. In the reported simulations, the thick disk extends in $[Fe/H]$ variously from about -1.5 to an upper limit in the range -0.1 to -0.5 . The thick disk’s $[\alpha/Fe]$ at the upper limit in two of the four reported simulations remained separated from the thin disk’s $[\alpha/Fe]$ and in the other two approached but did not merge with the $[\alpha/Fe]$ of the thin disk (i.e., the simulations do not predict a knee). The lower $[\alpha/Fe]$ of the thin disk results from contamination of the thin disk by ejecta from Type Ia supernovae from thick disk binaries. The thin disk has a metallicity spread of -0.5 to $+0.4$ in three of the four simulations and -0.9 to -0.1 in the fourth. Halo stars extend to $[Fe/H]$ of about -0.9 to -0.6 with a $[\alpha/Fe]$ very similar to that of the thick disk in three simulations and about 0.2 dex larger in the fourth simulation.

Our data on thick and thin disk abundances may be used to characterize the pollution of the gas by SN Ia ejecta (and AGB stars). Ages of thin and thick disk stars show (Figure 24) that several Gyr elapsed between the formation of the first thick and the first thin disk stars and, thus, time aplenty for SN Ia’s (and AGB stars) to cause pollution. Compositions of thick disk stars up to the most metal-rich (in our interpretation) at $[Fe/H] = -0.3$ are dominated by

contributions from SN II. Addition of SN Ia ejecta to gas, as recognised in a classic paper by Tinsley (1979), increases the abundance ratio of the iron-group elements to α -elements.

This episode in chemical evolution of the Galactic disk is represented schematically by Figure 26 in which we plot $[X/\alpha]$ versus $[\alpha/H]$. The α abundances are dominated by SN II products but not without a SN Ia contribution, especially for the heavier α -elements. Oxygen would probably provide a cleaner measure of SN II products, albeit with a bias to the SN II from the most massive stars, but, at present, we do not have non-LTE corrected O abundances for all of our stars. Evolution of the thick disk is represented by the track A to B; pristine gas is contaminated by SN II ejecta raising $[\alpha/H]$ and, in this example, also raising $[X/\alpha]$; X is here an element whose yield from SN II is metallicity-dependent. For elements whose yield from SN II is independent of metallicity, the track A to B will be parallel to the x -axis. Stars formed as the gas composition evolves from A to B become today's thick disk stars.

Star formation ceases as a thin disk forms from the gas of the satellites that gave the thick disk stars and infalling more metal-poor gas. On the assumption that the thick disk gas of the composition corresponding to point B is diluted with very metal-poor gas, the thin disk will initially have the composition corresponding to point C. Following the period of active merger, there will be a hiatus before star formation in the thin disk resumes. In and following the interval of very low star formation, SN Ia's pollute the gas. Pollution prior to resumption of star formation is represented by the track C to D; in this example, the SN Ia's products include noticeable amounts of X but not of the α -elements. (If α -elements are produced, the track C to D is slanted.) Finally, the composition of the gas (and stars) of the new thin disk evolves along the track D to E in response to contributions by the SN II arising from massive stars formed in the new thin disk, SN Ia in the thick disk and later of the thin disk, and AGB stars of the thick and thin disks.

Evolution from A to E will depend on the element X, as we illustrate in Figure 27, where derived abundances for four representative elements – Mn, Fe, Ni, and Eu – are shown with a track A to E superimposed with point B placed at $[\alpha/H] = -0.1$, and C placed, somewhat arbitrarily, at $[\alpha/H] = -0.6$. The increase in $[Mn/\alpha]$ along A to B is attributed to a metallicity-dependent Mn yield from SN II (McWilliam et al. 2003). This is supported by the observation that the track C to D for Mn is short. Iron offers a contrasting track: along the thick disk segment, A to B, $[Fe/\alpha]$ is essentially constant indicating that the relative yields of Fe and α -elements are metallicity independent; the large jump from C to D shows, as anticipated, that Fe is a principal product of SN Ia's; and the slope to the track D to E reflects the combined contributions of SN II and SN Ia to the continuing evolution of the thin disk. Nickel's behaviour is similar to iron's but the increment in $[X/\alpha]$ from C to D is less for Ni than for Fe. For Eu, $[Eu/\alpha]$ is approximately constant along the track A to B indicating a lack of a metallicity dependence of the Eu to α -element yields from SN II. The track C to D shows a decrease in $[Eu/\alpha]$ resulting from α -element production by SN Ia with the absence of Eu production. The track D to E is controlled by the yields from SN II and SN Ia. In summary, chemical evolution of the disk as depicted by Figure

26 offers a qualitative account of the compiled data on the abundances of thin and thick disk stars.

This scenario for the formation of the thick disk offers a fine account of the observed abundance pattern of the Galaxy's halo, thick and thin disks. Brook et al. describe how their simulations fit other observed characteristics of the Galaxy and external disk galaxies. They also remark that accretion of stars from satellites, after formation of the thin disk, may contribute to the population of the thick disk and halo, i.e., the first scenario (above) may have a role to play.

A potential problem with this scenario, pointed out by Dalcanton (2005), is that it will be the same gas from the merging blocks which will give birth to the thick disk stars first and to the thin disk population later. This situation could make it difficult to have quite different scale lengths for the two disks. However, as we discuss above, in order to match the observed abundances of thin and thick disk stars, a significant contribution of metal-poor gas must be made available before star formation begins in the thin disk. Only in this way, the last stars formed in the thick disk can have higher metal abundances than thin disk stars formed at a later time. In the models reported by Brook et al., the scale length of the thin disk, we note, is significantly different from that of the thick disk (a ratio of 1.6), but with the thick disk being more compact than the thin disk, which is opposite to the behaviour observed in most galaxies, including the Milky Way.

8 CONCLUDING REMARKS

On the basis of the available abundance data on the thin and thick disks and of the published simulations of disk formation through mergers in a Λ CDM universe, scenario (C) appears to be a plausible leading explanation for the origin of the thick and thin disks. In terms of a continued exploration of the observational frontiers, there is, for example, a need for (i) a detailed abundance analysis of stars apparently attributable to an extension of the thick disk to metallicities below $[Fe/H]$ of -1 , i.e., the so-called metal weak thick disk, which comprises only one per cent of the thick disk (Martin & Morrison 1998); (ii) a more complete investigation of the four dimensional space (U,V,W,[Fe/H]), e.g., the pursuit of stars at low W_{LSR} with $[Fe/H]$ less than about -0.7 , stars, which, if present, would be assigned to the thin disk; (iii) analysis of a larger sample of stars with $[Fe/H]$ greater than about -0.3 and well-determined kinematics is needed to confirm or deny the presence of the knee in the thick disk Mg-like abundances connecting to the thin disk abundances for the most metal-rich stars; (iv) a larger sample of thick disk stars is needed to determine radial and vertical gradients in compositions of thick disk stars. The vertical gradient, if any, appears to be very shallow (e.g; Bensby et al. 2005, Allende Prieto et al. 2005).

The realisation that thick and thin disk stars of the same $[Fe/H]$ differ in composition and the strong suggestion that thick and thin disk stars span overlapping but distinctly different ranges in $[Fe/H]$ (see, for example, Schuster et al. 2005) has consequences for the cottage industry providing models of chemical evolution of the Galactic disk, especially for models of the solar neighbourhood. The industry stan-

dard supposes that chemical evolution as represented by a plot of $[X/Y]$ vs $[Y/H]$, where Y is traditionally taken to be Fe or sometimes O, is a continuous process from the halo to the disk, i.e., initially metal-free gas experiences star formation leading to the halo stars, collapse of gas to a disk with enrichment from stellar nucleosynthesis and possibly continuing infall of gas leads to a steady continuous chemical evolution. No account is taken of the fact that the disk has the two components - thin and thick - from different origins and most probably covering different metallicity ranges. The time has come to change the industry standard!

9 ACKNOWLEDGMENTS

We thank Jocelyn Tomkin, Kameswara Rao, and Gajendra Pandey for many spirited and useful discussions. This research has been supported in part by the Robert A. Welch Foundation of Houston, Texas. This research has made use of the SIMBAD data base, operated at CDS, Strasbourg, France, and the NASA ADS, USA.

REFERENCES

- Abadi, M. G., Navarro, J. F., Steinmetz, M., Eke, V. R. 2003a, *ApJ*, 591, 499
- Abadi, M. G., Navarro, J. F., Steinmetz, M., Eke, V. R. 2003b, *ApJ*, 597, 21
- Adelman-McCarthy et al. 2005, *ApJS*, in press (arXiv:astro-ph/0507711)
- Allende Prieto, C., Barklem, P. S., Lambert, D. L., Cunha, K. 2004, *A&A*, 420, 183
- Allende Prieto, C., Beers, T. C., Wilhelm, R., Newberg, H. J., Rockosi, C. M., Yanny, B., & Lee, Y. S. 2005, *ApJ*, in press (arXiv:astro-ph/0509812)
- Alonso, A., Arribas, S., Martínez-Roger, C. 1996, *A&A*, 313, 873
- Andersson, Edvardsson, B. 1994, *A&A*, 290, 590
- Barbier-Brossat, M., Figon, P. 2000, *A&AS*, 142, 217
- Bensby, T., Feltzing, S., Lundström, I. 2003, *A&A*, 410, 527
- Bensby, T., Feltzing, S., Lundström, I. 2004, *A&A*, 415, 155
- Bensby, T., Feltzing, S., Lundström, I., Ilyin, I. 2005, *A&A*, 433, 185
- Bertelli, G., Bressan, A., Chiosi, C., Fagotto, F., Nasi, E. 1994, *A&AS*, 106, 275
- Bihain, G., Israelian, G., Rebolo, R., Bonifacio, P., Molaro, P. 2004, *A&A*, 423, 777
- Borkova, T.V., Marsakov, V.A. 2005, *ARep*, 49, 405
- Brewer, M., Carney, B.W. 2005, *AJ* (in press, ArXiv:astro-ph/0509267)
- Brook, C. B., Kawata, D., Gibson, B. K., Freeman, K. C. 2004, *ApJ*, 612, 894
- Brook, C. B., Gibson, B. K., Martel, H., Kawata, D. 2005a, *ApJ*, 630, 298
- Brook, C. B., Veilleux, V., Kawata, D., Martel, H., & Gibson, B. K. 2005b, To appear in the proceedings of "Island Universities: Structure and Evolution of Disk Galaxies" (eprint arXiv:astro-ph/0511002)
- Buser, R., Rong, J., Karaali, S. 1999, *A&A*, 348, 98
- Burris, D. L., Pilachowski, C. A., Armandroff, T. E., Sneden, C., Cowan, J. J., Roe, H. 2000, *ApJ*, 544, 302
- Cabrera-Lavers, A., Garzón, F., & Hammersley, P. L. 2005, *A&A*, 433, 173
- Carney, B. W., Latham, D. W., Laird, J. B., Aguilar, L. A. 1994, *AJ*, 107, 2240
- Chen, Y.Q., Nissen, P.E., Zhao, G., Zhang, H.W., Benoni, T. 2000, *A&AS*, 141, 491
- Cutri, R. M., et al. 2003, *VizieR Online Data Catalog*, 2246. Originally published in: University of Massachusetts and Infrared Processing and Analysis Center, IPAC/California Institute of Technology
- Dalcanton, J.J., Seth, A.C., Yoachim, P. 2005, ArXiv: astro-ph/0509700
- Degl'Innocenti, S., Prada Moroni, P.G., Ricci, B. 2005, astro-ph/0504611
- Dehnen, W., Binney, J.J. 1998, *MNRAS*, 298, 387
- Degl'Innocenti, S., Prada Moroni, P.G., Ricci, B. 2005, ArXiv:astro-ph/0504611
- Edvardsson, B., Andersen, J., Gustafsson, B., Lambert, D.L., Nissen, P.E., Tomkin, J. 1993, *A&A*, 275, 101
- Famaey, B., Jorissen, A., Luri, X., Mayor, M., Udry, S., Dejonghe, H., Turon, C. 2005, *A&A*, 430
- Feltzing, S., Bensby, T., Lundström, I. 2003, *A&AL*, 397, 1
- Feltzing, S., Gustafsson, B. 1998, *A&AS*, 129, 237
- Freeman, K., Bland-Hawthorn, J. 2002, *ARA&A*, 40, 487
- Fulbright, J.P. 2000, *AJ*, 120, 1841
- Fuhrmann, K. 1998, *A&A*, 338, 161
- Fuhrmann, K. 2004, *AN*, 325, 3
- Gehren, T., Liang, Y. C., Shi, J. R., Zhang, H. W., Zhao, G. 2004, *A&A*, 413, 1045
- Gilmore, G., Reid, N. 1983, *MNRAS*, 202, 1025
- Girardi, L., Bressan, A., Bertelli, G., Chiosi, C. 2000, *A&AS*, 141, 371
- Gratton, R.G., Carretta, E., Matteucci, F., Sneden, C. 1996, in ASP conference Series 92, Formation of the Galactic Halo ... inside and out, ed. H. Morrison & A. Sarajedini (San Francisco: ASP), 307
- Gratton, R. G., Carretta, E., Desidera, S. Lucatello, S. Mazzei, P. Barbieri, M. 2003, *A&A*, 406, 131
- Gustafsson, B., Karlsson, T., Olsson, E., Edvardsson, B., Ryde, N. 1999, *A&A*, 342, 426
- Hauck, B., Mermilliod, M. 1997, *yCat*, 2215, 0
- Hill, V. 2004, in "Origin and Evolution of the Elements", Carnegie Observatories, Pasadena: Ed. A. McWilliam and M. Rauch, P. 205
- Ibata, R. A., Wyse, R. F. G., Gilmore, G., Irwin, M. J., & Suntzeff, N. B. 1997, *AJ*, 113, 634
- Juric, M., et al. 2005, ArXiv Astrophysics e-prints, arXiv:astro-ph/0510520
- Kurucz, R.L. 1998, [HTTP://cfaku5.harvard.edu](http://cfaku5.harvard.edu)
- Latham, D. W., Stefanik, R. P., Torres, G., Davis, R. J., Mazeh, T., Carney, B. W., Laird, J. B., Morse, J. A. 2002, *AJ*, 124, 1144
- Majewski, S.R. 1993, *ARA&A*, 31, 575
- Malaroda S., Levato H., Galliani S. 2001, Complejo Astronomico El Leoncito (CASLEO), San Juan, Argentina
- Marsakov, V.A., Borkova, T.V. 2005, *AstL*, 31, 515
- Martin, J. C., Morrison, H. L. 1998, 116, 172
- Mishenina, T. V., Kovtyukh, V. V., Soubiran, C., Travaglio, C., Busso, M. 2002, *A&A*, 396, 189
- Mishenina, T.V., Soubiran, C., Kovtyukh, V.V., Korotin, S.A. 2004, *A&A*, 418, 551
- McWilliam, A.; Rich, R. M. 2004, in " Origin and Evolution of the Elements ", Carnegie Observatories, Pasadena: ed. A. McWilliam and M. Rauch, P38
- Neckel, Th., Klare, G., Sarcander, M. 1980, *A&AS*, 42, 252
- Nidever D.L., Marcy G.W., Butler R.P., Fischer D.A., Vogt S.S. 2002, *ApJS*, 141, 503
- Nissen, P. E., Chen, Y. Q., Schuster, W. J., Zhao, G. 2000, *A&A*, 353, 722
- Nissen, P.E., Chen, Y.Q., Asplund, M., Pettini, M. 2004, *A&A*, 415, 993
- Nordström, B., Mayor, M., Andersen, J., Holmberg, J., Pont, F.,

- Jorgensen, B.R., Olsen, E.H., Udry, S., Mowlavi, N. 2004, *A&A*, 418, 989
- Ojha, D. K., Bienaymé, O., Mohan, V., & Robin, A. C. 1999, *A&A*, 351, 945
- Ojha, D. K., Bienayme, O., Robin, A. C., Creze, M., & Mohan, V. 1996, *A&A*, 311, 456
- Ojha, D.K. 2001, *MNRAS*, 322, 426
- Peterson, R.C. 1981, *ApJ*, 244, 989
- Prochaska, J. X., McWilliam, A. 2000, *ApJL*, 537, 57
- Prochaska, J.X., Naumov, S.O., Carney, B.W., McWilliam, A., Wolfe, A.M. 2000, *AJ*, 120, 2513
- Quinn, P. J., Hernquist, L., Fullagar, D. P. 1993, *ApJ*, 403, 74
- Robin, A. C., Reyl, C.; Derrire, S.; , icaud, , S. 2003, *A&A*, 409, 523
- Ramírez, I., Allende Prieto, C., Lambert, D.L. 2006 (private communication)
- Reddy, B.E., Tomkin, J., Lambert, D.L., Allende Prieto, C. 2003, *MNRAS*, 340, 304
- Schuster, W.J., Moitinho, A., Marquez, A., Parrao, L., Covarrubias, E. 2005, *A&A*, (in press, ArXiv: astro-ph/0510313)
- Shetrone, M., Venn, K. A., Tolstoy, E., Primas, F., Hill, V., Kaufer, A. 2003, *AJ*, 125, 684
- Shi, J.R., Gehren, T., Zhao, G. 2004, *A&A*, 423, 683
- Shi, J.R., Zhao, G., Chen, Y.Q. 2002, *A&A*, 381, 982
- Simmerer, J., Sneden, C., Cowan, J. J., Collier, J., Woolf, V. M., Lawler, J. E. 2004, *ApJ*, 617, 1091
- Sneden, C. 1973, PhD. Thesis, Univ. of Texas, Austin
- Sneden, C., Gratton, R. G., Crocker, D. A. 1991, *A&A*, 246, 354
- Soubiran, C., Bienaymé, O., & Siebert, A. 2003, *A&A*, 398, 141
- Spite, M., Spite, F. 1980, *A&A*, 89, 118
- Takada-Hidai, M., Saito, Yu-Ji., Takeda, Y., Honda, S., Sadakane, K., Masuda, S., Izumiura, H. 2005, *PASJ*, 57, 347
- Tinsley, B.M. 1979, *ApJ*, 229, 1046
- Tull, R. G., MacQueen, P. J., Sneden, C., Lambert, D. L. 1995, *PASP*, 107, 251
- Venn, K. A., Irwin, M., Shetrone, M.D., Tout, C.A., Hill, V., Tolstoy, E. 2004, *AJ*, 128, 1177
- Yong, David., Lambert, D. L., Allende Prieto, C., Paulson, D. B. 2004, *ApJ*, 603, 697
- Yanny, B. et al. 2003, *ApJ*, 588, 824
- York et al. 2000, *AJ*, 120, 1579
- Wyse, R.F.G., Gilmore, G. 2005, (ArXiv: astro-ph/0510025) in "Resolved Stellar Populations", ASP Conf. Ed. D. Valls-Gabaud and M. Chavez

Table 2. Atmospheric parameters and kinematic data for the programme stars. The columns 1-11 are self explanatory. The value in column 5 is the heliocentric radial velocity(R_v). Errors for the values in columns 5-8 are discussed in the text. See text for explanatory note about the probability (%P) in column 12.

Star HIP	[Fe/H]	T_{eff} (K)	$\log g$ (cm s^{-2})	R_v	U_{LSR} (km s^{-1})	V_{LSR}	W_{LSR}	R_m (kpc)	e	Z_{max} (kpc)	τ_9 (Gyrs)	%P
Thick Disk												
3086	-0.23	5697	4.14	-29.2	-159	-50	56	8.55	0.51	0.70	$7.9^{+2.4}_{-1.8}$	95±1
3185	-0.65	5344	3.81	-45.3	-37	-84	45	6.20	0.40	0.43	$11.3^{+2.7}_{-2.2}$	87±0
3441	-0.50	5723	4.50	-108.3	89	-66	86	7.08	0.39	1.13	...	96±0
4039	-1.24	5803	3.92	-5.3	-116	-92	46	6.75	0.52	0.47	$13.0^{+2.6}_{-2.1}$	95±1
4544	-0.87	5832	4.51	-112.2	-33	-133	-74	5.35	0.61	0.81	...	90±6
5122	-0.62	5204	3.80	8.9	-93	-73	48	6.93	0.42	0.50	$12.6^{+3.0}_{-2.4}$	91±2
5315	-0.47	5014	3.45	-94.0	59	-117	44	5.68	0.56	0.41	$8.8^{+6.7}_{-3.8}$	96±1
5336	-0.86	5300	4.67	-99.6	-31	-154	-27	4.99	0.72	0.22	...	91±1
5775	-0.59	5547	4.62	81.8	-59	-97	-74	6.10	0.47	0.90	...	96±1
6159	-0.67	5653	4.56	-6.7	148	-68	-40	7.78	0.52	0.43	...	93±9
6607	-0.41	5454	4.59	84.7	-15	-80	-68	6.26	0.36	0.71	...	97±0
7961	-0.64	5565	3.96	-8.6	-86	-71	40	6.83	0.41	0.37	$10.7^{+2.9}_{-2.3}$	78±1
8674	-0.60	5455	4.62	41.8	28	-88	-43	6.10	0.41	0.37	...	86±11
9080	-0.37	5162	4.65	-14.2	-83	-85	52	6.53	0.45	0.48	...	96±1
10652	-0.67	5499	4.58	-20.5	-90	-86	90	6.61	0.46	1.21	...	93±2
12579	-0.80	5770	4.60	-12.5	-2	-54	-67	6.84	0.24	0.70	...	94±13
13366	-0.70	5669	4.19	7.0	45	-99	-74	5.97	0.47	0.83	$11.8^{+4.3}_{-3.2}$	96±1
15405	-0.73	5107	3.56	17.8	-137	-95	-40	6.91	0.57	0.39	$10.2^{+8.3}_{-4.6}$	94±1
17147	-0.87	5722	4.50	121.0	-100	-80	-38	6.74	0.46	0.35	...	88±2
17666	-1.03	5000	4.50	76.0	-108	-99	-73	6.04	0.55	0.78	...	93 ± 3
22020	-0.35	5604	4.27	28.1	-71	-85	-53	6.43	0.43	0.52	...	95 ± 14
22060	-0.63	5610	4.61	172.1	-184	-66	52	8.75	0.59	0.65	...	89 ± 7
23080	-0.32	5334	4.60	38.5	-46	-67	55	6.65	0.33	0.54	...	88 ± 1
24030	-1.00	5738	4.64	-15.7	20	-88	97	6.18	0.39	1.22	...	95 ± 1
25860	-0.35	5543	4.56	48.1	-14	-74	-59	6.38	0.34	0.59	...	94 ± 8
26452	-0.89	5749	4.64	-37.7	3	-96	47	5.93	0.43	0.44	...	94 ± 1
26828	-0.34	6180	4.12	77.7	-63	-81	40	6.42	0.42	0.35	$3.20^{+3.6}_{-1.7}$	80 ± 1
27128	-0.81	5802	4.16	180.7	-162	-68	-66	8.11	0.56	0.91	$12.3^{+2.8}_{-3.3}$	91 ± 0
29269	-0.68	5484	3.95	-32.0	-95	-85	-74	6.64	0.47	0.89	$12.2^{+3.7}_{-2.8}$	95 ± 1
31188	-0.59	5789	4.54	3.3	19	-26	71	7.68	0.12	0.77	...	92 ± 3
34642	-0.44	5747	4.14	-29.5	-13	-87	-55	6.09	0.40	0.53	$8.97^{+3.2}_{-2.4}$	95 ± 12
35989	-0.19	5185	4.60	6.3	-37	-41	-65	7.27	0.21	0.68	...	92 ± 13.
36849	-0.77	5843	4.40	-36.8	70	-84	-46	6.35	0.43	0.42	...	92 ± 17.
37233	-0.51	5627	4.01	52.8	13	-67	50	6.55	0.30	0.47	$9.3^{+2.6}_{-2.1}$	75 ± 2
38769	-0.79	5726	4.15	5.6	25	-65	69	6.63	0.30	0.74	$12.7^{+3.5}_{-2.8}$	97 ± 1
39893	-0.84	5249	4.69	-40.6	66	-127	-55	5.59	0.61	0.56	...	93 ± 3
40613	-0.62	5670	4.16	111.3	-27	-138	-36	5.18	0.65	0.30	$12.4^{+2.8}_{-2.3}$	94 ± 1
43393	-0.59	5256	4.65	33.4	32	-104	-79	5.88	0.47	0.93	...	95 ± 2
44075	-0.86	5783	4.09	149.6	-51	-111	86	6.25	0.39	0.87	$12.8^{+2.6}_{-2.2}$	92 ± 0
44347	-0.85	5798	4.62	-57.4	117	-64	31	7.34	0.45	0.29	...	70 ± 0
44860	-0.51	5654	4.27	65.5	-58	-67	-57	6.69	0.35	0.57	$12.6^{+3.8}_{-2.9}$	92 ± 5
45947	-0.46	4911	3.29	26.6	-16	-105	-60	5.77	0.48	0.60	$9.51^{+8.2}_{-4.4}$	97 ± 7
50005	-0.53	5394	4.64	60.1	101	-99	41	6.31	0.53	0.42	...	95 ± 4
50671	-0.48	5878	4.45	82.0	-60	-41	63	7.39	0.26	0.69	...	90 ± 1
50965	-0.57	5715	4.56	19.8	-51	-88	-84	6.26	0.42	1.02	...	96 ± 1
52673	-0.66	5541	4.62	74.7	52	-99	-39	5.97	0.47	0.35	...	92 ± 14
58843	-0.79	5663	4.63	6.8	109	-122	-52	6.01	0.63	0.53	...	91 ± 6
59233	-0.83	5333	3.71	-12.2	-181	-72	-37	8.38	0.60	0.38	...	91 ± 18
59750	-0.74	6069	4.44	-3.7	61	-61	-60	6.77	0.35	0.54	...	93 ± 2
60268	-0.72	5532	4.62	-81.8	6.7	-98	-37	5.86	0.45	0.32	...	88 ± 5
60956	-0.58	5362	4.63	6.1	7.3	-139	-64	5.21	0.63	0.73	...	91 ± 7
62240	-0.83	5663	4.46	-36.4	61	-68	-69	6.73	0.35	0.75	...	97 ± 4
64426	-0.71	5754	4.16	49.4	-72	-64	64	6.91	0.36	0.70	$11.3^{+3.4}_{-2.6}$	96 ± 0
65449	-0.44	5383	3.84	-21.6	-141	-55	-37	7.97	0.48	0.38	$9.7^{+4.5}_{-3.1}$	85 ± 2
70520	-0.62	5708	4.01	-48.2	96	-78	-65	6.79	0.45	0.75	$9.9^{+2.9}_{-2.2}$	97 ± 0
70681	-1.10	5396	4.70	-46.7	-12	-41	-69	7.21	0.18	0.71	...	94 ± 7

Table 2 – continued

Star HIP	[Fe/H]	T_{eff} (K)	$\log g$ (cm s ⁻²)	R_V	U_{LSR} (km s ⁻¹)	V_{LSR}	W_{LSR}	R_m (kpc)	e	Z_{max} (kpc)	$\log \tau_9$ (yrs)	%P
71819	-0.14	5825	4.35	-18.1	-65	-101	38	6.01	0.50	0.33	...	94 ± 0
72407	-0.54	5567	4.56	1.5	-88	-60	48	7.10	0.38	0.47	...	81 ± 6
72803	-0.73	5159	3.57	-98.9	-98	-85	-45	6.65	0.47	0.40	9.6 ^{+5.0} _{-3.3}	94 ± 1
74033	-0.85	5574	3.95	-59.9	-104	-120	33	5.99	0.62	0.28	13.8 ^{+2.2} _{-1.9}	94 ± 2
74067	-0.75	5572	4.63	-61.1	-20	-60	-61	6.72	0.27	0.62	...	91 ± 3
81748	-0.01	5559	4.29	-76.0	-4	-65	-56	6.56	0.29	0.55	...	86 ± 4
84781	-0.29	5259	3.86	-93.9	-91	-60	49	7.17	0.35	0.54	12.1 ^{+2.8} _{-2.3}	85 ± 7
84803	-0.52	5524	3.87	-90.5	-47	-79	-51	6.36	0.39	0.49	8.4 ^{+3.9} _{-2.6}	91 ± 13
84862	-0.41	5605	4.49	-79.3	35	-76	-57	6.40	0.35	0.55	...	93 ± 1
85373	-0.82	5351	4.66	-74.1	-57	-103	75	5.99	0.49	0.87	...	95 ± 2
85378	-0.51	5709	4.22	-72.7	-55	-100	73	6.00	0.48	0.82	...	96 ± 0
85757	-0.70	5414	3.81	3.5	24	-75	71	6.40	0.34	0.78	9.9 ^{+4.2} _{-2.9}	98 ± 0
86013	-0.70	5630	4.58	-138.0	-156	-57	87	8.36	0.51	1.35	...	88 ± 6
86830	-0.59	5305	3.74	-82.6	165	-100	52	7.33	0.63	0.60	11.5 ^{+3.8} _{-2.9}	88 ± 5
87089	-0.30	5142	4.63	-96.3	-47	-120	47	5.58	0.56	0.44	...	96 ± 1
87533	-0.21	5727	3.97	-115.9	-68	-106	-33	5.93	0.52	0.28	5.8 ^{+2.0} _{-1.5}	93 ± 8
88039	-0.81	5680	4.01	-18.5	4	-108	83	5.73	0.49	0.99	12.2 ^{+3.1} _{-2.5}	94 ± 1
88166	-0.76	5305	4.67	-12.7	51	-97	75	6.06	0.46	0.85	...	96 ± 0
90393	-0.72	5541	3.97	-85.0	-56	-110	91	5.86	0.52	1.18	13.5 ^{+2.3} _{-1.9}	90 ± 3
94129	-0.27	5630	4.35	-45.3	5	-122	41	5.43	0.56	0.36	...	96 ± 0
96902	-0.29	5697	4.05	-104.7	-3	-109	-54	5.67	0.50	0.52	6.9 ^{+2.4} _{-1.8}	96 ± 2
97846	-0.18	5259	3.81	-73.1	-82	-49	55	7.33	0.33	0.58	11.3 ^{+3.2} _{-2.5}	85 ± 4
98020	-1.61	5170	4.73	-192.2	-142	-108	69	6.77	0.62	0.87	...	84 ± 0
98532	-1.13	5518	3.71	-14.0	84	-123	50	5.78	0.61	0.49	11.1 ^{+4.2} _{-3.1}	94 ± 3
99224	-0.12	5580	4.20	0.4	19	-87	-68	6.11	0.40	0.72	9.9 ^{+3.0} _{-2.3}	97 ± 1
104659	-1.07	5730	4.34	-45.3	102	-111	-51	6.16	0.57	0.51	13.2 ^{+4.0} _{-3.1}	94 ± 1
106947	-0.35	5305	4.63	-107.0	-55	-68	76	6.71	0.34	0.89	...	98 ± 0
107294	-1.14	5929	4.63	-95.0	139	-101	62	6.85	0.59	0.72	...	90 ± 6
108056	0.14	5928	4.39	-98.3	5	-67	118	6.72	0.28	1.73	...	92 ± 6
109384	-0.38	5126	4.64	-64.8	-5	-55	-59	6.84	0.24	0.59	...	85 ± 7
110291	-0.93	5729	4.55	-104.4	75	-87	37	6.31	0.46	0.33	...	84 ± 1
111517	-0.45	5471	3.88	-11.6	-88	-95	-107	6.45	0.49	1.59	9.0 ^{+3.7} _{-2.6}	84 ± 11
112666	-0.42	5208	4.62	-97.4	-31	-103	-70	5.80	0.48	0.77	...	96 ± 1
112811	-0.70	5347	4.64	-4.0	38	-84	-55	6.21	0.40	0.53	...	95 ± 11
113514	-0.63	5720	4.57	-119.8	-46	-128	33	5.51	0.58	0.24	...	95 ± 0
116421	-0.51	5617	4.15	-112.0	-55	-108	69	5.85	0.51	0.76	11.7 ^{+2.6} _{-2.1}	95 ± 0
117029	-0.77	5436	3.86	-71.7	-61	-99	89	6.12	0.47	1.15	12.4 ^{+2.2} _{-1.9}	93 ± 0

Thin Disk

2909	-0.28	5634	4.15	24.9	38	-60	-21	6.75	0.29	0.18	8.9 ^{+2.7} _{-2.1}	88 ± 3
14086	-0.65	5075	3.72	42.6	18	-78	-13	6.27	0.36	0.10	8.3 ^{+4.3} _{-2.8}	78 ± 2
14241	-0.49	5457	4.61	-19.7	14	-63	33	6.60	0.29	0.28	...	75 ± 2
19696	-0.24	5554	4.45	-5.5	-2	-49	40	6.95	0.22	0.34	...	77 ± 3
26437	0.10	5911	4.40	-63.8	23	-55	-38	6.83	0.26	0.32	...	74 ± 3
39616	-0.41	5936	4.43	3.7	-53	-36	-35	7.48	0.23	0.30	...	87 ± 2
40118	-0.47	5484	4.58	28.4	-36	-55	-32	6.86	0.27	0.27	...	81 ± 2
64924	-0.03	5515	4.53	-8.4	-13	-41	-24	7.13	0.19	0.19	...	95 ± 0
73078	-0.11	5189	3.76	10.6	-26	11	21	8.87	0.09	0.18	11.7 ^{+3.4} _{-2.6}	98 ± 0
74933	-0.39	5712	4.24	9.3	9	-44	39	7.06	0.20	0.33	...	82 ± 0
81681	-0.38	5565	4.52	-41.0	1	-53	-38	6.85	0.24	0.32	...	77 ± 3
84506	0.09	5610	4.05	-62.6	-10	-45	-38	7.04	0.21	0.33	5.70 ^{+2.0} _{-1.5}	82 ± 5
86568	-0.40	5214	4.64	-51.3	-5	-71	28	6.40	0.32	0.23	...	74 ± 2

Table 2 – continued

Star HIP	[Fe/H]	T_{eff} (K)	$\log g$ (cm s^{-2})	R_v	U_{LSR} (km s^{-1})	V_{LSR}	W_{LSR}	R_m (kpc)	e	Z_{max} (kpc)	$\log \tau_9$ (yrs)	%P
Halo												
3026	-1.04	6060	4.47	-50.2	146	-231	-33	166.	0.99	57.2	...	97 ± 2
10449	-0.87	5566	4.64	27.9	-196	-196	65	6.46	0.94	0.77	...	75 ± 0
12294	-0.95	6069	4.58	54.6	-188	-149	69	6.97	0.80	0.81	...	99 ± 3
16072	-1.39	5608	4.72	-13.3	-31	-279	-49	4.88	0.76	0.46	...	99 ± 13
28671	-1.01	5357	4.69	-190.7	245	-234	99	361.	0.99	9.07	...	99 ± 0
52771	-1.98	5354	4.77	81.5	163	-339	102	7.44	0.63	1.74	...	99 ± 0
55592	-0.94	5886	4.60	97.2	-95	-239	13	24.9	0.99	5.54	...	96 ± 2
57450	-1.50	5315	4.74	64.0	-221	-270	60	7.48	0.89	0.77	...	99 ± 0
58229	-0.83	5740	4.61	167.9	-66	-201	57	27.5	0.99	3.01	...	73 ± 3
62882	-0.98	5619	3.83	152.6	280	-201	-103	61.9	0.99	2.28	12.2 ^{+3.6} _{-2.8}	99 ± 0
73385	-1.46	5435	3.86	175.6	51	-361	61	6.41	0.38	0.64	...	99 ± 0
78640	-1.34	5665	3.92	-152.3	119	-261	-16	5.25	0.86	0.12	14.9 ^{+1.7} _{-1.6}	99 ± 0
80837	-0.80	5724	4.10	-47.3	96	-258	-70	4.88	0.86	0.64	13.3 ^{+2.4} _{-2.0}	99 ± 0
86321	-0.87	5760	4.59	-241.8	-75	-260	-45	4.84	0.86	0.41	...	99 ± 0
86431	-0.54	5648	4.48	33.9	215	-112	91	8.55	0.74	1.63	...	78 ± 5
94449	-1.12	5545	3.68	-65.4	156	-310	60	6.61	0.73	0.69	10.1 ^{+5.3} _{-3.5}	99 ± 0
100568	-0.99	5566	4.67	-170.7	-145	-240	-65	8.76	0.96	1.48	...	99 ± 0
109067	-0.79	5362	4.69	-198.4	-24	-213	36	182.	0.99	9.61	...	73 ± 1
111549	-0.95	5704	4.13	-296.0	190	-261	41	6.39	0.90	0.33	14.2 ^{+2.5} _{-2.1}	99 ± 0
115704	-1.78	5691	4.65	-110.3	-167	-189	-49	5.96	0.90	0.53	...	88 ± 0

Thin/Thick Disk												
5163	-0.74	5547	4.63	26.1	-21	-59	-38	6.74	0.27	0.35	...	31 ± 12
8720	-0.74	5079	4.70	-3.7	90	-59	-42	7.14	0.38	0.40	...	69 ± 44
10711	-0.69	5585	4.57	49.6	-82	-56	-43	7.19	0.35	0.42	...	64 ± 20
12381	-0.16	6151	4.24	45.9	26	-62	-46	6.65	0.29	0.45	...	58 ± 14
15126	-0.82	5305	4.68	88.1	145	-52	35	8.15	0.48	0.36	...	80 ± 12
15394	-0.27	5211	3.73	4.9	29	-52	-46	6.92	0.25	0.43	10.6 ^{+4.2} _{-3.1}	58 ± 15
16738	0.37	6000	3.99	60.0	-91	-62	37	7.07	0.39	0.34	...	62 ± 20
21227	-0.45	5701	4.48	65.7	-93	-71	17	6.90	0.42	0.14	...	41 ± 14
21306	-0.65	5532	4.63	-83.0	-120	-92	-23	6.72	0.53	0.21	...	86 ± 30
21703	0.15	5386	4.53	-19.7	23	-62	40	6.66	0.29	0.35	...	39 ± 1
21921	-0.41	5285	4.61	-33.0	30	-43	55	6.86	0.30	0.46	...	68 ± 6
24037	-0.49	5473	4.60	64.4	-9	-51	-52	6.92	0.23	0.48	...	58 ± 8
30990	-0.87	5655	3.99	61.3	-77	-58	45	7.06	0.35	0.43	13.2 ^{+2.6} _{-2.2}	58 ± 3
33382	-0.05	5513	4.49	-10.1	59	-55	-34	6.94	0.31	0.29	...	72 ± 4
34511	-0.15	5710	4.51	42.6	-24	-50	-39	6.94	0.24	0.34	...	76 ± 6
35148	-0.30	5710	4.16	41.5	22	-56	49	6.80	0.26	0.45	9.0 ^{+2.5} _{-1.9}	57 ± 6
40023	-0.12	5250	3.45	-45.0	49	-46	-45	7.16	0.25	0.41	4.6 ^{+2.5} _{-1.6}	39 ± 5
42734	-0.70	5635	4.03	57.9	-28	-65	38	6.59	0.30	0.30	11.6 ^{+3.0} _{-2.4}	40 ± 2
47588	-0.47	5610	4.06	41.1	14	-76	-48	6.72	0.26	0.59	10.7 ^{+2.9} _{-2.3}	77 ± 21
52015	-0.02	5641	4.03	42.8	24	-57	38	6.77	0.27	0.33	6.32 ^{+2.1} _{-1.6}	71 ± 3
53535	0.11	5575	4.03	-85.5	56	-68	-33	6.61	0.36	0.32	5.9 ^{+1.9} _{-1.4}	39 ± 8
54196	-0.39	5800	4.04	-0.9	-81	-46	-40	7.38	0.32	0.36	6.9 ^{+2.2} _{-1.7}	42 ± 7
64103	-0.21	5482	4.59	-57.2	-71	-43	-46	7.40	0.29	0.43	...	48 ± 6
74442	-0.23	5649	4.22	-60.4	20	-41	-48	7.17	0.20	0.45	...	38 ± 5
74443	-0.59	5116	4.68	-60.5	-29	-64	-40	6.62	0.30	0.36	...	43 ± 8
80162	-0.66	5058	4.67	-9.0	8	-83	37	6.16	0.38	0.32	...	61 ± 3
82265	0.09	5446	4.52	-75.3	-54	-58	-37	6.89	0.31	0.32	...	34 ± 5
85653	-0.43	5300	4.61	-83.8	-16	-50	-53	6.94	0.23	0.50	...	61 ± 3
89583	-0.20	5492	4.55	-57.1	-29	-51	-40	6.95	0.25	0.35	...	74 ± 7
90745	-0.50	5663	4.10	-77.3	-59	-62	39	6.83	0.33	0.35	10.5 ^{+2.8} _{-2.2}	47 ± 9
94615	0.20	5634	4.48	-81.4	-49	-54	38	6.93	0.29	0.32	...	30 ± 13
99938	-0.54	5732	4.48	-111.2	-105	-70	-36	7.04	0.44	0.33	...	74 ± 11

Table 2 – continued

Star HIP	[Fe/H]	T_{eff} (K)	$\log g$ (cm s^{-2})	R_v	U_{LSR} (km s^{-1})	V_{LSR}	W_{LSR}	R_m (kpc)	e	Z_{max} (kpc)	$\log \tau_9$ (yrs)	%P
Thick Disk/Halo												
7452	-1.53	5735	4.59	-151.2	34	-193	-46	4.45	0.90	0.38	...	97 ± 36
14594	-1.88	5522	4.55	-140.8	167	-118	-59	7.00	0.69	0.72	...	73 ± 9
20298	-0.84	5547	4.65	36.6	-94	-133	81	5.64	0.66	1.02	...	79 ± 13
23922	-0.66	5663	4.58	-107.8	42	-132	-116	5.46	0.62	1.74	...	38 ± 37
26617	-0.75	5429	4.67	127.2	-50	-224	33	93.8	0.99	140.	...	99 ± 34
42864	-1.47	5356	4.76	-13.7	16	-212	-39	583.	1.00	756.	...	98 ± 64
43595	-0.84	5506	4.67	49.9	-71	-148	-94	5.30	0.71	1.23	...	63 ± 62
48209	-0.65	5415	4.64	-35.2	-121	-125	-86	6.20	0.65	1.15	...	73 ± 21
51477	-1.25	5326	4.07	102.9	75	-173	-78	4.92	0.82	0.81	...	87 ± 24
60331	-0.64	5346	4.50	-152.0	-16	-105	-135	6.57	0.34	1.31	...	64 ± 3
62507	-0.24	5730	4.09	-42.0	-71	-79	-36	6.51	0.41	0.33	$6.8^{+2.3}_{-1.7}$	73 ± 11
71019	-0.39	5204	3.85	70.4	125	-109	-117	6.68	0.59	1.99	$13.0^{+2.8}_{-2.3}$	64 ± 39
85650	-0.39	5521	4.17	-31.8	147	-133	76	6.42	0.71	1.00	...	62 ± 20
107236	-0.5	5300	4.61	-41.2	-71	-80	34	6.48	0.42	0.30	...	72 ± 5

Table 5 – *continued*

HIP	[Fe1/H]	C	O	Na	Mg	Al	Si	Ca	Sc	Ti	V
84862	-0.41	0.40	0.61	0.07	0.35	0.28	0.22	0.16	0.23	0.18	0.06
85373	-0.82	...	0.42	0.01	0.18	0.26	0.34	0.05	0.30	0.15	0.19
85378	-0.51	0.27	0.57	0.12	0.34	0.35	0.21	0.23	0.12	0.23	-0.01
85757	-0.70	0.40	0.72	0.14	0.36	0.37	0.29	0.23	0.08	0.23	0.11
86013	-0.70	0.49	0.72	0.07	0.31	0.16	0.21	0.14	0.18	0.14	0.07
86830	-0.59	0.43	0.69	0.17	0.35	0.35	0.30	0.23	0.07	0.21	0.14
87089	-0.30	0.37	0.47	-0.12	...	0.06	0.14	0.10	0.16	0.26	0.24
87533	-0.21	0.12	0.22	0.08	0.15	0.16	0.04	0.08	-0.06	0.0	0.04
88039	-0.81	0.41	0.66	0.15	0.43	0.34	0.30	0.18	0.12	0.15	0.20
88166	-0.76	...	0.73	0.13	0.34	0.28	0.28	0.14	0.15	0.21	0.12
90393	-0.72	...	0.11	0.04	0.26	0.17	0.07	0.11	0.30	0.33	0.34
94129	-0.27	0.23	0.45	0.04	0.25	0.24	0.15	0.03	0.10	0.14	0.11
96185	-0.56	0.30	0.68	0.15	0.22	0.31	0.22	0.19	0.07	0.16	0.09
96902	-0.29	0.20	0.34	0.12	0.25	0.25	0.14	0.14	0.06	0.17	0.14
97846	-0.18	0.38	0.45	0.04	...	0.23	0.14	0.10	0.11	0.10	0.07
98020	-1.61	1.1	0.25	0.31	...	0.44	0.20	0.22	0.03	0.39
98532	-1.13	0.65	0.01	0.34	0.33	0.29	0.25	-0.03	0.15	0.10
99224	-0.12	0.18	0.40	0.05	0.01	0.16	0.14	0.0	0.00	-0.01	0.00
104659	-1.07	0.47	0.75	0.06	0.35	0.26	0.25	0.18	0.06	0.31	0.11
106947	-0.35	0.43	0.34	-0.01	...	0.15	0.15	0.09	0.21	0.20	0.20
107294	-1.14	0.73	0.23	0.25	0.26	0.25	0.22	0.09	0.27	0.24
108056	0.14	0.20	0.25	0.00	0.09	0.03	0.07	-0.08	0.08	-0.13	-0.01
109384	-0.38	0.50	0.65	0.02	0.30	0.17	0.26	0.10	0.20	0.12	0.24
110291	-0.93	0.52	0.82	0.06	0.36	0.17	0.21	0.11	0.15	0.12	0.11
111517	-0.45	0.44	0.49	0.17	0.31	0.36	0.23	0.15	0.07	0.18	0.10
112666	-0.42	0.25	0.44	0.07	...	0.21	0.21	0.13	0.14	0.10	0.17
112811	-0.70	...	0.65	0.01	0.30	0.24	0.25	0.12	0.15	0.24	0.21
113514	-0.63	0.42	0.66	0.09	0.29	0.19	0.21	0.16	0.19	0.13	0.03
116421	-0.51	0.38	0.60	0.13	0.31	0.34	0.26	0.21	0.22	0.23	0.13
117029	-0.77	0.46	0.77	0.14	0.33	0.38	0.27	0.17	0.11	0.20	0.10
Thin Disk											
2909	-0.28	0.37	0.40	0.13	0.19	0.23	0.15	0.08	0.04	0.10	0.04
14086	-0.65	0.34	0.54	0.09	0.39	0.29	0.27	0.19	0.21	0.27	0.20
14241	-0.49	0.33	0.57	0.10	...	0.24	0.23	0.13	0.27	0.22	0.11
19696	-0.24	0.34	0.44	0.05	0.12	0.13	0.14	0.02	0.10	0.05	0.01
26437	0.10	0.02	0.07	0.00	0.07	0.06	0.01	0.00	-0.09	-0.03	-0.02
39616	-0.41	0.15	0.32	0.10	0.15	0.06	0.08	0.02	0.05	0.01	-0.04
40118	-0.47	0.41	0.54	0.08	0.21	0.22	0.21	0.10	0.23	0.15	0.08
64924	-0.03	0.18	0.07	-0.06	0.02	-0.01	0.05	-0.02	0.08	-0.06	0.00
73078	-0.11	0.30	0.47	0.04	0.15	1.3	0.18	-0.03	0.02	-0.13	-0.04
74933	-0.39	0.33	0.52	0.0	0.11	0.19	0.12	0.05	0.16	-0.02	-0.05
81681	-0.38	0.31	0.50	0.04	0.27	0.23	0.18	0.10	0.19	0.16	0.10
84506	0.09	0.50	0.43	0.14	0.04	0.24	0.20	-0.03	0.09	-0.08	-0.01
86568	-0.40	0.35	0.62	0.03	...	0.21	0.24	0.07	0.19	0.17	0.22
Halo											
3026	-1.04	0.47	0.07	0.19	...	0.09	0.11	0.13	0.20	...
10449	-0.87	...	0.71	-0.04	0.26	0.18	0.24	0.18	0.19	0.12	-0.09
12294	-0.95	0.24	0.22	0.07	0.14	...	0.28	0.14	0.07	0.15	...
16072	-1.39	1.2	0.41	0.45	...	0.49	0.28	...	0.26	0.33
28671	-1.01	0.79	-0.03	0.14	...	0.17	0.16	-0.06	0.16	0.26
52771	-1.98	1.1	...	0.21	0.10	...	0.11	...
55592	-0.94	0.390	0.59	0.08	0.31	0.21	0.18	0.15	-0.01	0.15	0.11
57450	-1.5	0.99	0.18	0.36	...	0.34	0.20	0.23	0.10	0.26

Table 5 – *continued*

HIP	[FeI/H]	C	O	Na	Mg	Al	Si	Ca	Sc	Ti	V
58229	-0.83	...	0.67	0.06	0.18	0.13	0.10	0.07	-0.03	0.10	...
62882	-0.98	0.200	0.80	-0.02	0.26	0.12	0.27	0.19	-0.12	0.08	0.10
73385	-1.46	1.0	1.6	0.49	0.32	0.0	0.33	0.0
78640	-1.34	0.78	...	0.29	...	0.23	0.26	-0.18	0.26	0.22
80837	-0.80	0.46	0.72	0.14	0.36	0.26	0.24	0.16	0.17	0.21	0.12
86321	-0.87	0.30	0.55	0.02	0.15	0.07	0.15	0.13	0.13	0.12	0.06
86431	-0.54	0.39	0.57	0.05	0.24	0.19	0.15	0.07	0.15	0.08	0.04
94449	-1.12	0.66	0.95	0.11	0.46	0.48	0.36	0.37	-0.06	0.24	0.08
100568	-0.99	...	0.68	0.01	0.20	...	0.14	0.11	0.00	0.08	0.00
109067	-0.79	0.48	0.68	0.07	0.28	0.24	0.24	0.13	0.21	0.15	0.11
111549	-0.95	...	0.40	-0.42	0.03	0.17	-0.3	0.12	0.00
115704	-1.78	0.67

Thin/Thick Disk

5163	-0.74	0.44	0.68	0.12	0.27	0.31	0.23	0.13	0.18	0.17	0.06
8720	-0.74	...	0.82	0.08	0.40	0.28	0.28	0.13	0.24	0.16	0.20
10711	-0.69	0.40	0.71	0.00	0.25	0.23	0.22	0.09	0.08	0.11	0.02
12381	-0.16	0.08	0.30	0.02	0.17	0.12	0.01	0.04	-0.01	-0.02	0.02
15394	-0.27	0.09	0.19	0.04	0.26	0.17	0.13	0.04	0.06	-0.02	-0.01
16738	0.37	-0.01	0.18	0.31	0.32	0.14	0.12	-0.08	-0.08	-0.17	-0.07
21227	-0.45	0.45	0.52	0.06	0.12	0.18	0.13	-0.01	0.16	0.04	-0.05
21306	-0.65	0.59	0.79	0.09	0.23	0.25	0.28	0.12	0.22	0.14	-0.02
21703	0.15	-0.01	0.17	-0.14	-0.06	-0.06	0.06	-0.14	0.08	-0.07	-0.06
21921	-0.41	0.32	0.65	0.12	0.21	0.25	0.26	0.11	0.27	0.15	0.17
24037	-0.49	0.28	0.48	0.07	...	0.19	0.19	0.08	0.15	0.17	0.11
30990	-0.87	...	0.87	0.14	0.34	0.30	0.26	0.16	0.18	0.17	-0.01
33382	-0.05	0.07	-0.01	-0.08	0.07	0.01	0.06	-0.05	0.03	-0.08	-0.04
34511	-0.15	0.19	0.17	-0.03	0.04	0.01	0.05	-0.02	0.08	-0.08	-0.04
35148	-0.30	0.22	0.36	0.02	0.17	0.12	0.06	0.0	0.00	-0.05	-0.03
40023	-0.12	0.01	0.08	0.03	0.03	0.13	0.04	0.05	-0.12	0.08	0.07
42734	-0.70	0.42	0.68	0.19	0.31	0.32	0.24	0.21	0.08	0.22	0.26
47588	-0.47	0.34	0.53	0.23	0.28	0.29	0.20	0.10	0.22	0.16	0.23
52015	-0.02	0.13	0.26	0.09	0.05	0.16	0.11	-0.01	0.02	-0.05	-0.01
53535	0.11	0.25	0.35	0.11	-0.06	0.15	0.17	-0.03	0.04	-0.11	-0.05
54196	-0.39	0.11	0.24	0.01	0.16	0.06	0.04	0.04	-0.05	0.02	0.03
62077	-0.59	0.53	0.76	0.13	0.31	0.27	0.23	0.11	0.25	0.21	0.10
62507	-0.24	0.16	0.27	0.06	0.15	0.14	0.09	0.03	-0.12	-0.03	0.01
64103	-0.21	0.16	0.19	-0.09	0.13	0.04	0.04	-0.03	0.02	-0.02	0.02
74442	-0.23	0.52	0.41	-0.01	0.16	0.10	0.09	0.04	0.03	-0.08	-0.09
74443	-0.59	0.62	0.63	0.13	0.12	0.26	0.25	0.14	0.21	0.26	0.25
80162	-0.66	0.75	0.73	0.10	0.06	0.34	0.31	0.11	0.26	0.25	0.22
82265	0.09	0.05	0.08	-0.06	0.17	0.06	0.05	-0.02	0.11	0.02	0.03
85653	-0.43	0.35	0.45	0.06	...	0.23	0.19	0.13	0.11	0.21	0.19
89583	-0.20	0.05	0.22	0.0	0.27	0.16	0.13	0.04	0.26	0.11	0.06
90745	-0.50	0.42	0.64	0.12	0.36	0.25	0.20	0.10	0.07	0.09	0.04
94615	0.20	-0.01	-0.06	-0.16	-0.01	-0.05	-0.02	-0.06	0.11	-0.02	0.06
99938	-0.54	0.36	0.72	0.05	0.30	0.15	0.16	0.09	0.34	0.17	0.06
102081	0.09	0.12	0.20	-0.04	0.20	0.05	0.05	-0.03	0.00	-0.11	-0.09
107236	-0.50	0.43	0.60	0.10	0.29	0.21	0.22	0.06	0.19	0.09	0.05
115721	-0.46	0.45	0.53	0.11	0.26	0.19	0.16	0.12	0.16	0.08	0.07

Thick Disk/Halo

7452	-1.53	0.78	...	0.18	0.65	0.77	0.20	0.24	0.28	...
14594	-1.88	0.58	0.64	0.28	...	0.50	...
20298	-0.84	0.67	0.93	0.08	0.42	0.41	0.38	0.28	0.20	0.23	0.00
23922	-0.66	...	0.63	0.05	0.29	0.12	0.18	0.13	0.19	0.18	0.08
26617	-0.75	0.50	0.83	0.04	0.23	0.25	0.25	0.19	0.13	0.13	0.08
42864	-1.47	0.95	...	0.40	...	0.55	0.20	...	0.22	0.34
43595	-0.84	0.52	0.71	0.05	0.29	0.32	0.17	0.13	0.12	0.24	0.06
48209	-0.65	0.39	0.66	0.10	0.21	0.24	0.22	0.11	0.22	0.18	0.08
51477	-1.25	1.4	0.14	0.44	0.49	0.53	0.26	0.08	0.11	0.09

Table 6. Abundance ratios $[X/Fe]$ for elements from V to Eu for the programme stars

HIP	[Fe/H]	Cr	Mn	Co	Ni	Cu	Zn	Y	Ba	Ce	Nd	Eu
Thick Disk												
3086	-0.23	-0.04	-0.18	0.02	-0.03	-0.06	0.14	-0.16	-0.15	0.04	0.14	0.23
3185	-0.65	0.08	-0.19	0.12	0.04	-0.09	0.14	0.04	-0.06	0.12	0.34	0.60
3441	-0.50	-0.03	-0.32	0.08	0.05	-0.08	0.23	0.04	-0.09	0.18	0.26	0.42
4039	-1.20	0.07	-0.51	0.28	-0.08	-0.48	0.08	0.05	0.30	0.88
4544	-0.87	-0.09	-0.40	0.13	0.0	-0.05	0.08	-0.02	-0.14	...	0.58	0.53
5122	-0.62	0.00	-0.22	0.11	0.05	0.11	0.09	-0.03	-0.16	-0.02	0.20	0.40
5315	-0.47	0.00	-0.18	0.12	0.03	0.14	0.23	0.07	-0.20	0.08	0.19	0.43
5336	-0.86	0.00	-0.23	0.18	0.12	0.02	0.16	-0.02	-0.23	0.05	0.14	0.34
5775	-0.58	0.06	-0.16	0.12	0.04	0.00	0.21	0.22	0.08	0.07	...	0.43
6159	-0.67	-0.04	-0.26	0.06	0.04	0.03	0.08	-0.01	-0.14	0.22	0.25	0.46
6607	-0.41	-0.01	-0.15	0.14	0.04	0.02	0.01	0.06	-0.08	0.21	0.36	0.41
7961	-0.64	-0.01	-0.28	0.07	0.02	-0.2	0.1	-0.03	-0.20	-0.04	0.07	0.28
8674	-0.60	-0.03	-0.24	0.08	-0.01	0.01	0.26	0.69	0.57	0.64	0.89	0.45
9080	-0.37	-0.05	-0.04	0.10	0.11	0.03	0.02	-0.28	-0.11	0.21	0.27	0.19
10652	-0.67	-0.01	-0.33	0.06	0.02	-0.02	0.10	-0.07	-0.09	-0.07	...	0.39
12579	-0.80	-0.08	-0.42	0.17	-0.05	-0.09	0.11	0.05	-0.04	-0.05	0.20	0.37
13366	-0.70	-0.06	-0.30	0.06	-0.01	-0.05	0.14	-0.07	-0.15	-0.10	0.18	0.29
15126	-0.82	-0.04	-0.40	0.11	-0.03	-0.14	0.13	-0.05	-0.07	0.49
15405	-0.73	-0.05	-0.30	0.07	-0.03	0.04	0.11	-0.13	-0.12	0.16	0.08	0.24
17147	-0.87	-0.03	-0.39	0.11	-0.02	-0.08	0.15	0.22	0.00	0.13	0.25	0.42
17666	-1.0	-0.03	-0.29	0.22	-0.01	-0.13	0.21	0.31	0.11	0.25	0.43	0.57
22020	-0.35	-0.03	-0.23	0.09	-0.01	0.04	0.11	-0.13	-0.06	0.02	...	0.21
22060	-0.63	-0.07	-0.28	0.02	0.00	0.00	0.14	0.10	-0.05	0.23	-0.02	0.47
23080	-0.32	-0.03	-0.13	0.15	0.04	0.09	0.11	0.08	-0.06	0.24	0.16	0.40
24030	-1.0	-0.05	-0.53	0.02	0.04	-0.33	0.13	0.21	0.02
25860	-0.35	0.01	-0.20	0.16	0.04	0.10	0.17	0.07	-0.08	0.26	0.22	0.35
26452	-0.89	-0.03	-0.38	0.2	-0.01	-0.08	0.13	0.09	-0.20	...	0.24	0.41
26828	-0.34	-0.07	-0.28	0.05	-0.04	-0.10	0.02	-0.13	-0.12	0.13
27128	-0.81	-0.14	-0.39	0.16	-0.02	-0.09	0.11	-0.02	-0.12	-0.01	...	0.40
29269	-0.68	0.00	-0.28	0.05	0.01	-0.03	0.17	-0.14	-0.10	-0.08	0.07	0.29
31188	-0.59	-0.12	-0.15	0.03	-0.06	-0.07	-0.02	-0.06	-0.07	-0.01	0.04	0.17
34642	-0.44	-0.04	-0.27	0.02	-0.02	-0.10	-0.04	-0.16	0.00	-0.23	0.08	0.15
35989	-0.19	-0.04	-0.11	-0.02	-0.03	-0.25	-0.02	-0.33	-0.21	0.18	0.01	0.13
36849	-0.77	-0.14	-0.40	0.02	-0.04	-0.10	0.10	-0.10	-0.12	0.02	...	0.39
37233	-0.51	0.00	-0.27	0.10	0.02	-0.04	-0.03	-0.11	-0.12	-0.12	0.04	0.36
38769	-0.79	-0.06	-0.54	0.02	0.01	0.0	0.17	-0.05	-0.12	0.00	...	0.26
39893	-0.84	-0.02	-0.25	0.16	0.02	-0.05	0.19	-0.16	-0.14	0.18	0.31	0.53
40613	-0.62	-0.03	-0.31	0.09	-0.04	-0.04	0.10	-0.05	-0.19	-0.15	0.07	0.24
43393	-0.59	-0.01	-0.28	0.09	0.02	0.02	0.10	-0.10	-0.22	-0.02	0.15	0.33
44075	-0.86	-0.07	-0.35	0.11	-0.06	-0.12	0.10	0.09	-0.06	0.12	0.14	0.35
44347	-0.85	-0.08	-0.43	0.21	0.05	-0.13	0.19	0.13	0.10	0.13	0.35	0.52
44860	-0.51	0.00	-0.20	0.14	0.05	0.09	0.17	0.09	-0.10	0.08	0.08	0.39
45947	-0.46	0.04	-0.21	0.06	0.03	0.22	0.13	0.06	-0.11	-0.04	0.13	0.57
50005	-0.53	0.02	-0.22	0.23	0.03	0.14	0.05	0.09	-0.19	0.42
50671	-0.48	-0.02	-0.13	-0.02	0.02	0.05	0.09	-0.05	0.03	-0.01	0.02	0.17
50965	-0.57	-0.04	-0.22	0.13	0.02	0.00	0.10	0.03	-0.07	0.02	...	0.34
52673	-0.66	0.02	-0.20	0.11	0.04	0.02	0.23	0.15	-0.01	0.03	0.19	0.40
58843	-0.79	0.00	-0.33	0.13	0.03	-0.03	0.09	0.18	0.00	0.08	0.09	0.44
59233	-0.83	0.07	-0.08	0.06	-0.01	0.02	0.17	-0.40	-0.25	-0.08	0.05	0.12
59750	-0.74	-0.09	-0.35	0.09	0.02	-0.08	0.12	0.07	-0.14	0.32
60268	-0.72	0.02	-0.26	0.10	0.05	0.08	0.17	0.00	-0.14	0.07	0.17	0.41
60956	-0.58	-0.02	-0.18	0.08	0.05	0.04	0.15	0.06	-0.10	0.22	0.29	0.44
62240	-0.83	0.03	-0.32	0.19	0.07	-0.11	0.04	0.04	-0.28	0.21	0.22	0.57
64426	-0.71	-0.09	-0.36	0.09	-0.04	-0.08	0.04	-0.07	-0.21	0.09	0.21	0.21
65449	-0.44	0.03	-0.22	0.04	-0.01	0.09	0.04	-0.16	-0.14	-0.27	0.00	0.29
70520	-0.62	0.00	-0.25	0.12	0.01	-0.02	0.09	-0.06	-0.22	0.11	0.07	0.28
70681	-1.1	-0.06	-0.47	0.07	-0.01	-0.33	0.08	0.29	0.10	...	0.34	0.53
71819	-0.14	-0.01	-0.07	0.02	0.0	0.01	0.02	-0.02	-0.06	0.03	0.16	0.03
72407	-0.54	0.05	-0.20	0.14	0.10	0.08	0.17	0.13	-0.13	0.09	0.29	0.56
72803	-0.73	-0.05	-0.26	0.11	0.09	0.01	0.09	-0.01	-0.28	0.07	0.19	0.42
74033	-0.85	0.00	-0.35	0.20	0.03	-0.09	0.18	0.17	-0.11	0.02	0.19	0.34
74067	-0.75	-0.06	-0.32	0.01	0.01	-0.07	0.14	0.09	-0.10	0.14	0.21	0.48

Table 6 – *continued*

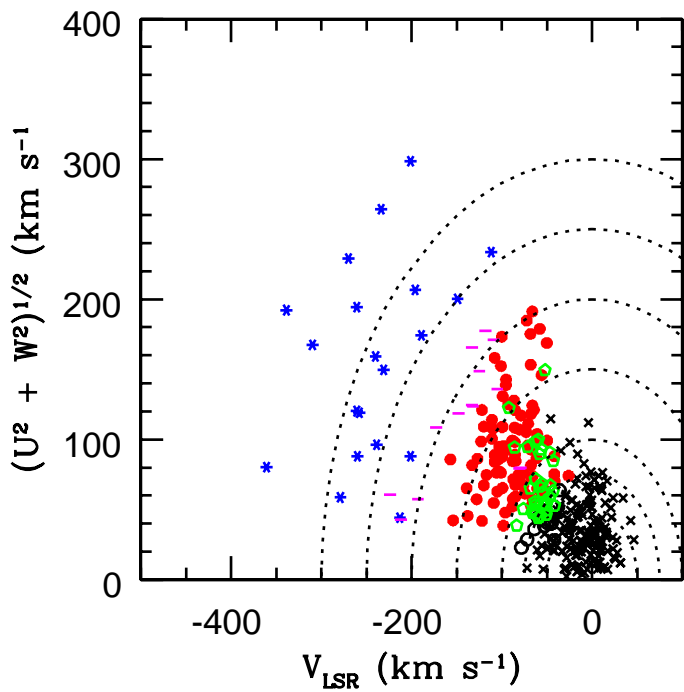
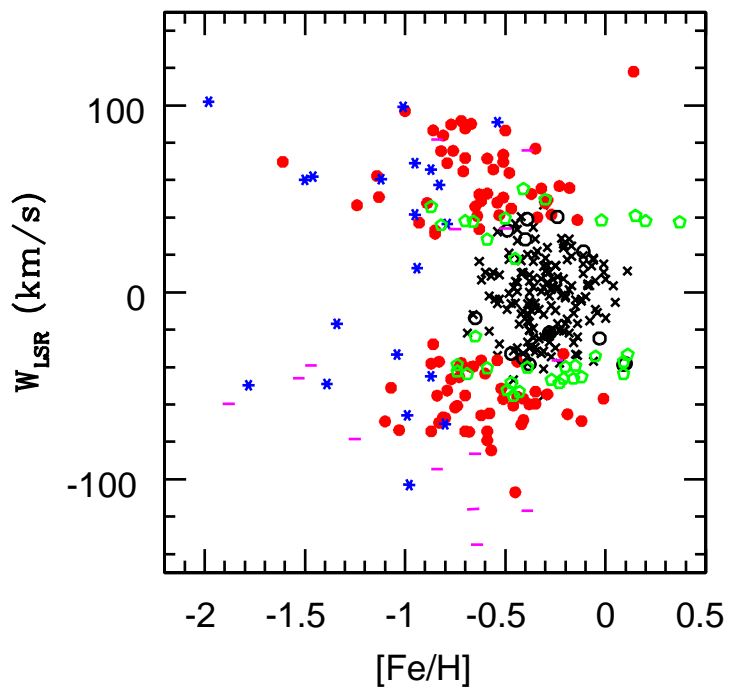
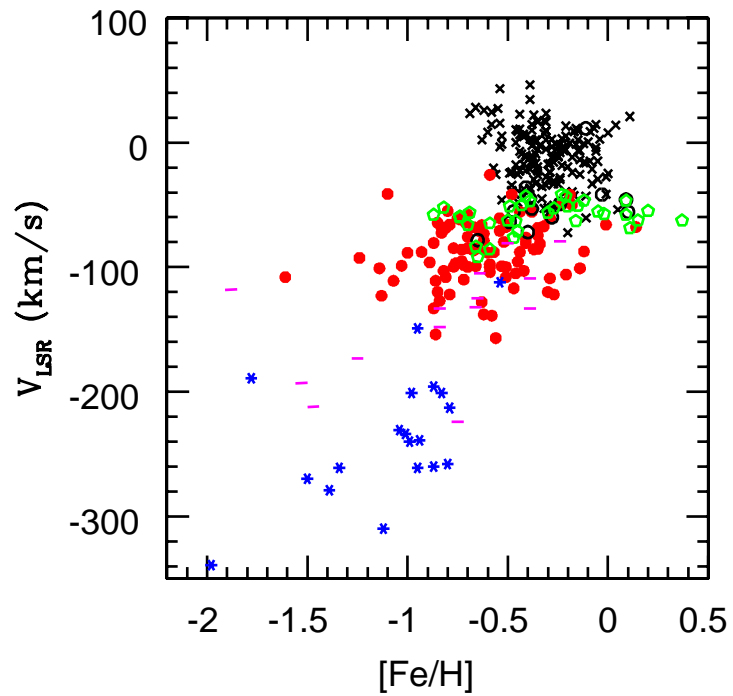
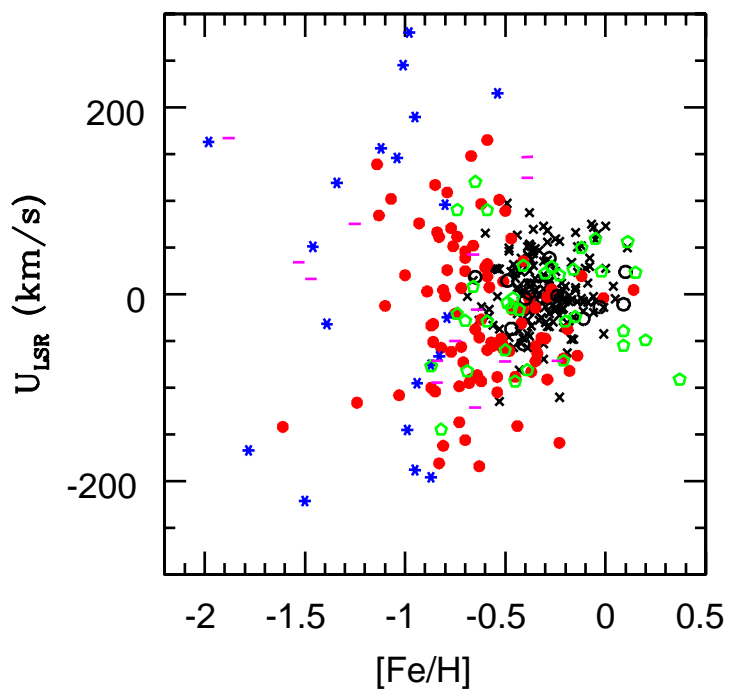
HIP	[Fe/H]	Cr	Mn	Co	Ni	Cu	Zn	Y	Ba	Ce	Nd	Eu
84862	-0.41	-0.03	-0.24	0.12	0.04	0.02	0.26	0.10	-0.12	0.06	0.32	0.45
85373	-0.82	0.04	-0.30	0.23	0.08	-0.2	0.10	0.05	-0.31	...	0.63	0.71
85378	-0.51	-0.04	-0.24	0.09	0.04	-0.02	0.09	-0.01	-0.15	0.08	0.22	0.36
85757	-0.70	-0.03	-0.29	0.10	0.03	-0.02	0.10	0.03	-0.17	-0.10	0.14	0.09
86013	-0.70	-0.11	-0.32	0.08	-0.03	-0.13	0.11	0.02	-0.13	-0.02	0.30	0.35
86830	-0.59	0.01	-0.22	0.14	0.05	0.00	0.04	-0.09	-0.27	-0.07	0.10	0.25
87089	-0.30	-0.03	-0.05	0.12	0.06	0.06	0.04	0.05	-0.10	0.32	0.28	0.46
87533	-0.21	-0.01	-0.12	-0.04	-0.02	-0.04	-0.01	-0.13	-0.14	-0.08	-0.06	-0.06
88039	-0.81	-0.09	-0.35	0.07	0.04	-0.07	0.22	0.01	-0.14	0.04	0.09	0.26
88166	-0.76	-0.01	-0.27	0.11	0.03	-0.05	0.14	0.09	-0.21	0.26	0.17	0.52
90393	-0.72	0.05	-0.15	0.14	0.05	-0.06	0.04	0.09	-0.24	0.23	0.61	...
94129	-0.27	-0.01	-0.17	0.10	0.01	0.03	0.13	0.00	0.06	-0.04	0.08	0.30
96185	-0.56	-0.09	-0.32	0.10	0.0	-0.03	0.04	0.01	-0.34	-0.06	0.17	0.20
96902	-0.29	-0.02	-0.17	0.09	0.03	0.09	0.08	-0.15	-0.22	-0.06	-0.02	0.14
97846	-0.18	0.01	0.02	0.08	0.04	0.08	0.19	-0.08	-0.02	0.03	0.19	0.12
98020	-1.6	-0.16	-0.48	0.16	0.00	-0.66	0.56	-0.01	-0.04	0.65	0.57	...
98532	-1.13	-0.03	-0.44	0.03	0.00	-0.40	0.07	0.20	0.04	0.05	0.23	0.31
99224	-0.12	-0.04	-0.16	0.02	-0.02	0.05	0.07	-0.04	-0.12	0.00	0.14	0.08
104659	-0.95	-0.19	-0.56	-0.06	-0.05	-0.23	0.11	-0.12	-0.18	0.27
106947	-0.39	-0.02	-0.05	0.12	0.05	0.11	0.13	0.0	0.05	0.28	0.24	0.47
107294	-1.14	-0.03	-0.28	0.25	0.11	-0.50	0.04	0.22	0.11
108056	0.14	-0.06	-0.14	-0.03	-0.01	0.04	0.04	0.06	0.15	-0.05	...	-0.12
109384	-0.38	-0.04	-0.06	0.16	0.04	0.04	0.19	0.13	-0.2	0.29	0.17	0.34
110291	-0.93	-0.12	-0.41	0.04	-0.04	-0.21	0.09	0.03	-0.03	...	0.03	0.40
111517	-0.49	0.06	-0.13	0.18	0.09	0.16	0.16	-0.08	-0.22	-0.11	-0.02	0.36
112666	-0.42	-0.03	-0.14	0.09	-0.01	0.01	0.07	-0.09	-0.13	0.27	0.16	0.43
112811	-0.63	-0.10	-0.37	0.07	-0.02	-0.11	0.00	0.07	-0.19	-0.10	-0.05	0.28
113514	-0.64	-0.05	-0.24	0.04	0.0	0.08	0.16	0.08	-0.03	0.07	0.35	0.43
116421	-0.50	-0.01	-0.24	0.12	0.03	0.0	0.07	0.03	-0.13	0.0	0.19	0.23
117029	-0.76	-0.02	-0.31	0.13	0.04	-0.03	0.11	-0.04	-0.27	0.05	0.18	0.25
Thin Disk												
2909	-0.28	-0.01	-0.15	0.08	0.03	0.04	-0.01	-0.08	-0.12	0.02	0.12	0.16
14086	-0.65	0.01	-0.23	0.14	0.05	0.07	0.06	0.09	-0.18	0.06	0.28	0.39
14241	-0.49	-0.01	-0.19	0.15	0.04	0.15	0.16	0.16	-0.06	0.13	0.22	0.48
19696	-0.24	-0.01	-0.14	0.06	0.00	0.10	0.19	0.08	0.02	0.07	0.20	0.25
26437	0.10	0.00	-0.05	-0.04	0.00	-0.02	-0.11	-0.05	-0.13	-0.16	0.02	-0.08
39616	-0.41	-0.05	-0.15	-0.02	-0.04	-0.06	0.06	0.05	0.12	0.21	0.27	0.12
40118	-0.47	-0.05	-0.19	0.10	0.01	0.10	0.16	0.00	-0.06	0.17	0.32	0.38
64924	-0.03	-0.03	-0.06	0.01	-0.05	0.00	0.07	-0.08	0.03	0.17	0.26	0.15
73078	-0.11	-0.04	-0.07	0.04	0.05	0.02	0.02	-0.09	-0.41	0.13	0.18	-0.10
74933	-0.39	-0.08	-0.20	-0.02	-0.04	-0.03	0.09	0.02	0.05	0.04	0.16	0.24
81681	-0.38	-0.05	-0.22	0.09	0.04	0.10	0.12	0.05	-0.15	0.10	0.35	0.30
84506	0.09	0.02	-0.07	0.08	0.06	0.15	0.05	0.01	-0.08	0.03	0.00	-0.11
86568	-0.40	-0.05	-0.16	0.17	0.04	0.04	0.13	-0.07	-0.07	0.20	0.18	0.49
Halo												
3026	-1.0	-0.21	-0.52	0.31	-0.01	...	0.03	0.06	0.09
10449	-0.87	-0.01	-0.41	0.13	-0.06	-0.20	0.14	0.07	-0.01	0.29	...	0.49
12294	-0.95	0.09	-0.35	...	0.04	-0.37	...	0.01	-0.12	...	0.80	...
16072	-1.39	-0.02	-0.28	...	-0.01	-0.32	0.33	0.36	0.14
28671	-1.01	0.02	-0.48	0.01	-0.03	-0.42	0.15	0.10	-0.15	0.42
52771	-2.0	...	-0.47	0.78	-0.06	...	0.17	...	-0.27
55592	-0.94	-0.11	-0.42	-0.02	-0.05	-0.34	0.17	0.09	0.13	0.12	...	0.40
57450	-1.50	-0.09	-0.40	...	-0.11	-0.36	0.08	-0.04	-0.05

Table 6 – *continued*

HIP	[Fe/H]	Cr	Mn	Co	Ni	Cu	Zn	Y	Ba	Ce	Nd	Eu
58229	-0.83	-0.35	-0.40	0.26	-0.05	-0.44	0.02	0.03	-0.13
62882	-0.98	-0.07	-0.61	-0.15	-0.08	-0.55	0.12	0.08	-0.06	0.07	0.10	0.12
73385	-1.46	0.18	-0.39	...	0.07	-0.46	0.20	0.20	0.07	0.27	...	0.31
78640	-1.34	...	-0.34	0.41	-0.03	...	-0.07	-0.07	-0.28	...	0.14	0.06
80837	-0.80	0.05	-0.27	0.22	0.04	0.01	0.15	0.06	-0.13	-0.05	0.14	0.29
86321	-0.87	-0.07	-0.34	0.20	-0.04	-0.43	0.08	0.07	0.03	0.36
86431	-0.54	-0.08	-0.23	0.05	-0.05	-0.03	0.07	0.00	-0.07	0.03	0.33	0.30
94449	-1.12	-0.08	-0.36	0.14	-0.01	-0.40	0.03	-0.12	-0.27	0.11	...	0.10
100568	-0.99	-0.06	-0.51	-0.07	-0.12	-0.45	-0.06	-0.17	-0.23	0.11	0.14	0.41
109067	-0.73	-0.16	-0.40	0.06	-0.05	-0.22	0.1	0.13	-0.10	0.04	0.01	...
111549	-0.95	-0.04	-0.34	-0.06	-0.07	-0.40	-0.03	-0.29	-0.24	...	-0.01	0.27
115704	-1.78

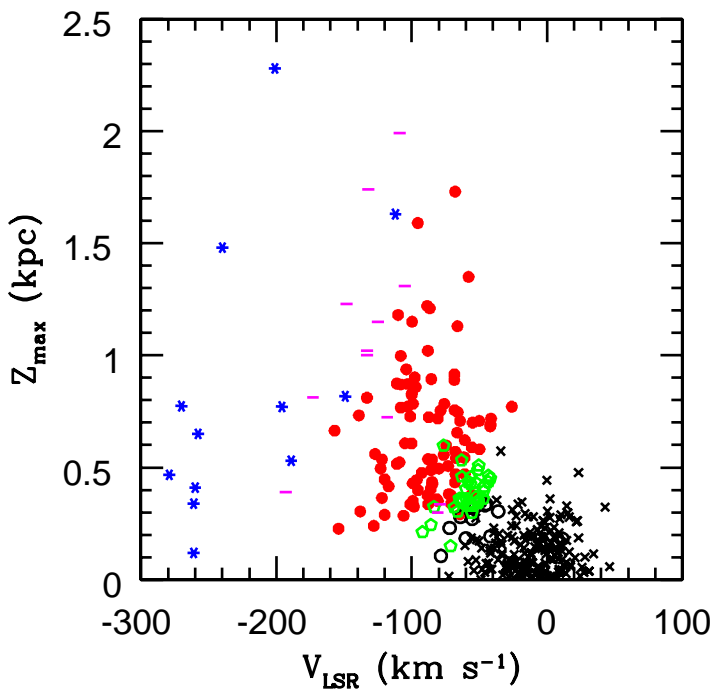
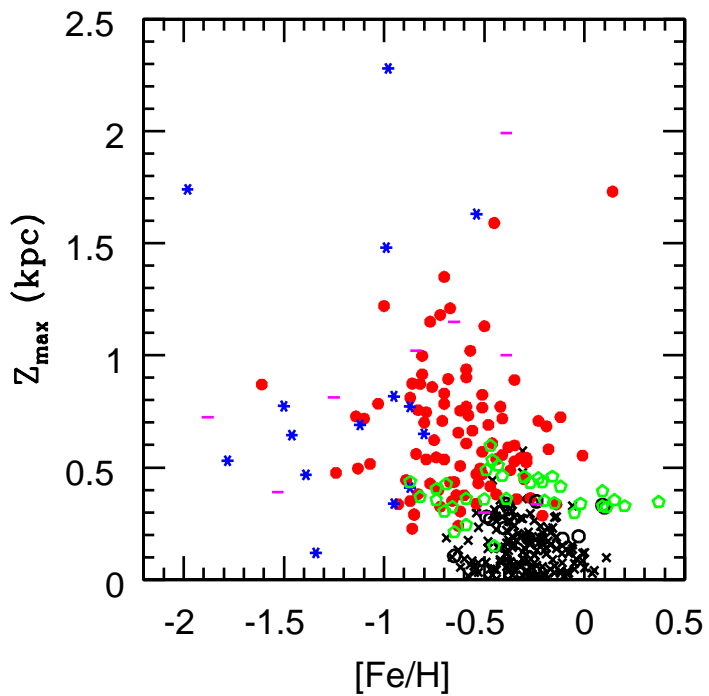
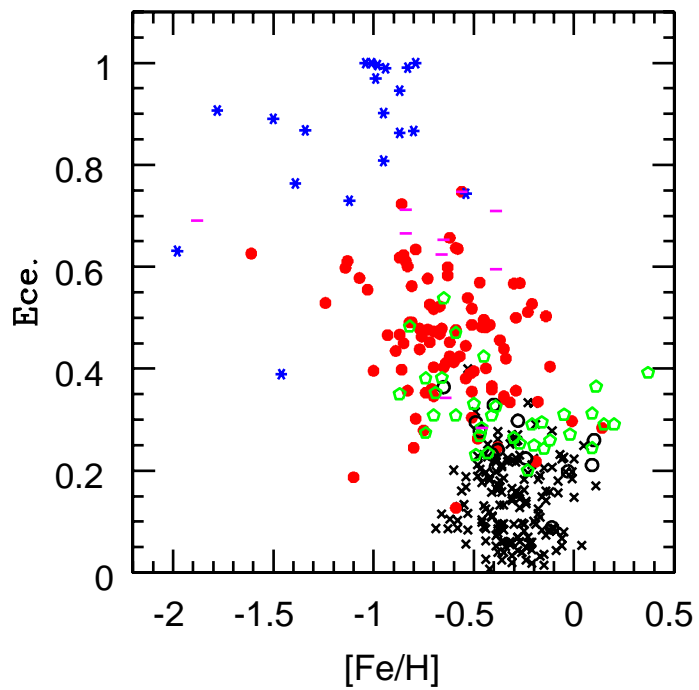
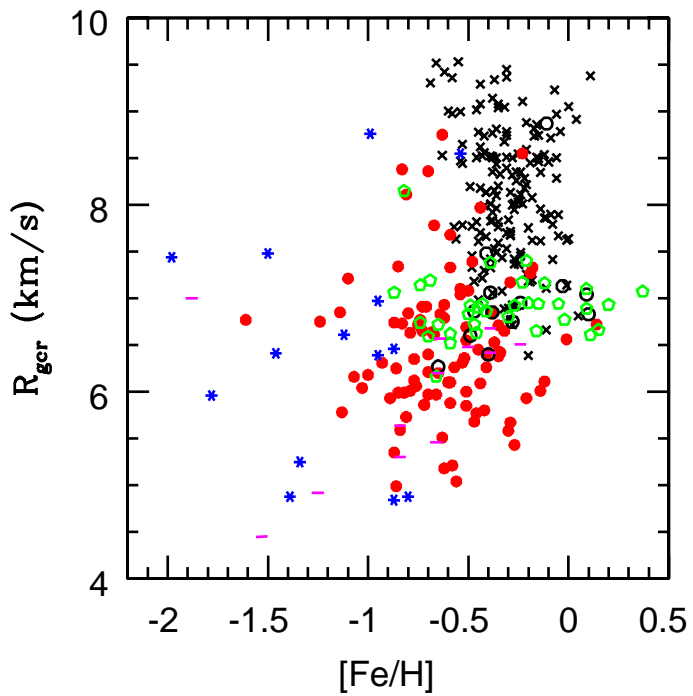
Thin/Thick Disk												
5163	-0.74	0.00	-0.25	0.10	0.06	0.07	0.06	0.03	-0.09	0.25	...	0.38
8720	-0.74	-0.03	-0.19	0.25	0.07	-0.01	0.13	0.02	-0.20	0.17	0.15	0.45
10711	-0.69	-0.11	-0.42	0.11	-0.06	-0.13	0.11	0.02	-0.13	0.13	...	0.27
12381	-0.16	-0.06	-0.25	0.0	-0.09	-0.01	-0.07	0.12	-0.02	-0.27	...	0.14
15394	-0.27	0.00	-0.09	0.02	0.01	-0.02	0.12	-0.08	-0.15	0.02	0.09	0.09
16738	0.37	-0.01	0.01	0.03	0.06	0.22	0.18	-0.08	0.12
21227	-0.45	-0.12	-0.26	0.0	-0.02	-0.04	0.03	0.02	-0.08	0.08	0.49	0.37
21306	-0.67	-0.05	-0.33	0.08	0.02	-0.05	0.17	0.07	-0.10	0.24	0.24	0.29
21703	0.15	-0.08	-0.09	-0.01	0.01	-0.01	-0.01	0.13	-0.04	0.14	0.15	0.14
21921	-0.41	-0.01	-0.20	0.12	0.03	0.02	0.11	0.06	-0.13	0.12	0.39	0.47
24037	-0.49	-0.01	-0.19	0.13	0.04	0.15	0.14	0.05	-0.07	0.06	0.33	0.38
30990	-0.87	-0.07	-0.48	0.14	-0.01	-0.15	0.12	-0.10	-0.21	0.04	...	0.29
33382	-0.05	-0.05	-0.12	-0.01	-0.03	0.01	-0.08	-0.04	-0.04	0.04	0.13	0.08
34511	-0.15	-0.03	-0.09	-0.06	-0.05	-0.01	-0.03	0.11	0.11	0.09	0.25	0.11
35148	-0.30	-0.06	-0.17	-0.04	-0.07	-0.06	-0.07	-0.16	-0.15	-0.12	0.05	0.08
40023	-0.12	0.04	-0.04	0.02	-0.03	0.08	-0.10	-0.18	-0.04	-0.07	-0.01	-0.05
42734	-0.70	0.05	-0.23	0.12	0.01	0.01	0.11	-0.14	-0.13	-0.01	0.02	0.34
47588	-0.47	-0.03	-0.22	0.19	0.02	0.08	0.10	-0.05	-0.19	-0.20	0.07	0.26
52015	-0.02	0.00	-0.04	0.04	-0.01	0.05	0.02	-0.08	-0.10	-0.02	0.06	-0.03
53535	0.11	0.00	-0.08	0.07	0.01	0.10	0.02	-0.13	-0.11	-0.06	0.20	-0.16
54196	-0.39	-0.04	-0.21	0.04	-0.04	0.00	0.03	-0.10	-0.14	-0.13	-0.03	0.17
62077	-0.59	-0.02	-0.22	0.17	0.02	0.10	0.09	-0.03	0.01	0.05	...	0.36
64103	-0.21	-0.06	-0.13	-0.06	-0.05	-0.03	0.01	-0.05	-0.02	0.11	0.14	0.17
74442	-0.23	-0.06	-0.13	-0.05	-0.02	-0.02	0.05	-0.02	-0.14	0.08	0.0	0.07
74443	-0.59	0.01	-0.08	0.20	0.06	0.00	0.13	-0.06	-0.22	-0.03	0.07	0.44
80162	-0.66	-0.02	-0.17	0.12	0.08	0.05	0.16	-0.01	-0.20	0.15	0.15	0.41
82265	0.09	-0.03	-0.04	0.04	0.01	0.04	-0.03	0.01	-0.04	0.14	0.14	0.22
85653	-0.43	0.00	-0.22	0.13	0.05	0.11	0.12	0.37	0.17	0.10	0.39	0.41
89583	-0.20	-0.05	-0.15	0.10	0.03	0.11	0.03	0.03	-0.04	0.06	0.19	0.40
90745	-0.50	-0.01	-0.20	0.06	0.02	0.04	0.06	-0.02	-0.11	-0.04	0.07	0.22
94615	0.20	0.01	-0.07	1.3	-0.02	0.06	-0.02	0.07	0.12	0.23	0.19	0.06
99938	-0.54	-0.10	-0.26	0.03	0.0	-0.03	0.06	0.02	-0.08	0.05	0.21	0.37
102081	0.09	-0.06	-0.09	0.0	-0.03	-0.03	0.04	0.04	-0.02	0.00	-0.04	-0.01
115721	-0.46	-0.01	-0.29	0.04	-0.01	0.11	0.17	-0.02	-0.02	0.07	0.05	0.30

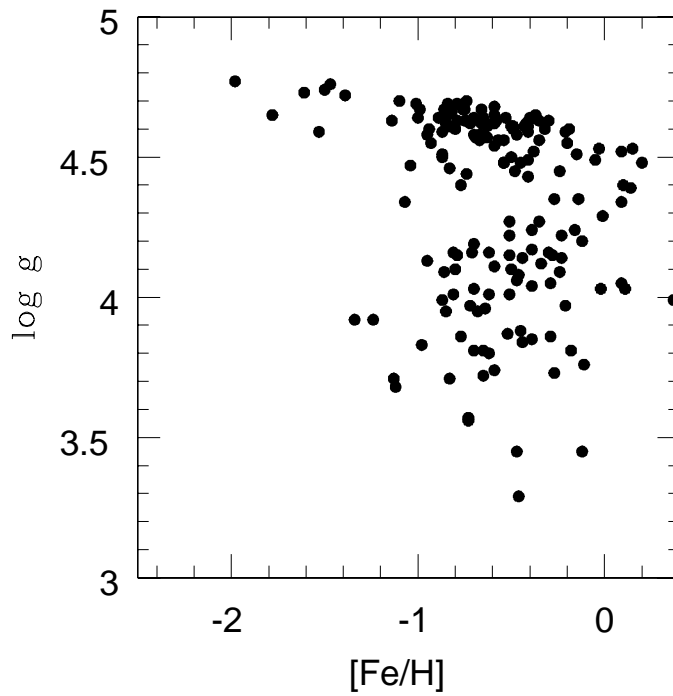
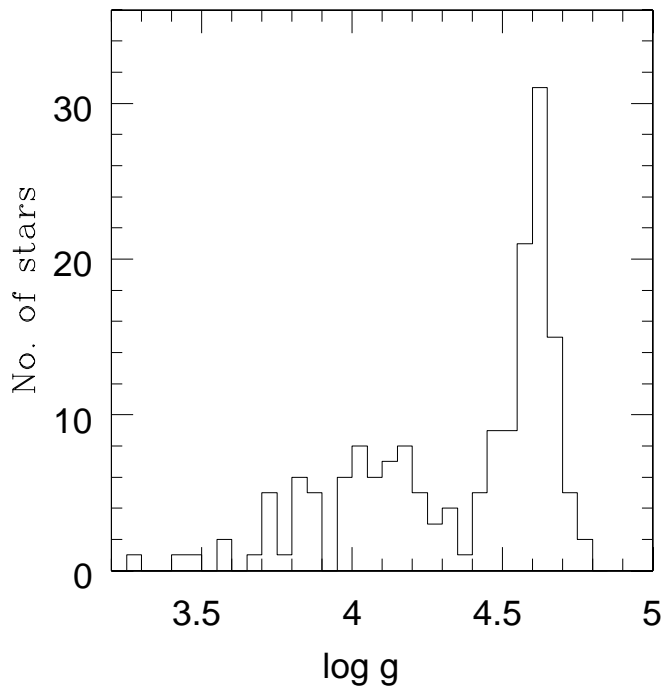
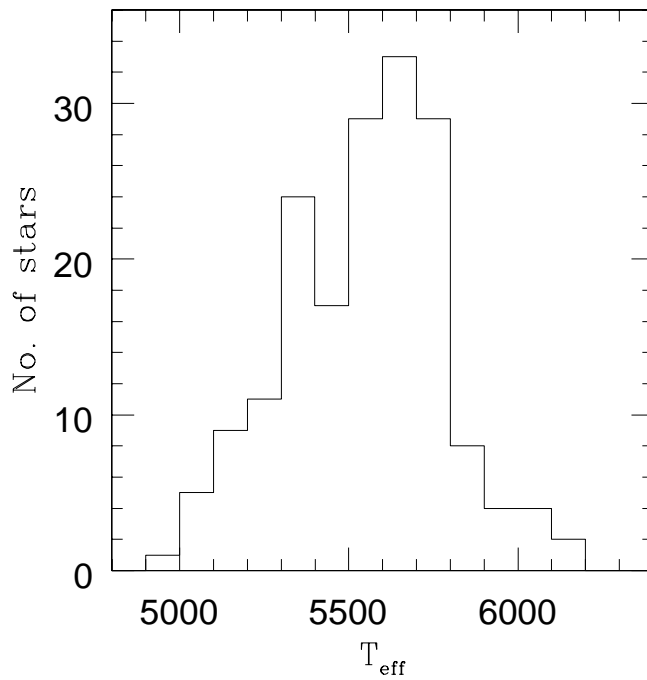
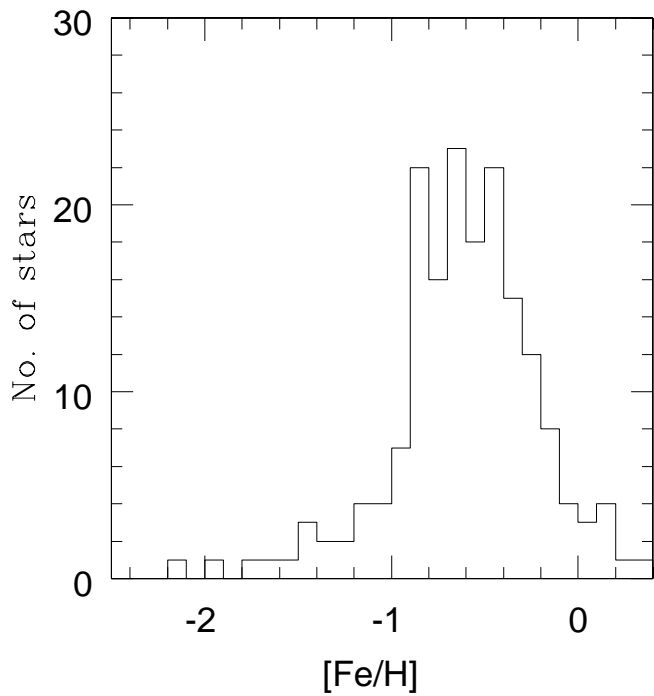
Thick Disk/Halo												
7452	-1.53	0.38	0.02	0.23	-0.01	0.12
14594	-1.88	0.91	0.44	...	0.33	...	-0.16	1.0e+03	1.0e+03	1.0e+03
20298	-0.84	-0.04	-0.43	0.07	-0.07	0.05	0.20	0.34	-0.02	0.16	0.28	0.29
23922	-0.66	-0.08	-0.31	0.07	-0.02	-0.04	0.17	0.09	-0.11	-0.09	0.11	0.35
26617	-0.75	-0.05	-0.30	0.18	0.0	-0.21	0.09	0.12	-0.06	0.21	0.25	0.39
42864	-1.47	-0.17	-0.58	...	0.24	-0.16	0.39	...	0.04
43595	-0.84	-0.04	-0.29	0.14	-0.01	-0.03	0.20	0.07	-0.11	0.26	0.23	0.36
48209	-0.65	-0.01	-0.18	0.09	0.06	0.06	0.12	0.04	-0.09	0.09	0.10	0.35
51477	-1.2	0.00	-0.47	0.15	0.01	-0.24	0.22	0.26	0.02	0.11	0.25	0.29
60331	-0.64	0.21	-0.35	0.17	-0.06	...	0.28	-0.05	-0.25	-0.08	...	0.58
62507	-0.24	-0.04	-0.12	0.01	-0.02	0.04	0.12	0.16	0.17	0.20	0.07	0.05

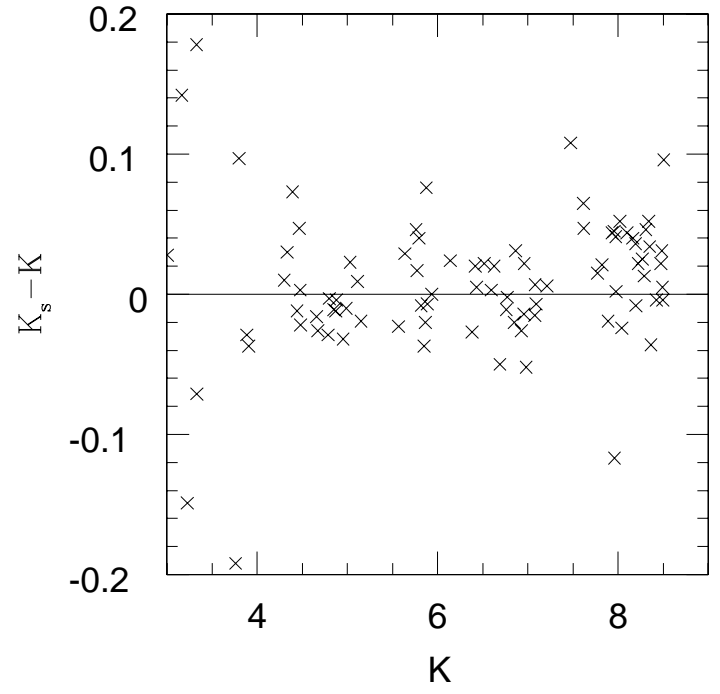
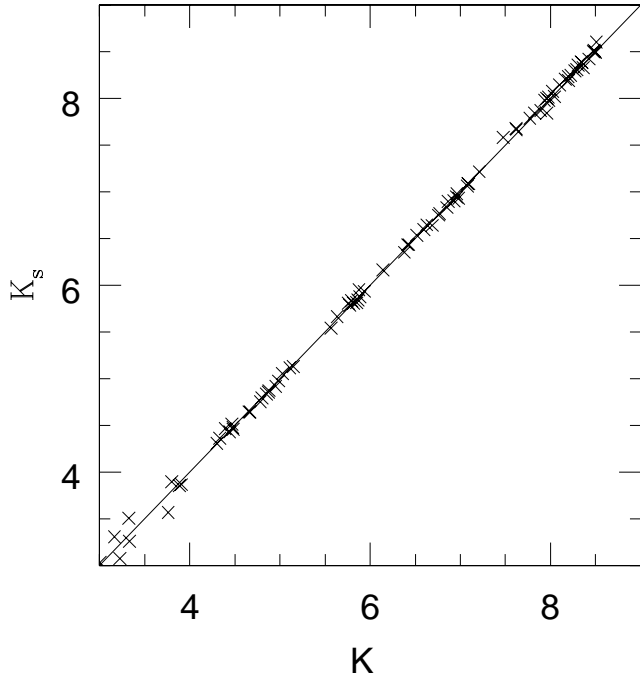


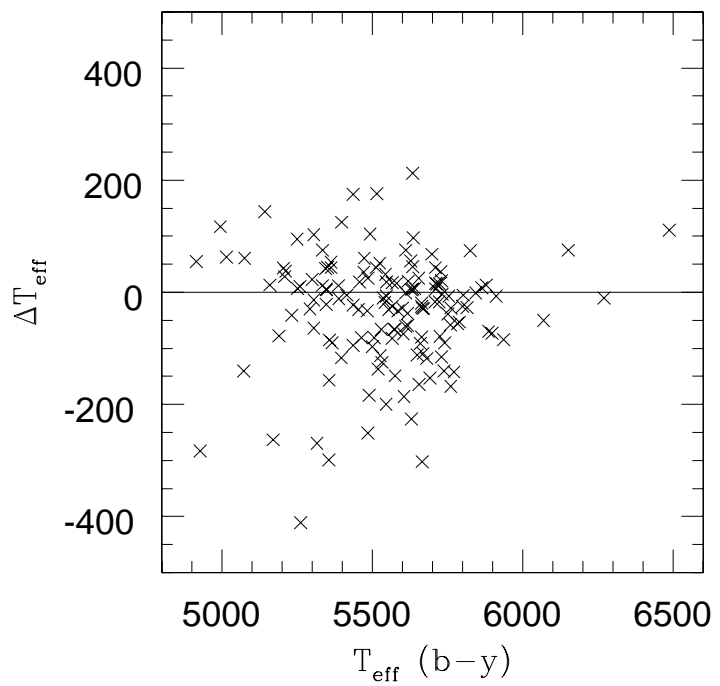
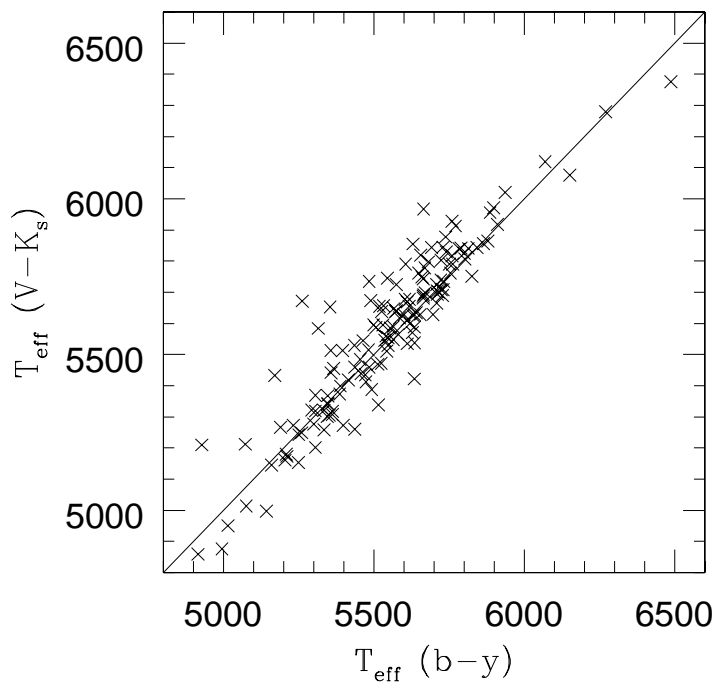
This figure "reddy_fig2.jpg" is available in "jpg" format from:

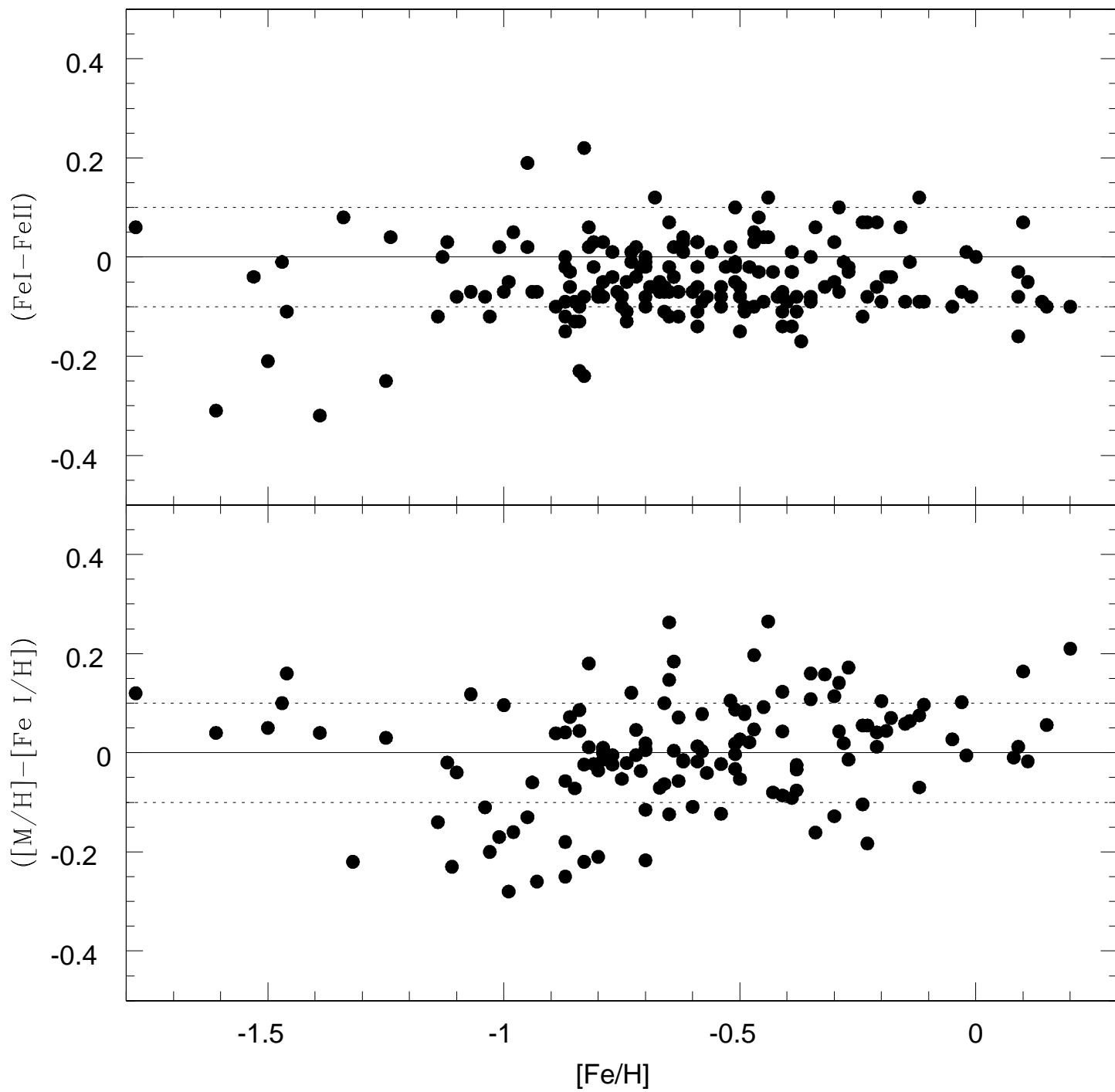
<http://arxiv.org/ps/astro-ph/0512505v1>

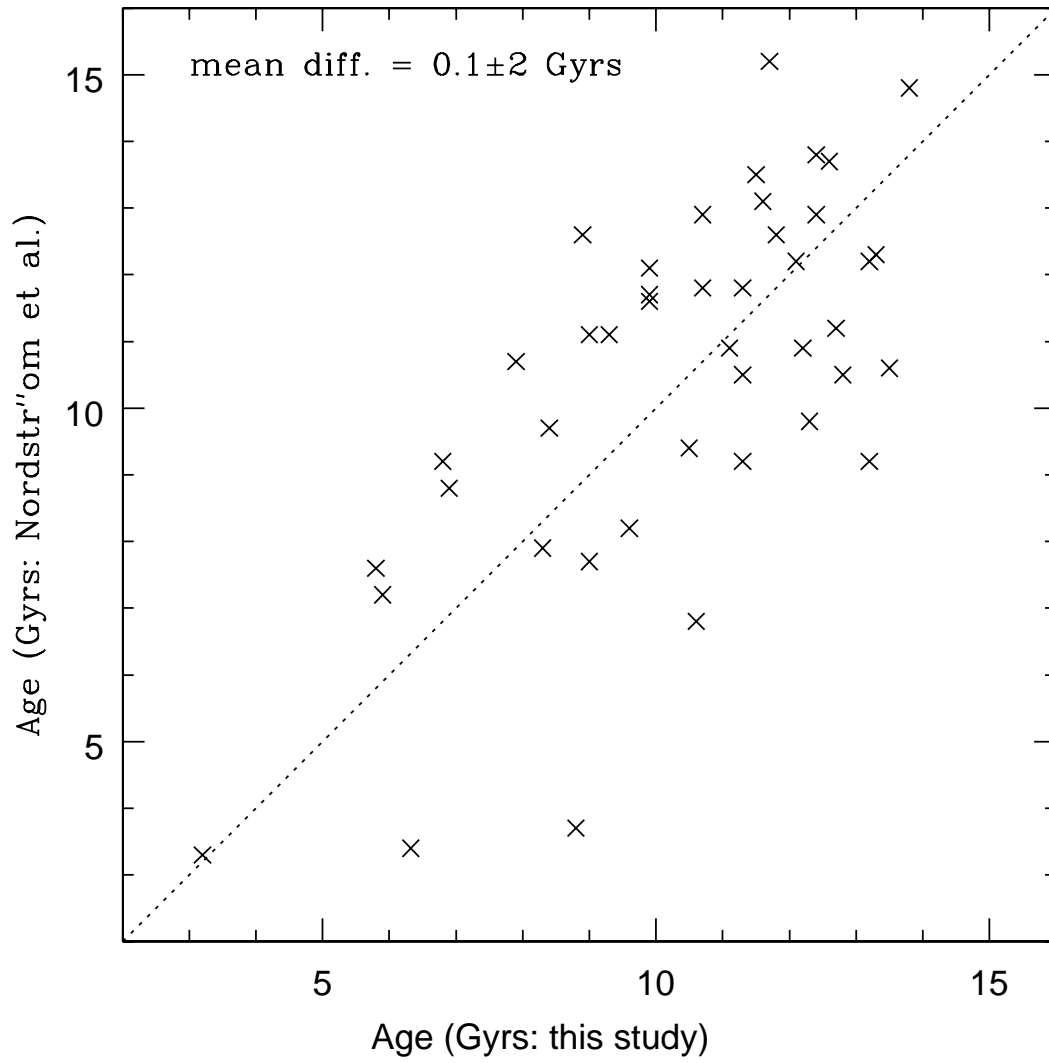


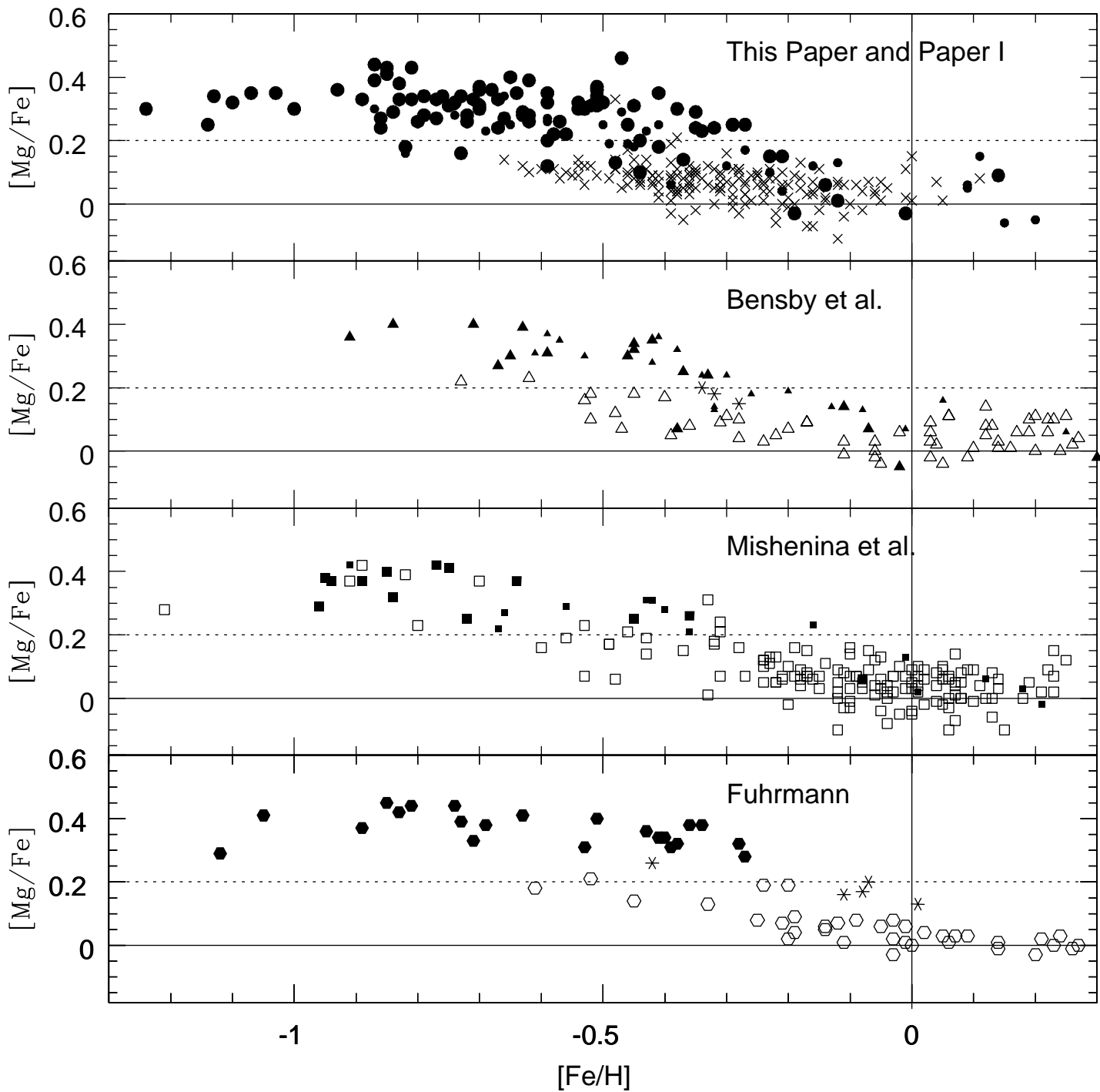


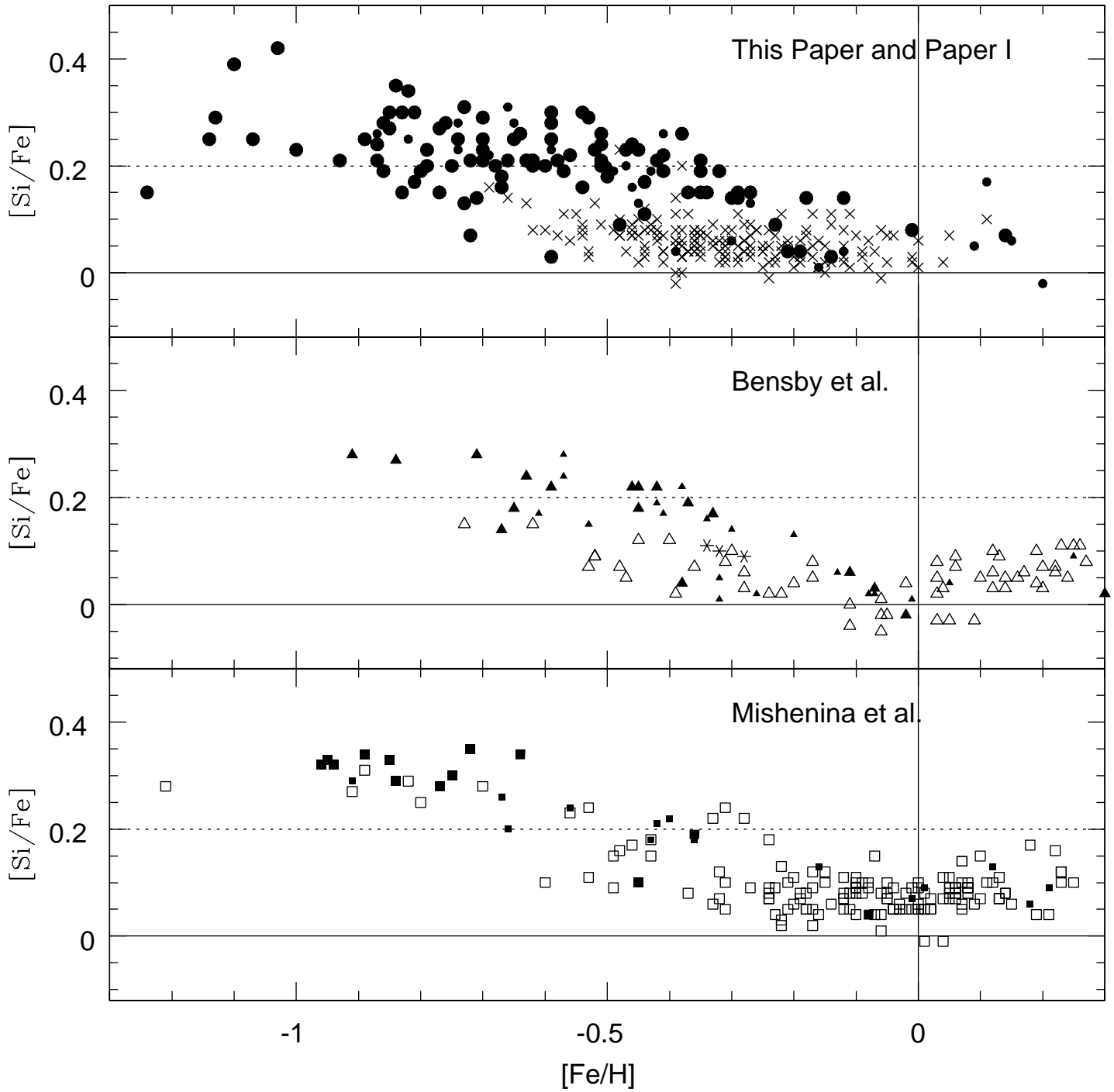


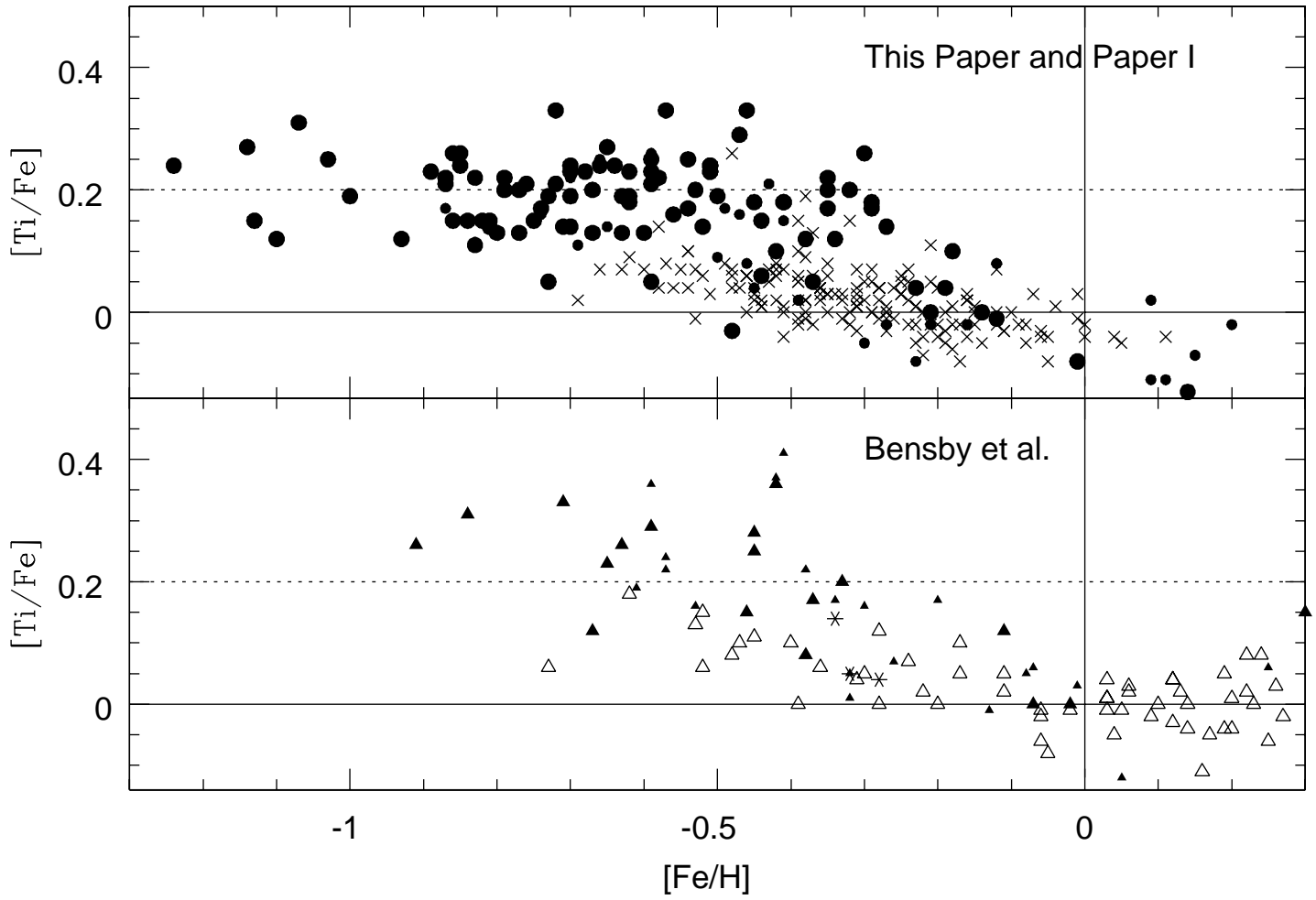


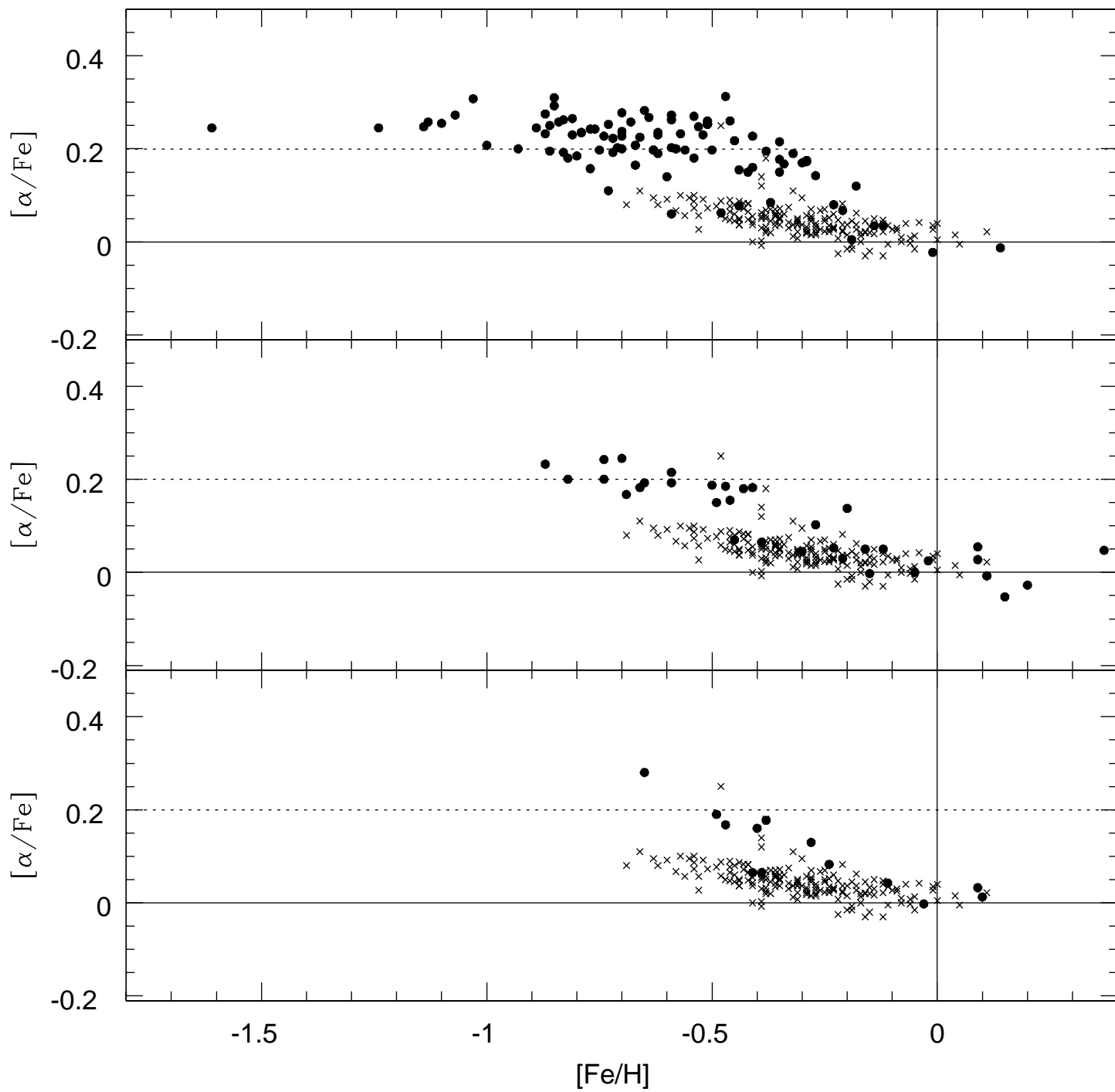


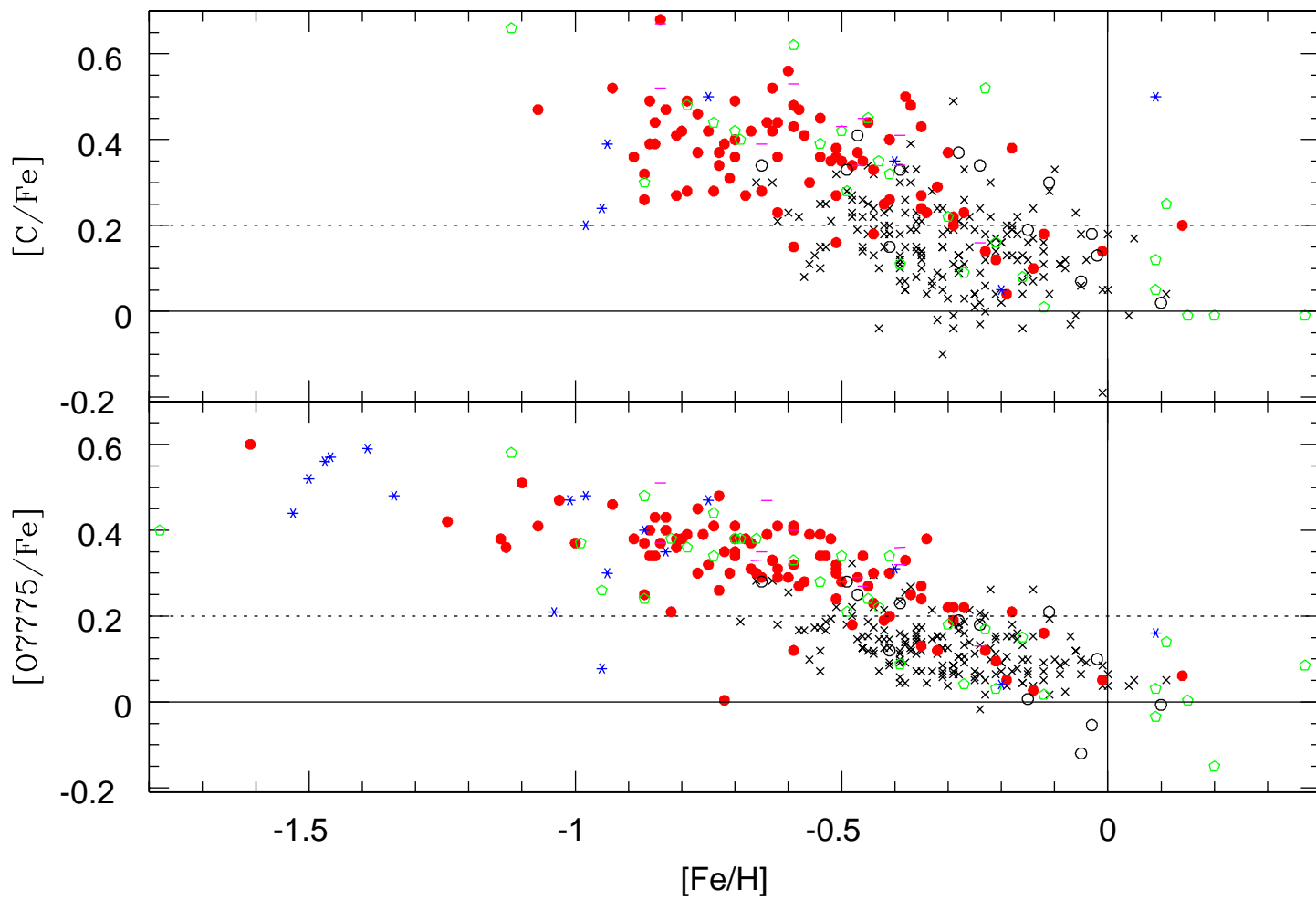


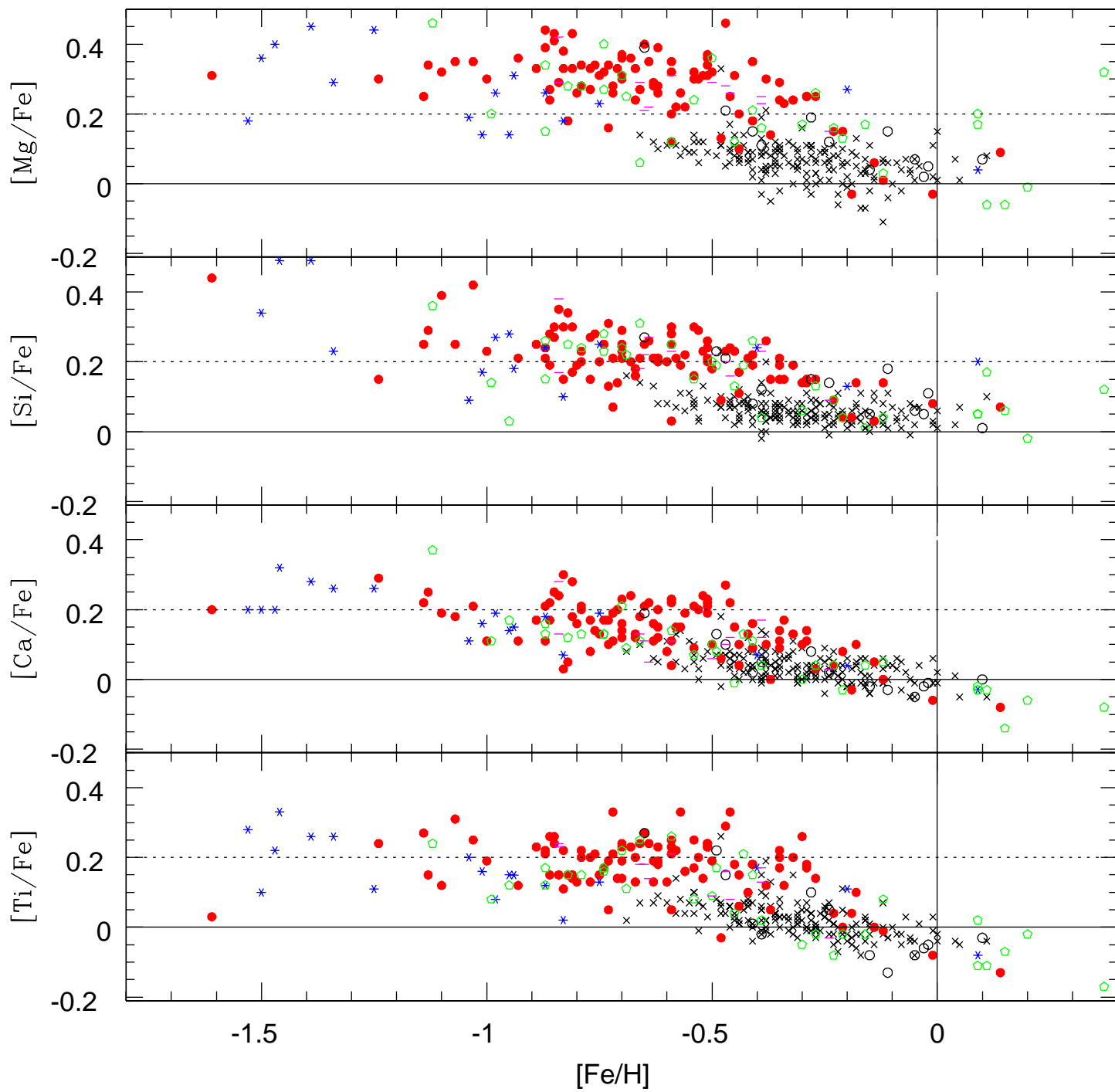












This figure "reddy_fig15.jpg" is available in "jpg" format from:

<http://arxiv.org/ps/astro-ph/0512505v1>

This figure "reddy_fig16.jpg" is available in "jpg" format from:

<http://arxiv.org/ps/astro-ph/0512505v1>

